

# Enzymatic strategies for carbon-sulfur bond formation in ergothioneine biosynthesis

**Inauguraldissertation**

Zur  
Erlangung der Würde eines Doktors der Philosophie  
vorgelegt der  
Philosophisch-Naturwissenschaftlichen Fakultät  
der Universität Basel

Von

**Reto Burn**

Adelboden, Bern

Basel, 2021

«Originaldokument gespeichert auf dem Dokumentenserver der Universität Basel  
edoc.unibas.ch»

Genehmigt von der Philosophisch-Naturwissenschaftlichen Fakultät auf Antrag von

Prof. Dr. Florian P. Seebeck

Prof. Dr. Thomas R. Ward

Basel, den 25.06.2019

Prof. Dr. Martin Spiess  
Dekan der Philosophisch-  
Naturwissenschaftlichen Fakultät







---

„Wir können nicht entscheiden, ob das,  
was wir Wahrheit nennen, wahrhaft Wahrheit ist,  
oder ob es uns nur so scheint.“  
- Heinrich von Kleist

---

---

## Abstract

Sulfur-containing molecules are abundant in nature and in pharmaceutical and agrochemical industries. Many chemical and enzymatic strategies for C-S bond formation have been identified and used to create novel compounds. Recently, there has been a considerable amount of interest in direct C-H bond functionalization, especially in reactions which have been developed to directly transform C-H to C-S bonds. Such transformations have also been observed in nature, for example, in ergothioneine biosynthesis. In **Chapter 1**, a brief overview on sulfur-containing molecules and synthetic/biosynthetic strategies to synthesise these is given.

Ergothioneine is a sulfur-containing derivative of histidine with antioxidant properties. In the following sections of this thesis, a novel biosynthetic enzyme for direct C-H to C-S bond transformation is described; the anaerobic ergothioneine biosynthetic enzyme, EanB.

The enzymes for oxygen-dependent ergothioneine biosynthesis (EgtA-E) were described a few years ago. In **Chapter 3**, the identification of an oxygen-independent ergothioneine biosynthetic pathway is described. The pathway involves only two enzymes - the methyl transferase EanA and the sulfurtransferase EanB. In addition to the *in vitro* reconstitution of oxygen-independent ergothioneine biosynthesis, we could show that the extremely halophilic bacterium, *Salinibacter ruber*, an organism carrying genetic information only for anaerobic ergothioneine biosynthesis, could produce ergothioneine in similar concentrations as has been described for those carrying the genetic information for aerobic ergothioneine biosynthesis.

This study was followed up by a structural and mechanistic investigation of the EanB-catalyzed C-S bond formation, described in **Chapter 4**. Based on structural and kinetic data, a mechanistic model for the direct C-H to C-S bond transformation catalyzed by EanB was elucidated. EanB is suggested to follow a ping-pong mechanism where, in a first step, a persulfide is formed on an active site cysteine residue of EanB and, in a second step, a sulfane sulfur is transferred to the unactivated carbon 2 of the imidazole ring of *N*- $\alpha$ -trimethylhistidine. The use of a single turnover assay allowed us to investigate the sulfur transfer from the enzyme to the substrate isolated from the formation of the active site persulfide.

In **Chapter 5**, the focus is set on the non-heme iron-dependent ergothioneine biosynthetic enzyme, EgtB. EgtB catalyzes the oxygen-dependent C-S bond formation in aerobic ergothioneine biosynthesis. We designed substrate analogs to probe the binding interactions between the two substrates, *N*- $\alpha$ -trimethyl histidine and cysteine/ $\gamma$ -glutamyl cysteine. The

---

result of this study led to the development of bisubstrates which revealed the importance of substrate alignment for efficient C-S bond formation.

Additionally, we analyzed substrate binding and regulation of the SAM-dependent methyl transferase EgtD, the only enzyme common to all known ergothioneine biosynthetic pathways. This study, described in **Chapter 6**, provides a good basis for further inhibitor design.

This thesis gives an insight into two different strategies of C-S bond formation in ergothioneine biosynthesis. Our findings contribute to a further understanding of the role of ergothioneine *in vivo* and its molecular mechanism of action.

---

## Abbreviations

3,4-AHBAL	3-Amino-4-hydroxybenzaldehyde
ACV	$\delta$ -(L- $\alpha$ -Aminoadipoyl)-L-cysteinyl-D-valine
AIBN	Azobis(isobutyronitril)
APS	Adenosine 5'-phosphosulfate
BioB	Biotin snyhtase
CDO	Cysteine dioxygenase
<i>CthEgtB</i>	EgtB from <i>Candidatus chloracidobacterium thermophilum</i>
CYP	Cytochrome P450
Cys	L-cysteine
DMH	N- $\alpha$ -dimethyl-L-histidine
EanA/B	Ergothioneine anaerobic biosynthetic enzyme A/B
EDTA	Ethylenediaminetetraacetic acid
ESI	Electrospray ionization
FAD	Flavin adenine dinucleotide
FMN	Flavin mononucleotide
$\gamma$ GluCys	$\gamma$ -Glutamyl-L-cysteine
HAT	Hydrogen atom transfer
HRMS	High-resolution mass spectrometry
IPNS	Isopenicillin-N-synthase
KIE	Kinetic isotope effect
KSIE	Kinetic solvent isotope effect
LipA	Lipoate synthase
MOA	Monoamine oxidase
<i>MthEgtB</i>	EgtB from <i>Mycobacterium thermoresistibile</i>
NADPH	Nicotinamide adenine dinucleotide phosphate
NHI	Non-haem iron-dependent
NMR	Nuclear magnetic resonance
OCTN1	Organic cation transporter 1
OvoA	L-cysteinyl-L-histidinylsulfoxide synthase
PAPS	3'-Phosphoadenylylsulfate

---

PLP	Pyridoxal phosphate
ROS	Reactive oxygen species
rSAM	Radical SAM
SAM	<i>S</i> -adenosyl-L-methionine
SET	Single electron transfer
TBHP	<i>tert</i> -butyl hydroperoxide
TCEP	Tris(2-carboxyethyl)phosphine
TMH	<i>N</i> - $\alpha$ -trimethyl-L-histidine

---

## Outline

1	Oxidative Carbon-Sulfur Bond Forming Reactions .....	1
1.1	Sulfur containing molecules .....	3
1.2	Chemical strategies for C-S bond formation .....	5
1.2.1	Metal catalyzed C-S bond formation <i>via</i> C-H bond activation .....	6
1.2.2	Metal-free reactions – radical .....	9
1.2.3	Metal free reactions – ionic .....	10
1.3	Enzymatic strategies for C-S bond formation .....	12
1.4	Ionic Mechanism for C-H functionalization with sulfur functional groups.....	14
1.4.1	Sulfur as a nucleophile .....	14
1.4.2	Sulfur as an electrophile.....	16
1.5	Radical Mechanism.....	17
1.5.1	CYP catalyzed C-S bond formation .....	17
1.5.2	Radical SAM enzyme catalyzed C-S bond formation .....	18
1.5.3	Flavin-dependent enzyme catalyzed C-S bond formation.....	21
1.5.4	Non-heme iron-dependent enzyme catalyzed C-S bond formation .....	22
1.6	Conclusion.....	26
2	Aim of the Thesis .....	27
3	Anaerobic Origin of Ergothioneine .....	29
4	Structural and mechanistic basis for anaerobic ergothioneine biosynthesis.....	37
5	Probing the Substrate-Substrate Interaction in Type I and Type II EgtB Catalysis .....	49
5.1	Introduction .....	49
5.2	Results .....	51
5.2.1	Probing the Substrate-Substrate Interaction for Binding and Catalysis .....	51
5.2.2	Bisubstrate analogs as substrates for EgtB .....	54
5.3	Discussion .....	56
5.3.1	Substrate-substrate interaction .....	56
5.3.2	Precise substrate positioning is essential for sulfoxide synthase activity.....	57
5.3.3	Inactivation of <i>CthEgtB</i> by the linked substrate.....	59
5.4	Conclusion.....	60
5.5	Experimental Part.....	61
6	Inhibition and Regulation of the Ergothioneine Biosynthetic Methyltransferase EgtD....	81
7	Literature .....	93
8	Acknowledgements.....	98





---

# 1 Oxidative Carbon-Sulfur Bond Forming Reactions

Making up 0.2% of the human body mass, sulfur is ranked as the 7<sup>th</sup> most abundant element found in body tissues.<sup>1</sup> What are the chemical properties of sulfur that make it so important for living organisms?

Sulfur belongs to the group of elements called the chalcogens and neighbors other essential elements of life in the periodic table, such as oxygen and phosphorous. In its elementary form, sulfur occurs as cyclooctasulfur (S<sub>8</sub>) and is relevant to only a few microorganisms. The sulfur atom has a larger diameter than oxygen and therefore is more polarizable.<sup>2</sup> Sulfur is highly reactive and reacts with almost all elements with exception for the noble gases and some inert metals. In comparison to oxygen, which occurs mainly in its oxidative state 0 as dioxygen or -1 and -2 in most organic compounds, sulfur can adopt oxidation states from -2 to +6.<sup>3</sup>

Most of the biologically available inorganic sulfur occurs as stable sulfate. Through activation of sulfate (OS(S) = +6), reduced sulfur species are generated and incorporated into organic molecules, such as cysteine and methionine (OS(S) = -2). Animals lack the ability to incorporate inorganic sulfate into cysteine, which makes cysteine and methionine to essential amino acids, whereby sulfur assimilation is mainly done by plants.<sup>1</sup>

The standard bond length of a C-S bond is 1.82 Å, which is longer than a C-C bond (1.52 Å) or a C-O bond (1.43 Å). With an electronegativity almost identical to carbon, the sulfenyl C-S bond is usually only slightly polarized. Thus, while replacing a methylene group with a sulfur atom does not change the polarity of the molecule, the geometry and size is changed.<sup>4</sup> The sulfhydryl group is chemically the most important form of sulfur to living organisms. The sulfhydryl groups are excellent nucleophiles and often scavenge toxic electrophiles or serve as activating groups in thioester chemistry in living organisms. Furthermore, thiolates are excellent chelators – they have the ability to remove toxic metals from organisms and prevent the formation of reactive oxygen species.<sup>5</sup>

One feature that makes sulfur indispensable for living organisms is the ability to form stable disulfide bonds (RS-SR). The relative stability of RS-SR bonds compared to RO-OR bonds is mainly due to the increased length of disulfide bonds (S-S approx. 2.04 Å) compared to peroxides (O-O 1.47 Å) leading to a decreased repulsion of the lone pairs. Additionally, the disulfide bond is stabilized by  $\pi$ -bonding interactions. Disulfide bonds are hydrolytically stable and keep protein structures together, however they can be easily reduced to free thiols by enzymes or intracellular reductants, such as glutathione.

---

Additionally, positively-charged sulfur species, such as sulfonium ions are relatively stable even under physiological conditions. Again, they are stable enough that their half-life is long enough to be a valuable metabolite, but also reactive enough that the bond can be broken if needed. This property makes the sulfonium ion *S*-adenosyl-L-methionine (SAM) to nature's analog of methyl iodide.<sup>6</sup>

Organisms have developed many systems to exploit these unique features of sulfur, some of which will be discussed in the following chapter.

---

## 1.1 Sulfur containing molecules

Sulfur-containing molecules have important roles as primary and secondary metabolites in all living organisms.<sup>7</sup> They are represented in all major classes of biomolecules, such as in proteins, nucleic acids, sugars, vitamin cofactors and metabolites. The sulfur-containing amino acids, methionine and cysteine, are essential for catalysis, structure and stability of proteins. Thiol-containing molecules are responsible for maintaining the cellular redox potential, protein thiol disulfide ratios, and to neutralize intracellular reactive oxygen species (ROS) formation.<sup>8</sup> Most prominent examples are glutathione (**1, figure 1**), mycothiol (**2, figure 1**), and ergothioneine (**3, figure 1**). Other sulfur-containing molecules are important for chemical defense (penicillin, **4, figure 1**), are cosubstrates for the biosynthesis of other biomolecules (SAM, **5, figure 1**) or contribute to other central biochemical processes, such as transcription (s<sup>2</sup>C and s<sup>4</sup>U in tRNA, **6, figure 1**), fatty acid metabolism (coenzyme A, **7, figure 1**) or carbohydrate and amino acid catabolism (thiamine, **8, figure 1**).<sup>9-11</sup> Due to the importance of sulfur-containing molecules to all living organisms, understanding their biosynthetic pathways could lead to potential targets for novel antibiotics.<sup>12</sup>

However, it is not only nature that has made use of the versatile properties of sulfur - chemists have also discovered various methods of compound synthesis, exploiting the special chemical character of sulfur in its various forms. Sulfur-containing molecules are important in pharmaceutical and agricultural industries, as well as in material science.<sup>13,14</sup> Nine of the top ten selling drugs from 2000-2011 were sulfur-containing molecules.<sup>15</sup> Sulfur is found in the form of disulfides in antibodies, as thioethers, thiophenes, sulfoxides and as sulfate ester and amides. Hence, the development of new methods to form carbon-sulfur bonds is an exciting and vivid field nowadays.

There are many strategies to form C-S bonds, both in nature and developed by synthetic chemists, from simple transformations, such as nucleophilic substitution and addition, to more sophisticated metal-catalyzed reactions.<sup>16-20</sup> The aim of this chapter is to give an overview on the strategies developed by chemists and nature to transform C-H bonds to C-S bonds.

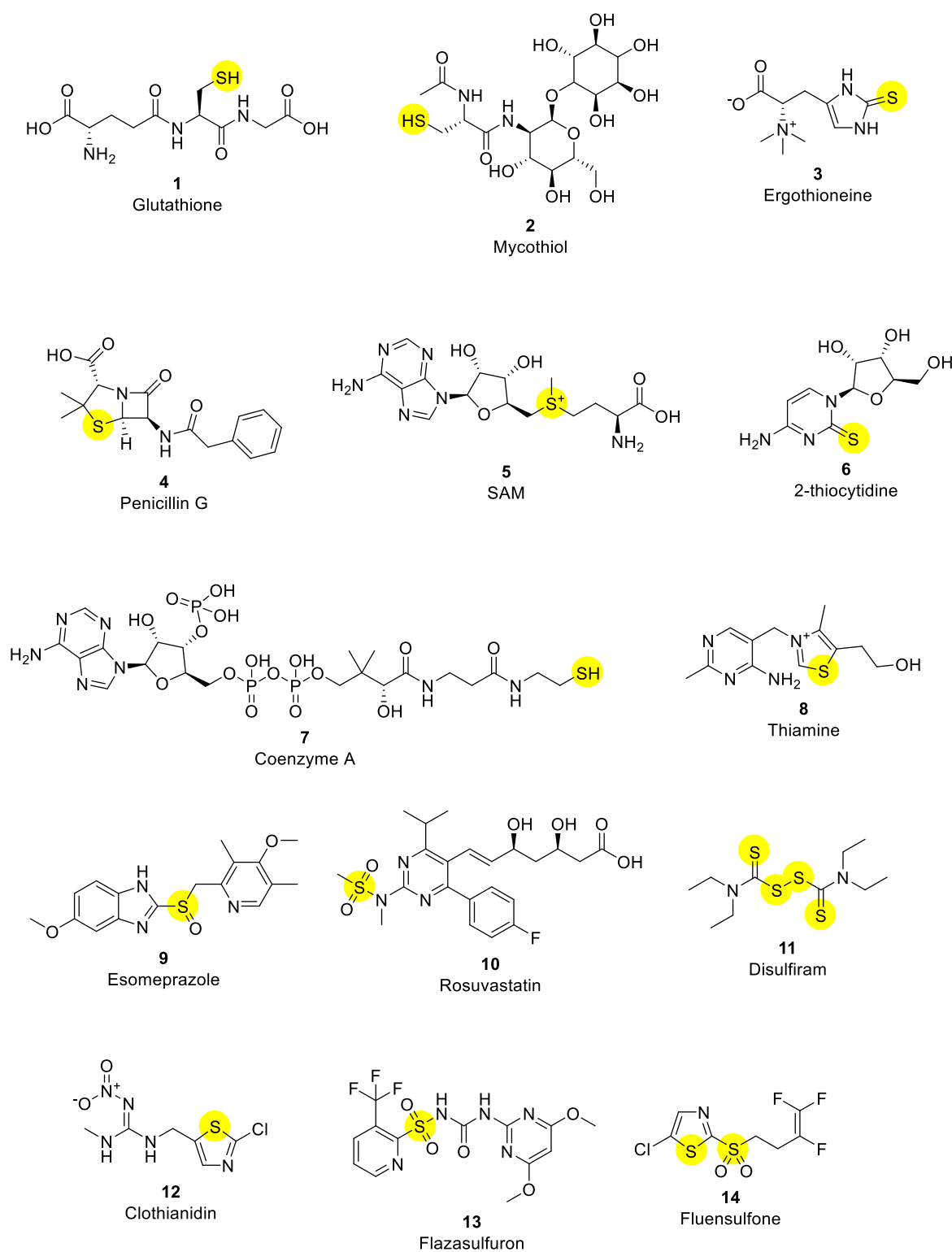


**Figure 1.** A selection of sulfur-containing small molecules. Compounds 1- 8 are biomolecules; Compounds 9-11 pharmaceuticals and Compounds 12-14 are agrochemicals.

## 1.2 Chemical strategies for C-S bond formation

Many reactions have been developed for the construction of new C-S bonds (**figure 2**).<sup>16</sup> The most common methods involve nucleophilic substitution or addition reactions of sulfur nucleophiles ((1) and (2), **figure 2**). Alternatively, a sulfur electrophile, such as a disulfide or S<sub>8</sub> ((3), **figure 2**) can be used for the construction of C-S bonds in the presence of an appropriate electrophile. Other common reaction types include the sulfonylation of C-H bonds ((4), **figure 2**), cross coupling reactions and photo-catalyzed reactions.<sup>17–20</sup> Reactions with sulfur electrophiles, sulfonylation reactions and metal-catalyzed reactions *via* C-H bond activation are most prominent and will be discussed in more detail.

Sulfonylation reactions are defined as reactions where a sulfonyl group (RS-, R ≠ H) is incorporated into a molecule. Such reactions have been known for a long time and have often involved the use of sulfur electrophiles, such as disulfides or sulfonyl halides in combination with carbon nucleophiles. Radical reactions have also been used for C-S bond construction by addition to alkenes ((6), **figure 2**), however, methods have been developed for direct C-H functionalization using radical chemistry.<sup>21,22</sup> More recently, methods have been developed for sulfonylation through selective C-H bond activation using transition metal catalysis.<sup>22</sup>

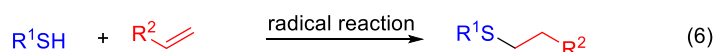
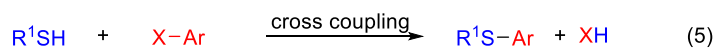
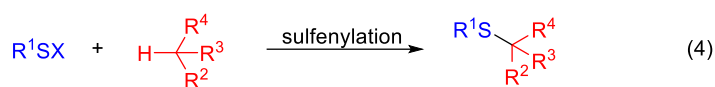
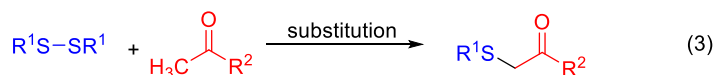
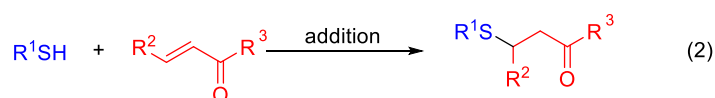
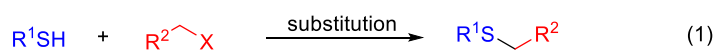


**Figure 2.** Different strategies used to form C-S bonds.

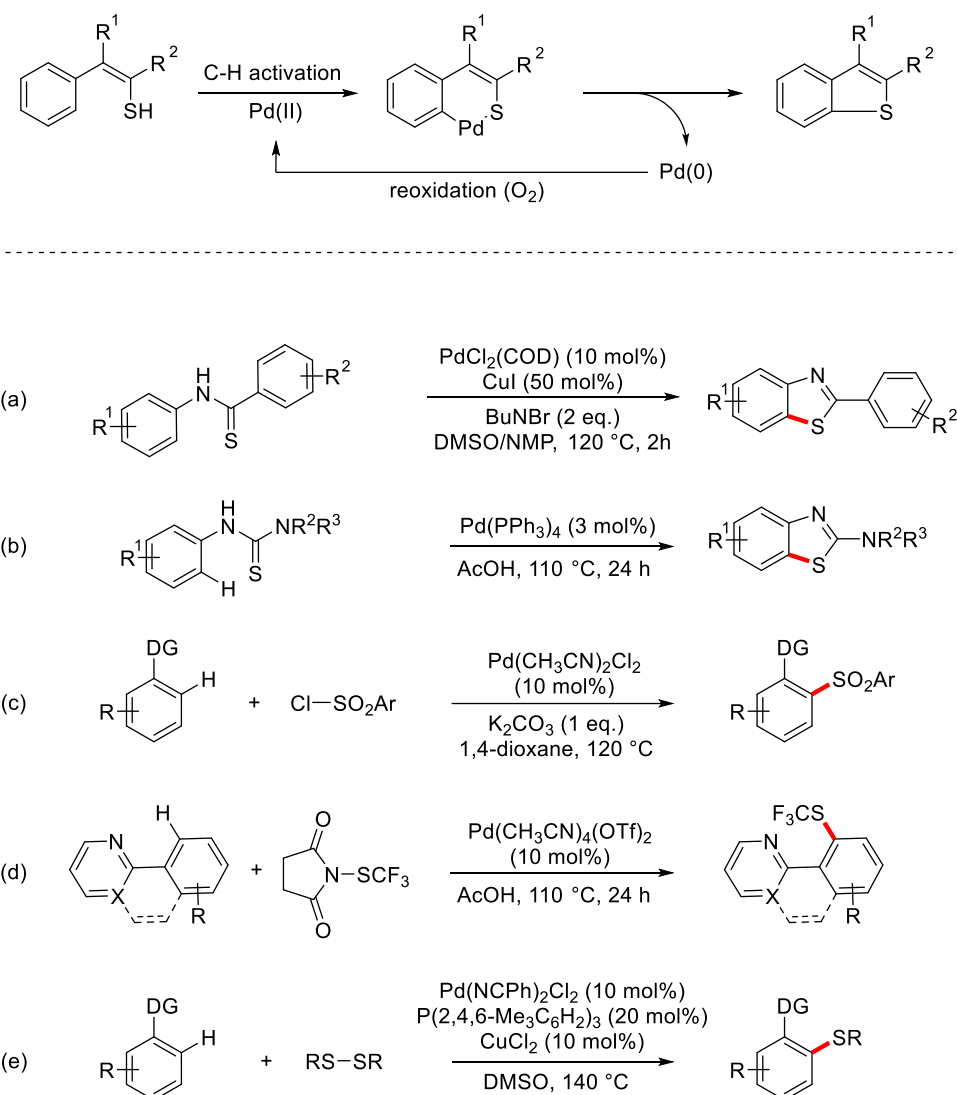


**Figure 3.** Top: Pd catalyzed cyclization reaction developed by Inamoto *et al.* Bottom: Some examples for Pd catalyzed C-S bond forming reactions via C-H bond activation.

### 1.2.1 Metal catalyzed C-S bond formation via C-H bond activation

Transition metal catalysis is a powerful tool for carbon-heteroatom bond formation through C-H bond activation. The catalytic power of transition metals lies in their ability to adopt various oxidative states and, hence, serve as electron sinks or donors. For example, Migita *et al.* reported transition metal catalyzed C-S bond formation in the late 1970's and early 1980's.<sup>23,24</sup> This reaction has been used to couple aryl iodides/bromides with thiols using Pd catalysts. Throughout the years, the reaction has been optimized to increase catalyst turnover number, scope and generality.<sup>25</sup> The Migita coupling has also been used in industrial set ups for large scale productions.<sup>25</sup> However, until recently, not much was known about transition metal catalyzed C-S bond formation via C-H bond activation.<sup>22</sup>

Then, in 2008, Inamoto *et al.*<sup>26</sup> reported the intramolecular C-S bond formation with  $\text{PdCl}_2$  and  $\text{PdCl}_2(\text{cod})$  catalysts (a, **figure 3**). These reactions became especially useful for the synthesis of benzothiazoles. The group of Inamoto developed Pd-catalyzed reactions to synthesize

---

benzothiazoles in water.<sup>27</sup> Other groups have developed other Pd-based catalyst systems to synthesize 2-aminoglycosylbenzothiazoles or 2-trifluoromethylbenzothiazoles.<sup>28,29</sup> This type of reaction is generally a two-electron oxidation of the substrate. The palladium catalyst is reduced and must be reoxidized to close the catalytic cycle. Most of these reactions are run under aerobic conditions, using oxygen as oxidant (top, **figure 3**).

More recently, protocols for intermolecular C-S bond formation have been developed. The first report was a C-H sulfonylation with arylsulfonylchlorides by Zhao *et al.* (c, **figure 3**).<sup>30</sup> They managed to synthesize sulfones by C-H activation/cross-coupling. Phenyl pyridine was used as substrate due to the well-known coordinating ability of pyridine moieties and the prevalence of pyridine moieties in medicinal chemistry. Interestingly, depending on the conditions the C-H bond could also be oxidized to a C-C bond or C-Cl bond.

Pd-based catalysts have also been used to introduce trifluoromethylthiol groups *via* C-H activation (d, **Figure 3**).<sup>31</sup> The trifluoromethylthio group is mainly interesting due to the high lipophilicity, facilitating the crossing of lipid membranes for pharmaceuticals and agrochemicals. N-trifluoromethylthio succinimide was used in combination with aryl pyrimidines. The reaction was proposed to have a Pd(III) or Pd(IV) intermediate.

Iwasaki *et al.* recently reported a Pd and Cu co-catalysis system for the direct sulfenylation of arenes bearing a directing group using phenyl disulfides as substrates.<sup>32</sup> Since both sulfenyl moieties could be incorporated, they suggested that the reaction proceeds *via* a Pd(II)/Pd(IV) mechanism. DMSO serves as the terminal oxidant (e, **figure 3**).

The most prominent metal catalyst used for direct C-S functionalization of C-H bonds is copper. The first Cu catalyzed C-S bond forming reactions *via* C-H activation were reported in 2006 by Chen *et al.*<sup>33</sup> They achieved C-H bond sulfenylation with both, thiophenol and dimethyl disulfide. This reaction was proposed to proceed through a single electron transfer (SET) from Cu(II) to the coordinated phenyl ring (**A, figure 4**).

Another interesting example employs disulfides as substrates for cyclization of benzothiazoles. The reaction was originally performed under an argon atmosphere and gave a 1:1 mixture of the benzothiazole and 2,3-dihydro-2-benzothiazole (**B, figure 4**).<sup>33</sup> Because there was no oxidant present in reaction, the disulfide served as the oxidant. After 0.5 turnovers, all disulfides were reduced to the respective thiol and the reaction stopped. When the reaction was run in the presence of oxygen, quantitative formation of the benzothiazole product was observed (**B, figure 4**).<sup>34,37</sup> With similar methods, a variety of compounds have been sulfenylated, such as thiazoles, oxazoles, pyrroles, thiophenes and arenes.<sup>22</sup> Another interesting example of Cu-catalyzed C-S bond formation was reported in 2014 by Chen *et al.*<sup>35</sup> where a C-S and C-N bond were constructed in one step using elemental sulfur (**C, figure 4**). Finally, a procedure for copper-catalyzed sulfonylations of C-H bonds had been developed

using sulfonyl chlorides or sodium sulfonates as starting materials (**D**, **figure 4**).<sup>36,38</sup> These examples show the strength of Cu catalyzed C-S bond formation. Substrate used for these transformations are generally more versatile in comparison with Pd catalyzed transformations.

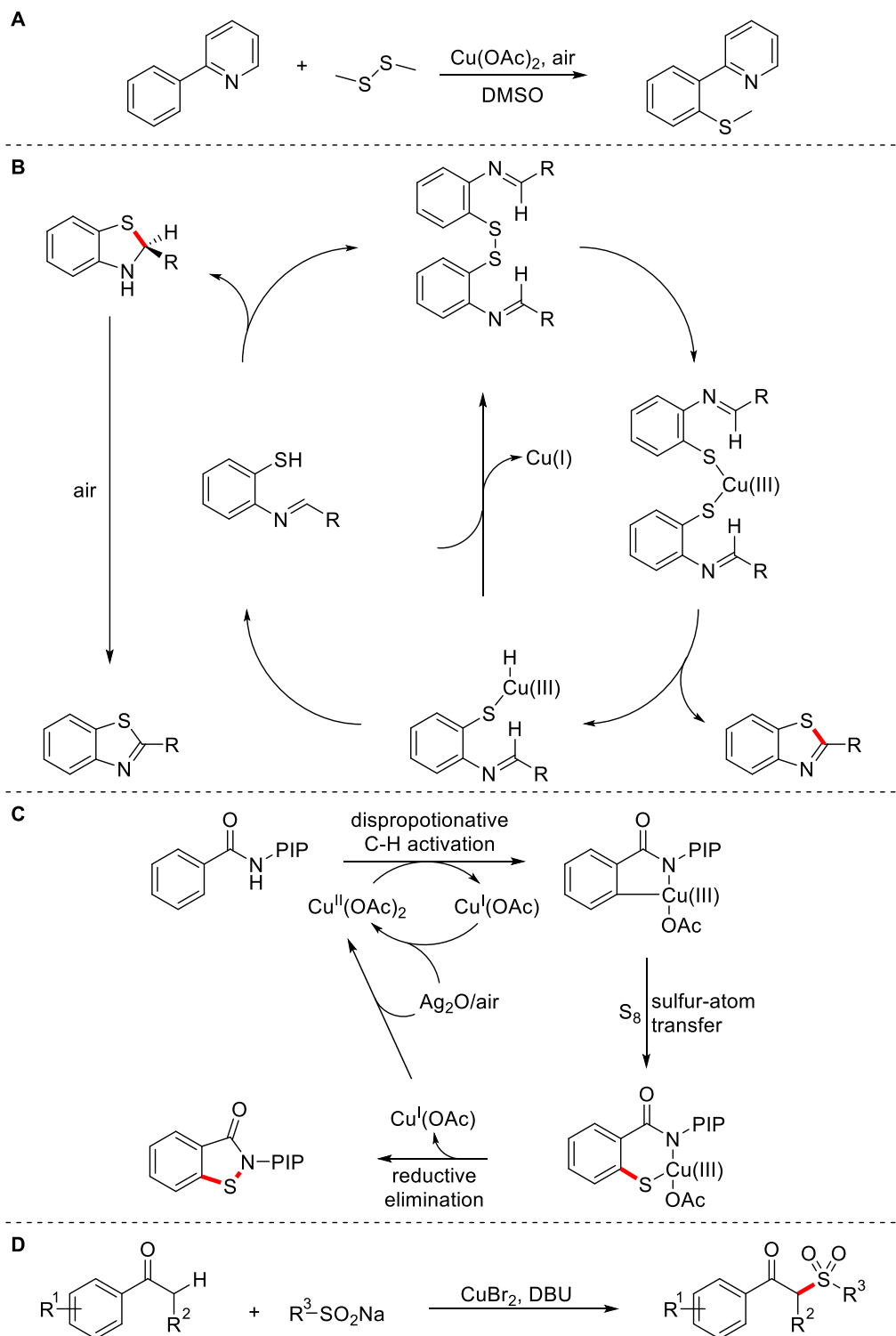


**Figure 4.** Some representative reactions for Cu-catalyzed C-S bond formation via C-H activation. **A:** The first Cu catalyzed C-S bond forming reactions via C-H activation reported by Chen et al.<sup>33</sup> **B:** Proposed mechanism for the Cu-catalyzed formation of benzothiazoles developed by Srogl et al.<sup>34</sup> **C:** The synthesis of benzoisothiazolone via C-S and C-N bond formation.<sup>35</sup> **D:** The  $\alpha$ -sulfonylation of arylketones.<sup>36</sup>



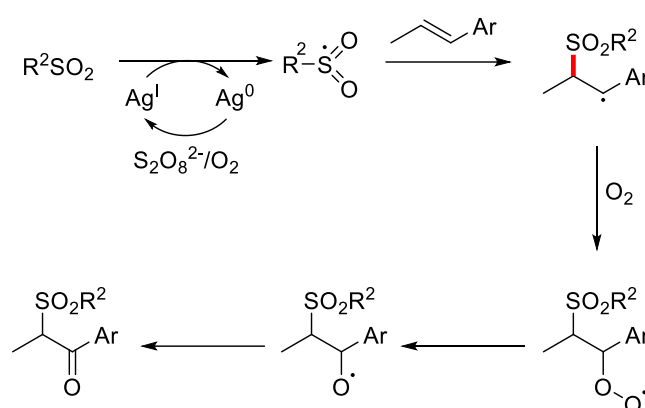
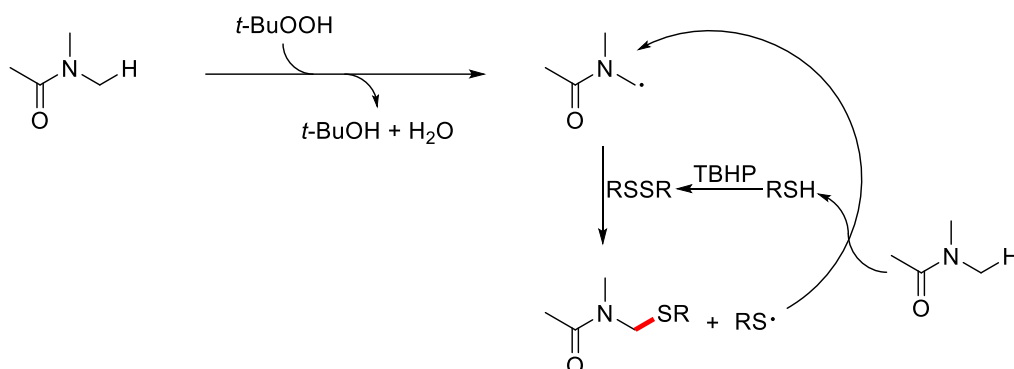


**Figure 5.** Top: Possible mechanism for the radical sulfenylation of amides.<sup>40</sup> Bottom: Suggested mechanism for the oxysulfonylation of alkenes.<sup>42</sup>

As a thiophilic metal, copper is especially useful when disulfides are used as substrates. These reactions generally use oxygen as an oxidant, or a stoichiometric amount of copper can also be used.<sup>22</sup> Copper-catalyzed reactions have several advantages over their palladium-catalyzed equivalents; for example, the catalysts are generally cheaper and, for example, if  $S_8$  or sulfides are used as the source of sulfur, palladium catalysts are more often affected by uncontrolled poisoning or deactivation of the metal center.

Further examples of transition metal-catalyzed C-S bond forming reactions use Rh or Ru catalysts. The substrate scope is very similar to Pd and Cu catalyzed reactions. In general, the methods for C-S bond formation through C-H bond activation are still quite limited.

### 1.2.2 Metal-free reactions – radical

An early example for C-S bond formation following a radical mechanism includes the sulfenylation of orthoesters with trichloromethyl sulfonyl chloride and AIBN as radical initiator, whereby a thiyl radical was proposed as the intermediate.<sup>39</sup> Recently, such transformations have gained the attention of researchers, and several conditions have been developed to directly transform C-H bonds to C-S bonds with radical initiators. Generally, these reactions use disulfides as substrates. The processes are oxidative and hence require an

---

oxidant. This often is the same molecule as the radical initiator, such as with *tert*-butyl hydroperoxide (TBHP) (*top*, **figure 5**).<sup>40,41</sup> The reduced thiolate can react with the TBHP to form sulfenic acid and *tert*-butanol. The sulfenic acid reacts with another thiolate forming a disulfide and water. Other examples of radical-based C-S bond formation use aryl alkenes/alkynes and sulfinic salts to synthesize  $\beta$ -keto sulfones under aerobic conditions (*bottom*, **figure 5**).<sup>42,43</sup>

### 1.2.3 Metal free reactions – ionic

The sulfenylation of nucleophilic carbon atoms with electrophilic sulfenyl species has been well established. These methods have been extensively used to functionalize electrophilic carbon atoms  $\alpha$  to a carbonyl group or heterocyclic compounds, such as indoles.<sup>16</sup> A common variant of this reaction is performed with iodine as a catalyst to form sulfenyl iodides as sulfenyl electrophiles (**A, figure 6**). Different sulfur substrates can be used to generate sulfenyl iodides such as thiols, disulfides, sulfonylchlorides, sulfinic acids and others.<sup>20</sup> Depending on the oxidative state of the sulfur atom, the oxidant must be replaced with a reducing agent, such as triphenylphosphine, to reduce the sulfur to the disulfide-state, however the mechanism of C-S bond formation is in principal the same for most of these reactions. The nucleophilic carbon attacks the electrophilic sulfur atom with concomitant loss of iodide, followed by deprotonation. The iodide anion must then be reoxidized to iodine to close the catalytic cycle (**A, figure 6**).

Some examples have been reported of direct attack of a nucleophilic carbon on a disulfide, without the addition of any catalyst. In these reactions, the disulfide directly serves as oxidant.<sup>44,45</sup> Other catalyst-free variants use sulfenyl succinimides/phthalimides/imidazoles or similar derivatives as sulfur electrophiles (**B, figure 6**).<sup>16,46</sup>

Reports of reactions for direct sulfinylation of nucleophilic carbon atoms are rather rare. A recent example was reported by Miao *et al.*,<sup>47</sup> where an aryl sulfinyl cation generated from aryl sulfinyl salts serves as the sulfur electrophile. *N*-Alkyl pyrroles and indoles were used as carbon nucleophiles. The reaction conditions are generally very mild and could be run in water at room temperature without the addition of a catalyst (**C, figure 6**).

Friedel-Crafts-type sulfonylation reactions with sulfonyl halides and anhydrides, using  $\text{AlCl}_3$  as the catalyst, have been known since over a century ago.<sup>48</sup> Since then, conditions have been optimized and to achieve efficient transformations under milder conditions. Recently, milder reactions have been developed using  $\text{CeCl}_3$  as a catalyst in presence of iodine (**D, figure 6**).<sup>49</sup>

Another useful reaction to form C-S bonds is the thioesterification of aldehydes. This is achieved through *N*-heterocyclic carbene (NHC) catalysis. When disulfides serve as sulfur electrophiles, an oxidant such as DEAD must be used to obtain good yields. First, the disulfide can serve as oxidant, but after 50% conversion only the thiol is remaining. The reaction

involves the formation of a carbonyl umpolung to obtain a nucleophilic carbonyl carbon (**E**, **figure 6**).<sup>50,51</sup>

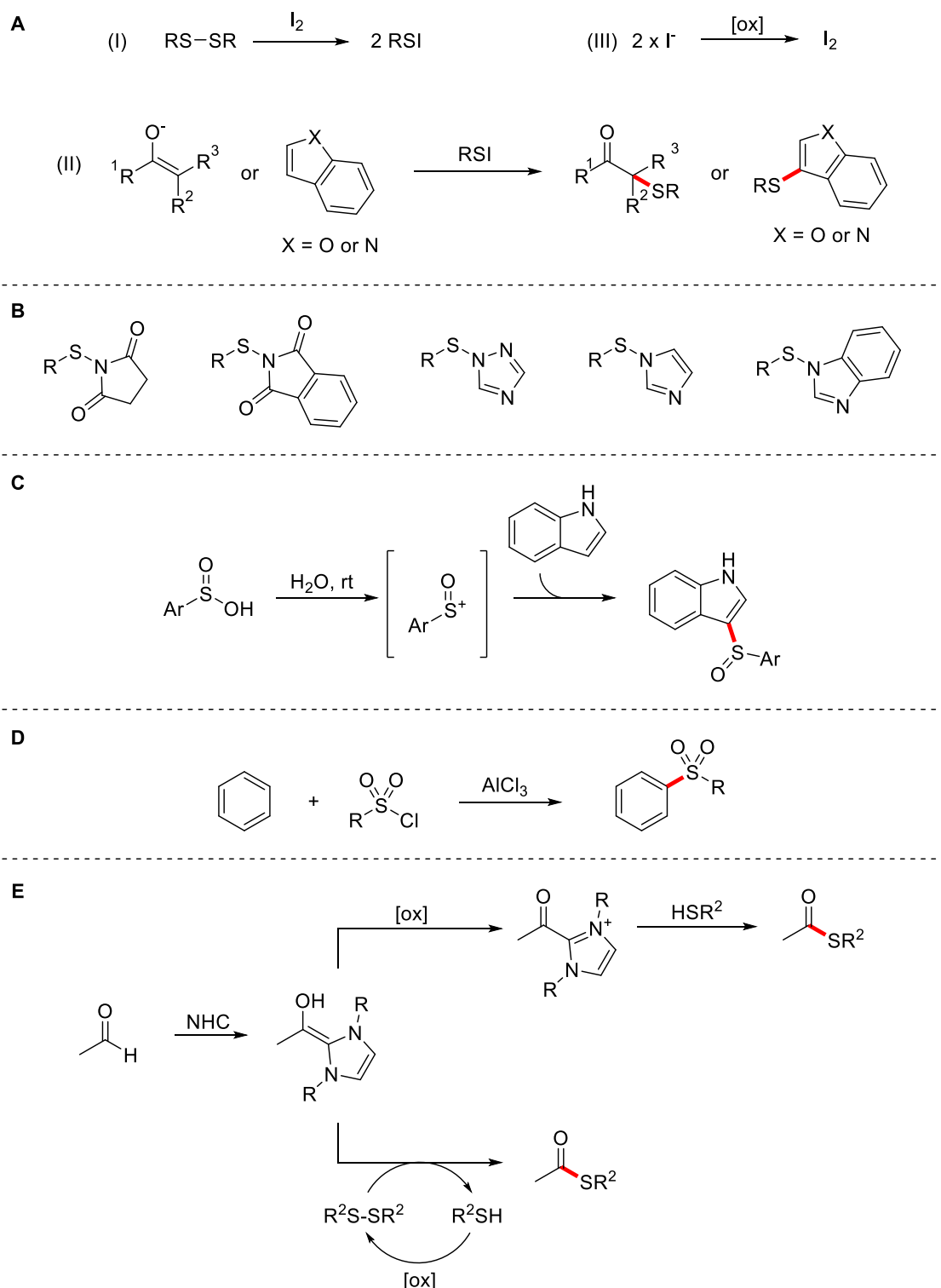


**Figure 6. A:** Basic steps in iodine-catalyzed sulfenylation of  $\alpha$ -carbonyl carbons or heterocyclic compounds. (I) Formation of the reactive sulfenyl iodide from a disulfide. (II) C-S bond formation by attack of the carbon nucleophile on the sulfur atom. (III) Oxidation of iodide to iodine. **B:** Electrophilic sulfenyl compounds used for sulfenylation of nucleophilic carbons  $\alpha$  to carbonyl groups and electron rich arenes. **C:** Sulfinylation of indole reported by Miao et al.<sup>47</sup> **D:** Friedel-Crafts sulfenylation of benzene.<sup>48</sup> **E:** NHC catalysis for thioester formation from aldehydes.

### 1.3 Enzymatic strategies for C-S bond formation

The pool of sulfur compounds which nature can use as substrates is relatively small even though sulfur is a versatile element occurring in various oxidation states. Moreover, some species, such as hydrogen sulfide or sulfur dioxide, are highly reactive and thus toxic for organisms. Concentrations of these sulfur species are usually kept at a low cellular concentrations, or are directly generated at the site where needed. Other species are rather unreactive, and their activation requires specialized enzymes, such as in sulfate activation in the cysteine biosynthesis.<sup>52</sup> Many different strategies have been evolved to keep balance between highly reactive and stable sulfur species. The central sulfur-containing biomolecules are the two amino acids, cysteine and methionine. The latter itself is *de novo* synthesized from cysteine and can be further transformed to its *S*-adenosyl derivative (SAM). Besides their important structural and catalytic roles in proteins, they are crucial in natural product biosynthesis. SAM is nature's most abundant methyl donor and more recently has been assigned to many other transformations such as C-S bond forming reactions.<sup>11,53</sup> Cysteine, which is synthesized from sulfate and serine through multiple steps, is involved in the biosynthesis of almost all sulfur-containing biomolecules (**figure 7** and **8**).<sup>10,54–57</sup> There are several metabolites where cysteine is a part of the core structure (*e.g.* glutathione). For other molecules, partial incorporation of the cysteine skeleton is involved (*e.g.* penicillin), but in many structures, the sulfur atom is the only remaining part of cysteine in the compound (*e.g.* ergothioneine). C-S bond cleavage to remove the amino acid moiety is generally catalyzed by PLP-dependent  $\beta$ -lyases.<sup>10</sup>

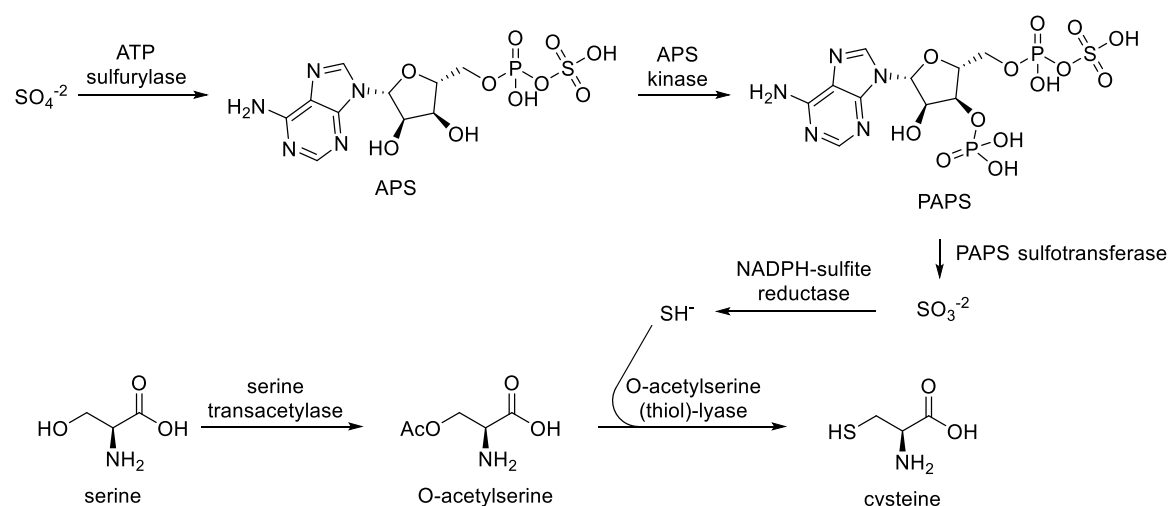


**Figure 7.** Cysteine biosynthesis starts with activation of sulfate to adenosine 5'-phosphosulfate (APS) by the ATP sulfurylase. Phosphorylation of APS by the APS kinase gives 3'-phosphoadenylylsulfate (PAPS). PAPS is reduced to sulfite by PAPS sulfotransferase, which is a thioredoxin enzyme. Sulfite is reduced by the FAD and FMN dependent NADPH-sulfite reductase. The sulfide is transferred to O-acetylserine to yield cysteine.

The synthesis of sulfur-containing biomolecules has been divided into two groups. The first group contains biosynthetic pathways where cysteine or a derivative thereof is the direct sulfur donor for the product. The other group contains biosynthetic pathways where the sulfur is introduced from a persulfidic sulfur. In the latter case, the sulfur often originates from cysteine. Sulfurtransferases can obtain a persulfidic sulfur from thiosulfate, mercaptopyruvate or from a cysteine  $\beta$ -lyase.<sup>56,58,59</sup>

Cysteine desulfurases (CSD) are PLP-dependent enzymes which can abstract the sulfur from cysteine and generate a persulfidic sulfur on an active site cysteine.<sup>58,60</sup> The sulfane sulfur is then shuttled either directly or *via* carrier proteins to the final acceptor. The biosynthesis of thiolated tRNA, iron sulfur clusters, molybdenum cofactor, and thiamine rely on this pathway. Another source for sulfane sulfur is cystine. Cystine  $\beta$ -lyases are PLP-dependent enzymes generating cysteine persulfide and pyruvate from cystine. Cysteine persulfide is then a substrate for C-S bond forming enzymes. Tropodithietic acid biosynthesis relies on this pathway.<sup>61</sup>

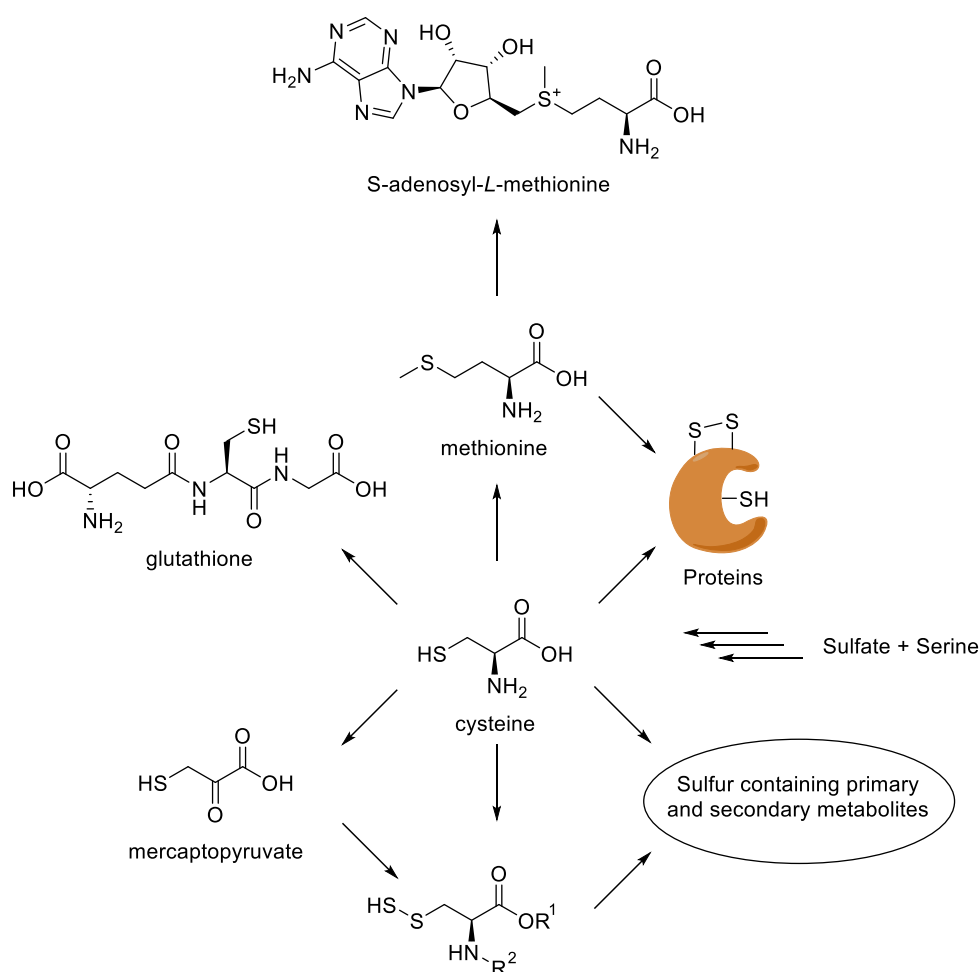


**Figure 8.** The central role of cysteine in sulfur metabolism.

## 1.4 Ionic Mechanism for C-H functionalization with sulfur functional groups

In ionic mechanisms, a carbon electrophile is attacked by a nucleophilic sulfur atom. The polarities are inverted in a few cases, i.e. a nucleophilic carbon attacks an electrophilic sulfur atom such as persulfidic sulfur or disulfides. In this section some examples of ionic C-S bond formation are discussed in more detail.

### 1.4.1 Sulfur as a nucleophile

Oxidative ionic carbon-sulfur bond formation often occurs in two steps. First, the substrate is oxidized by a cytochrome P450 monooxygenase (CYP) to generate a reactive electrophilic center. This activation of the substrate is followed by the attack of a thiolate nucleophile, either *via* addition or nucleophilic substitution. Such a reaction is often catalyzed by S-transferases, such as glutathione S-transferase. Some examples are found in the glucosinolate, thiolactomycin or gliotoxin (**figure 9**).<sup>10,62</sup> In some cases, the attack by the S-nucleophile may be enzyme-independent because of the high reactivity of the generated intermediate.

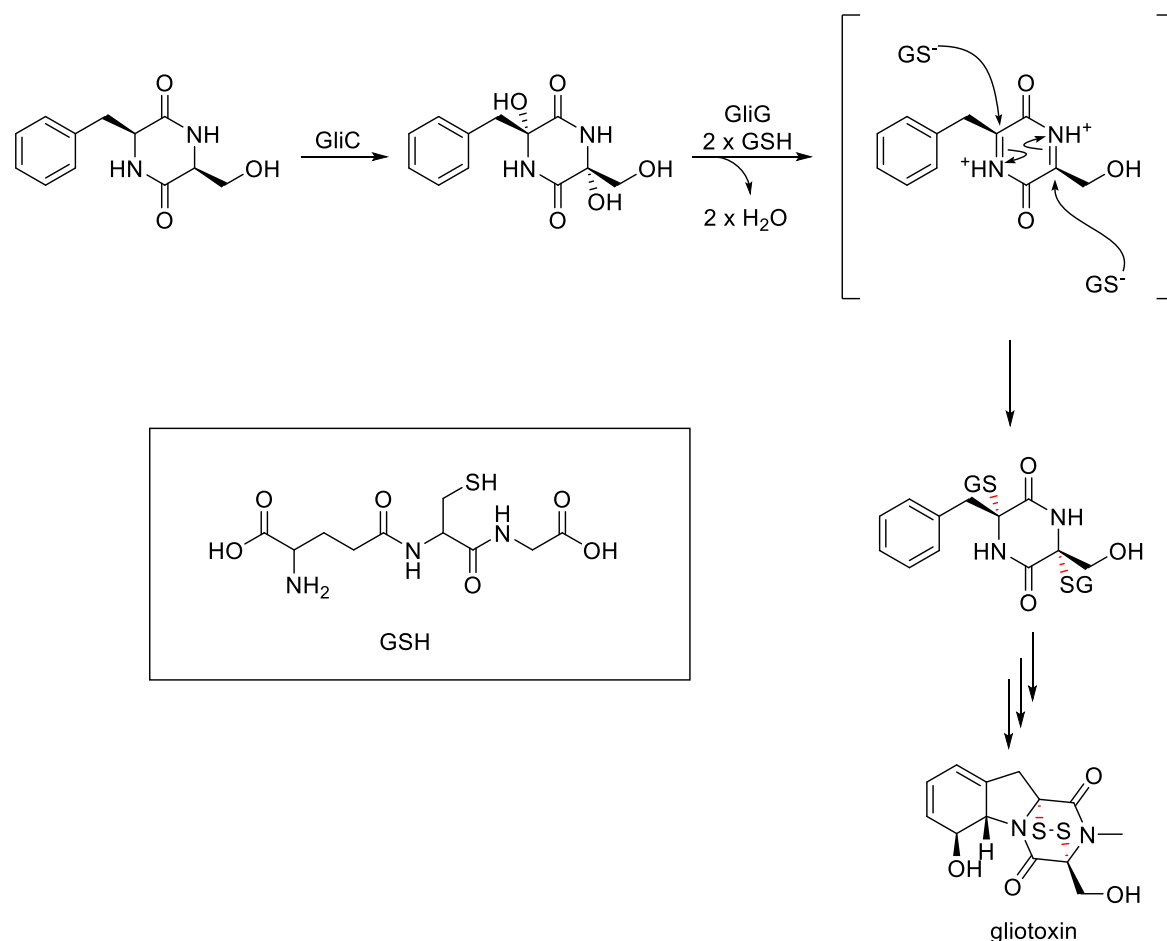


**Figure 9.** Gliotoxin biosynthesis. Oxidation of the Phe-Ser cyclic dipeptide by the CYP450 monooxygenase GliC and subsequent C-S bond formation catalyzed by the glutathione S-transferase GliG.<sup>53,64</sup>

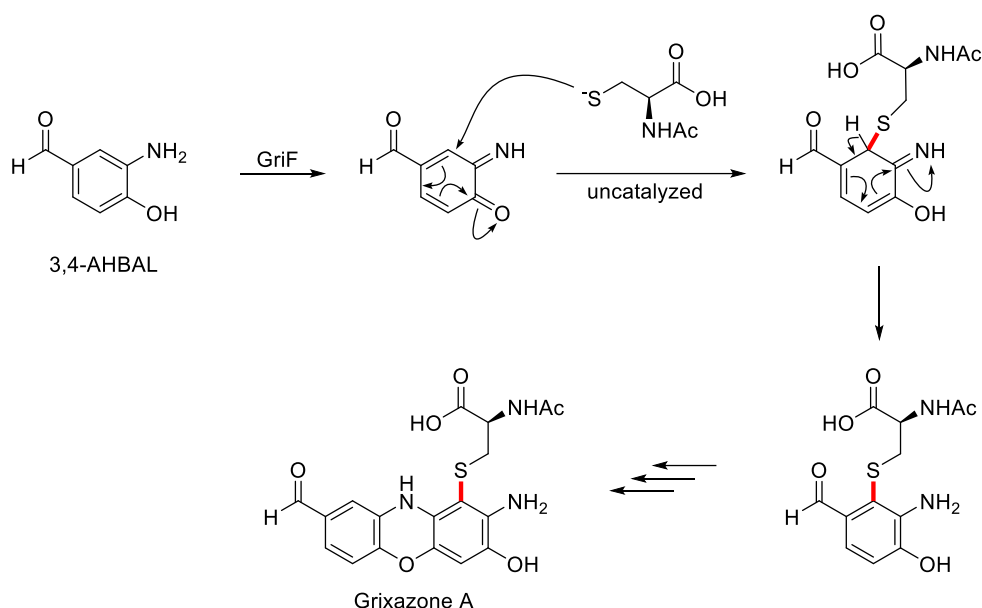


**Figure 10.** The uncatalyzed C-S bond formation in the biosynthesis of grixazone A.

A good example for uncatalyzed C-S bond formation has been observed in the biosynthesis of grixazone.<sup>65</sup> The precursor 3-amino-4-hydroxybenzaldehyde (3,4-AHBAL) is oxidized to the *ortho*-quinone by the tyrosinase homolog, GriF. The *ortho*-quinone is a good Michael acceptor and readily reacts with *N*-acetyl cysteine. *In vitro* studies have shown that this addition with subsequent aromatization occurs without any additional enzyme. The product can be re-oxidized and dimerize with another 3,4-AHBAL to form grixazone (**figure 10**).

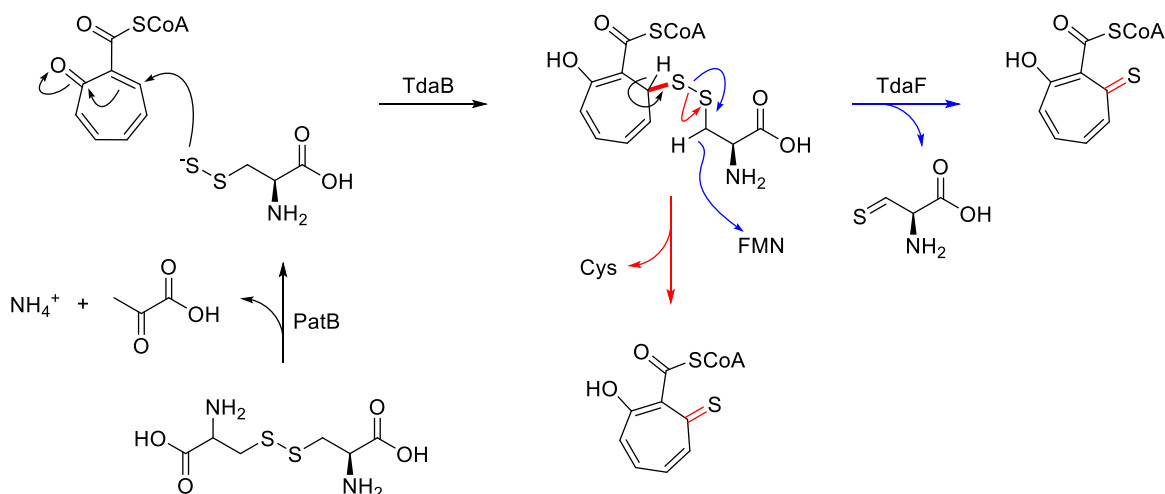


**Figure 11.** Proposed C-S bond formation in tropodithietic acid. Blue arrows represent the mechanism proposed by Brock *et al.*<sup>66</sup> The red arrows indicate an alternative pathway.

Cases where a direct oxidative ionic mechanism is occurring are rare. An example with a sulfur nucleophile is in the biosynthesis of tropodithietic acid. The oxidation of a C-H bond is coupled to the reduction of FMN. Tropodithietic acid biosynthesis is not fully understood yet. In 2014, Brock *et al.*<sup>66</sup> proposed a possible biosynthetic pathway which involves the Michael addition of cysteine persulfide onto an  $\alpha,\beta$  unsaturated ketone catalyzed by the glutathione-S-

transferase homolog, TdaB forming the disulfide intermediate. Dickschat *et al.*<sup>61</sup> identified PatB as the cystine lyase producing the cysteine persulfide required for the synthesis (**figure 11**). The role of TdaF is still very hypothetical and since the product of the Michael addition is expected to readily oxidize, a simple base-catalyzed pathway with elimination of cysteine should be considered too.

#### 1.4.2 Sulfur as an electrophile

An example with a carbon nucleophile is the detoxification of cyanide by rhodanese enzymes (sulfurtransferases, **figure 12**). Since the discovery of these enzymes in the 1930s, researchers have been interested in their function but until recently, not much has been reported about their functions.<sup>59</sup> Nowadays, only a few sulfurtransferases could be assigned with functions other than cyanide detoxification, such as those in the biosynthesis of thiamin and molybdopterin. The presence of an active site persulfide could be verified by X-ray in 1978.<sup>67</sup> These enzymes follow a double displacement mechanism (Ping-Pong mechanism). Firstly, the active site cysteine is persulfidated by thiosulfate or  $\beta$ -mercapto pyruvate to bring the enzyme into its active form. Once cyanide binds to the active site, the nucleophilic carbon of cyanide attacks the active site persulfide forming thiocyanate and the enzyme returns to its resting state.<sup>68,69</sup>

In chapter 3 of this thesis, the discovery of a sulfurtransferase from the anaerobic ergothioneine biosynthetic pathway (EanB), which catalyzes sulfur insertion into the C2-H bond of the imidazolyl moiety of *N*- $\alpha$ -trimethylhistidine will be described. Structural and kinetic data revealed that an active site persulfide serves as nucleophile and is then reductively cleaved. For more details see **Chapter 4**.

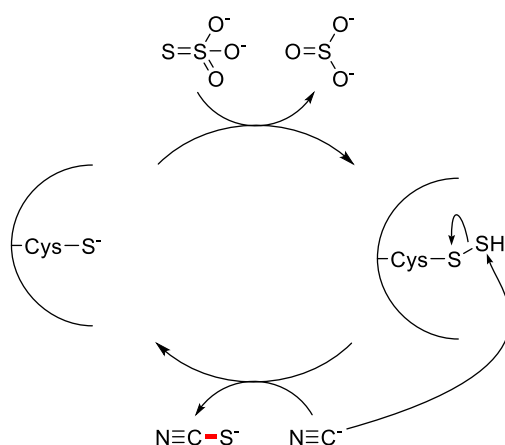


**Figure 12.** Mechanism of rhodanese-catalyzed detoxification of cyanide.



## 1.5 Radical Mechanism

For a long time, it was believed that most biologic reactions occurred through ionic mechanisms. While this still holds true for simple transformations, radical reactions are mostly involved in functionalization of unreactive C-H bonds.<sup>70,71</sup> Often intermediates with a high oxidative power are generated to abstract hydrogen atoms from the substrate. Reactions following a radical mechanism for C-S bond formation are often catalyzed by aerobic enzymes dependent on an iron cofactor using dioxygen as the oxidant or anaerobic enzymes using iron-sulfur ( $[4\text{Fe-4S}]^{2+}$ ) clusters. The latter are generally referred to as radical SAM enzymes. Due to the oxidative power of these reactions, most of the direct C-H to C-S bond oxidations are performed *via* radical reactions.

### 1.5.1 CYP catalyzed C-S bond formation

The main role of CYP enzymes in C-S bond formation has been discussed in the chapter about ionic reactions. There are only few examples of CYP enzymes which can catalyze direct C-S bond formation. A CYP-catalyzed reaction with a proposed radical mechanism for C-S bond formation has been reported in the biosynthesis of griseoviridin, a natural product with antimicrobial properties containing a unique thio-ene functional group.<sup>72,73</sup> The formation of such a group is also challenging for chemists and therefore the total synthesis of griseoviridin took more than 20 years. Synthetic strategies involved sulfenylation of carbons bearing an acidic proton with sulfur electrophiles.<sup>74,75</sup>

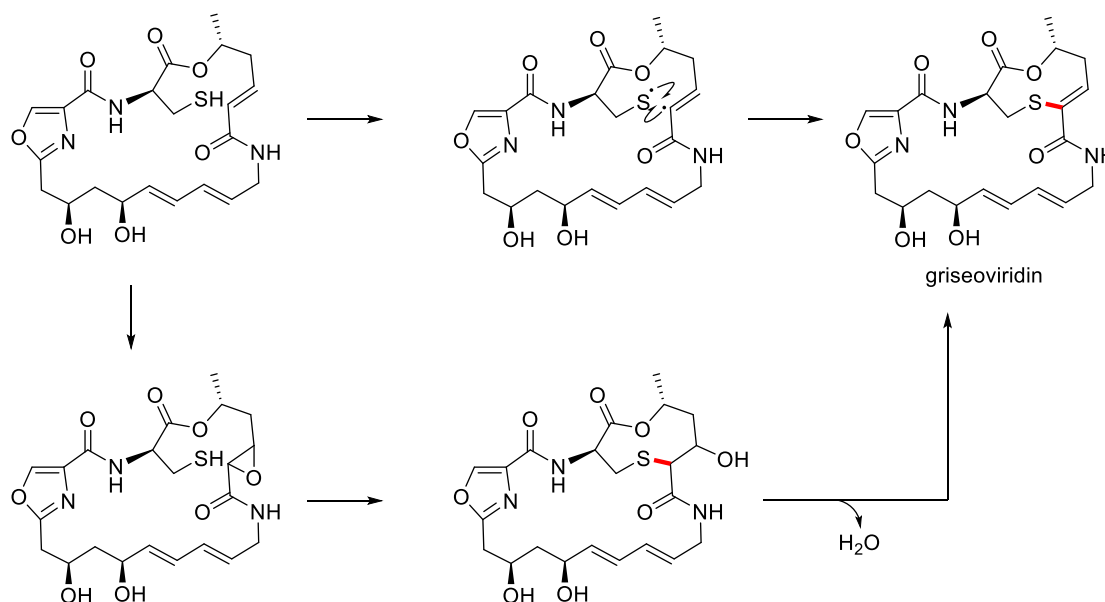


**Figure 13.** Two suggested mechanisms for CYP mediated C-S bond formation in the biosynthesis of griseoviridin.

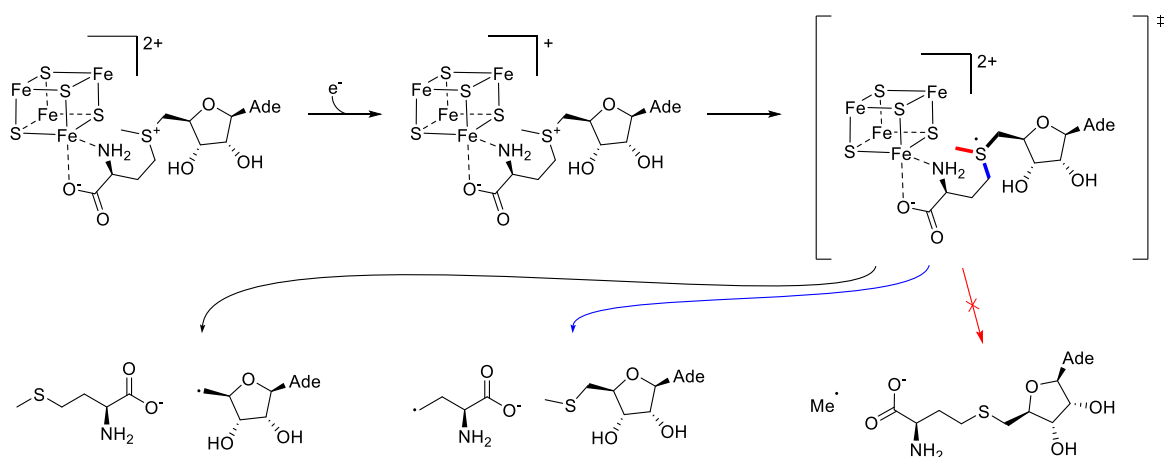


**Figure 14.** Formation of the different radicals from SAM and a  $[4\text{Fe-4S}]^{2+}$  cluster. The formation of a methyl radical is not yet described.

A few years after successful total syntheses reports, the biosynthetic machinery for griseoviridin was discovered and the CYP enzyme, SgvP, was identified to catalyze C-S bond formation.<sup>72,73</sup> Two mechanistic models have been proposed. A radical mechanism, where two electrons and two protons are abstracted from the cyclic substrate. The C-S bond is formed through recombination of the vinyl and thiyl radicals (*top*, **figure 13**). An alternative mechanism suggests the epoxidation of the double bond, with subsequent ring opening and dehydration (*bottom*, **figure 13**).<sup>72</sup> Either way, the reaction is a two-electron oxidation and hence reduces  $\frac{1}{2} \text{O}_2$  to  $\text{H}_2\text{O}$ . So far, no detailed study has been reported to understand the precise catalytic mechanism of SgvP and therefore it remains uncertain if direct C-S bond formation catalyzed by CYP enzymes occurs.

### 1.5.2 Radical SAM enzyme catalyzed C-S bond formation

Nature has found a very impressive solution to overcome the problem of direct C-H activation in the use of radical SAM enzymes. Reactions catalyzed by radical SAM enzymes are generally energetically very costly, and therefore only found for extremely challenging reactions. The first universal step in rSAM catalysis is the one-electron reduction of the  $[4\text{Fe-4S}]^{2+}$  cluster by single electron donors or flavodoxin. Upon activation of the cluster, C-S bond cleavage is initiated by a single electron transfer from the  $[4\text{Fe-4S}]^+$  cluster to the sulfur atom of SAM generating a sulfur-centered radical. Three different pathways from here are possible, whereby each of the C-S bonds can be cleaved homolytic to generate three different reaction intermediates. The classical and most common pathway for C-S bond forming reactions is the homolytic cleavage of the S-C(5') bond, generating a 5'-adenosyl radical and methionine (**figure 14**). These adenosyl radicals abstract a hydrogen atom from the substrate to generate a substrate-centered radical and 5'-deoxyadenosyl. In C-S bond forming reactions, these highly reactive radicals react then with a sulfur atom which is usually part of an auxiliary  $[4\text{Fe-4S}]^{2+}$

---

cluster or in the case of biotin, a [2Fe-2S] cluster. Methionine and 5'-deoxyadenosine are formed as by-products and the FeS-cluster is disintegrated.<sup>11</sup>

The homolytic cleavage of the S-C( $\gamma$ ) bond is rarer and has, to date, not been observed in any C-S bond forming reaction. However, an example for C-C bond formation *via* this pathway has been described for diphtamide synthesis.<sup>76</sup> On the other hand, a pathway which includes the formation of a methyl radical has not been described for any transformation. Pathway independent, one molecule of SAM performs a two-electron oxidation.

An interesting variation of C-S bond formation by rSAM enzymes is the methylthiolation of ribosomal S12 protein catalyzed by RimO (*top*, **figure 15**). In a first step of the reaction, a sulfur atom coordinated to a specific Fe atom of the [Fe-S] cluster is methylated, *via* nucleophilic substitution, to form thiomethane, and consuming one equivalent of SAM. In a subsequent radical step, the C-S bond between thiomethane and the C3 position of aspartyl 89 is formed, consuming a second equivalent of SAM.<sup>10</sup>

Two early reactions employing rSAM chemistry to catalyze sulfur insertion into C-H bonds were found in biotin and lipoic acid biosynthesis (*middle* and *bottom*, **figure 15**).<sup>71,77</sup> BioB and LipA are two well-studied examples of rSAM enzymes and the amount of research invested into the elucidation of their mechanisms displays the complexity of these reactions.<sup>77-79</sup>

Both reactions use the pathway described above for 5'-adenosyl radical generation through the reductive cleavage of SAM and subsequent hydrogen atom abstraction from the substrate. These substrate radicals undergo C-S bond formation with a sulfur atom from an Fe-S cluster. In the case of lipoic acid synthesis, it is an auxiliary [4Fe-4S] cluster, and for biotin, it is a [2Fe-2S] cluster. Methionine and 5'-dA are released from the enzyme and a second molecule of SAM binds to initiate the second cycle of C-S bond formation. During this transformation, the FeS clusters serving as sulfur donors are degraded and must be regenerated prior to the next catalytic cycle. For lipoyl cofactor synthesis, catalyzed by LipA, it could be shown that the reconstitution of the auxiliary [4Fe-4S] cluster is not rate limiting.<sup>79</sup>

These examples reflect the high cost at which such transformations are run. Two equivalents of SAM and (in some cases) a FeS cluster is used up during the reaction. However, the transformation of highly unreactive alkyl C-H bonds directly to C-S bonds occurs. The lack of alternatives might be the main reason for the choice of these enzymes.



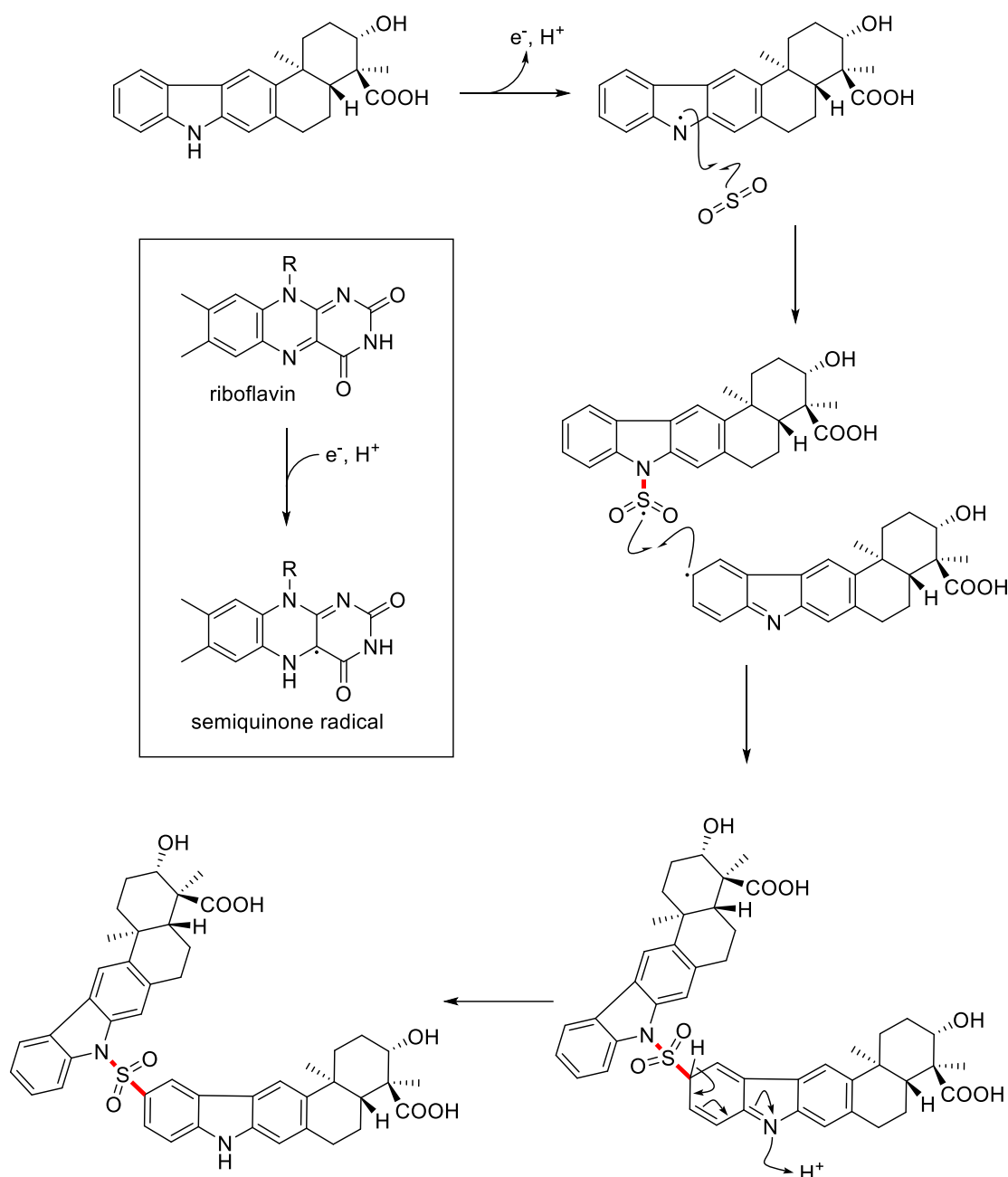


**Figure 16.** Suggested mechanism for the synthesis of sulfadixiamycins. Box: The flavin nucleotide serves as electron acceptor, a semiquinone radical is generated.

### 1.5.3 Flavin-dependent enzyme catalyzed C-S bond formation

Flavin nucleotides are used to catalyze a broad range of redox reactions. Flavin can undergo one-electron or two-electron redox reactions and is therefore the optimal link between cofactors restricted to either two-electron (NADPH) or one-electron transfers ( $\text{Fe}^{\text{II}}/\text{Fe}^{\text{III}}$ ). This feature is used, for example, by the CYP reductase enzymes. Flavins are generally tightly bound by the enzyme and are not released from the active site. Hence, flavin enzymes must undergo the reduction and oxidation half reaction to close a catalytic cycle. Single-electron transfer reactions of flavin-dependent enzymes are known for the activation of dioxygen. A superoxide radical anion and the semiquinone radical  $\text{FADH}^\bullet$  are formed by a single-electron transfer from

FADH<sub>2</sub> to dioxygen. The two radicals recombine to yield flavin hydroperoxide. The single electron oxidation of a substrate by FAD/FMN is not common but has been proposed for the monoamine oxidase (MOA).<sup>80</sup>

Catalysis by the FAD-dependent enzyme, XiaH, was suggested in the biosynthesis of sulfadixiamycins (**figure 16**). It was proposed that an electron and a proton are abstracted from the substrate by FAD to generate a resonance-stabilized substrate radical. This radical then captures a molecule of sulfur dioxide to form either a C-S or a N-S bond. Recombination of the sulfur-centered radical with another substrate radical and subsequent deprotonation leads to the formation of sulfadixiamycins.<sup>81</sup> Sulfonyl-bridged aromatic compounds are very rare and sulfadixiamycins were the first example where the biosynthetic enzymes of these compounds have been discovered. However, no detailed mechanistic studies have been published yet. Hence, as for the CYP-catalyzed direct C-S bond formation, the mechanism is rather speculative than solid.

#### 1.5.4 Non-heme iron-dependent enzyme catalyzed C-S bond formation

One of the important roles of non-heme iron-dependent (NHI) enzymes involves radical C-S bond formation. These are oxygen-dependent enzymes, which use an iron cofactor to activate the unreactive dioxygen. These reactions are four-electron oxidations. Natural products synthesized by NHI-enzymes are penicillin, ovothiol and ergothioneine.

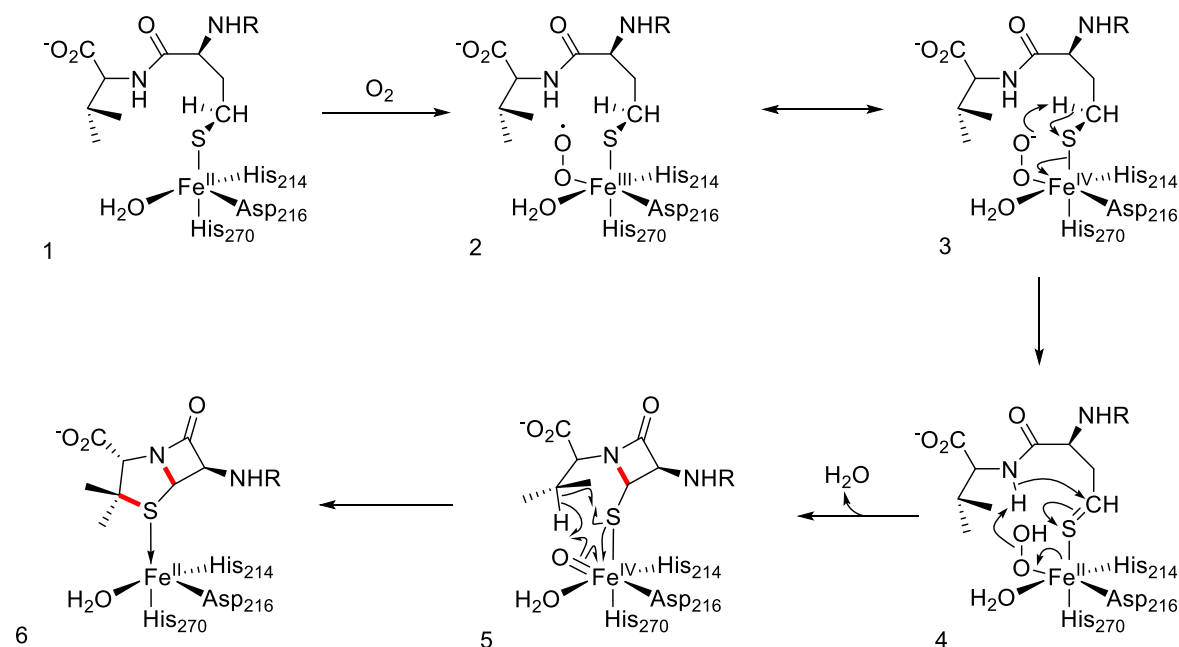


**Figure 17.** Mechanistic model for the formation of the  $\beta$ -lactam core of penicillins catalyzed by the NHI enzyme IPNS.

Isopenicillin-N-synthase (IPNS), which catalyzes the formation of the core  $\beta$ -lactam moiety of penicillin from  $\delta$ -(L- $\alpha$ -Aminoadipoyl)-L-cysteinyl-D-valine (ACV), has been studied extensively and a good mechanistic model has been elucidated (**figure 17**).<sup>82,83</sup> The active site of IPNS is hydrophobic, which protects the reactive intermediates from the solvent and prevent autooxidation of the enzyme. IPNS binds the central iron ion with a two histidine and one aspartate facial triad. The other three binding sites of the octahedral Fe<sup>II</sup> are occupied by two water molecules and a glutamine residue. ACV binding replaces one water and the glutamine residue leading to a penta coordinated Fe<sup>II</sup> with one vacancy for oxygen binding (1, **figure 17**). Oxygen binding leads to the formation of a superoxide radical anion and Fe<sup>III</sup> (2, **figure 17**). This species is in equilibrium with the ferryl-bound peroxide ion (3, **figure 17**). The peroxide can abstract a proton from the thiolate carbon, oxidizing it to a thione with concomitant reduction of the Fe (4, **figure 17**). In a next step, the C-N bond is formed. The peroxide abstracts a proton from the ACV amide and an oxoferryl species (Fe=O<sup>IV</sup>) is formed. Concomitantly, the amide attacks the thione, forming the  $\beta$ -lactam ring (5, **figure 17**). The highly oxidative oxoferryl species can abstract a hydrogen atom from the valine  $\beta$ -methylene group reducing the iron to its ferric state. The valine radical forms a bond with the thiolate forming the thiazolidine ring of the  $\beta$ -lactam core. The iron is concomitantly reduced to its ferrous state (6, **figure 17**).

*The ergothioneine biosynthetic enzyme, EgtB*

The mechanisms of the non-heme iron-dependent enzymes, OvoA from the ovothiol biosynthetic pathway, and EgtB from the ergothioneine biosynthetic pathway, have been investigated in structural, kinetic and computational detail.<sup>84–88</sup> Both enzymes catalyze the formation of a C-S bond between the thiolate of a cysteinyl substrate and the imidazole ring of a histidiny substrate and subsequent sulfoxidation. OvoA catalyzes the formation of the C-S bond at the imidazoyl C5, and EgtB at C2. Several mechanistic models have been proposed and the model based on the kinetic and structural data is depicted in **figure 18**.<sup>87</sup> The close relationship between the two types of enzymes could be demonstrated in a study by Liao *et al.*<sup>89</sup> An intrinsic EgtB activity can be observed in OvoA with only a few mutations OvoA fully adopts the EgtB activity. EgtB's which are most likely evolved from OvoA are denoted as EgtB<sub>(ovo)</sub> and are found in cyanobacteria. Overall, five different types of EgtB's have been distinguished so far.<sup>87</sup> Most studies have been performed on type I and II. The difference between these two types lies in the primary structure, the cysteinyl substrate (type I uses  $\gamma$ -glutamyl cysteine, type II uses cysteine) and active site architecture. Hereafter, the proposed mechanism of type II EgtB is discussed.

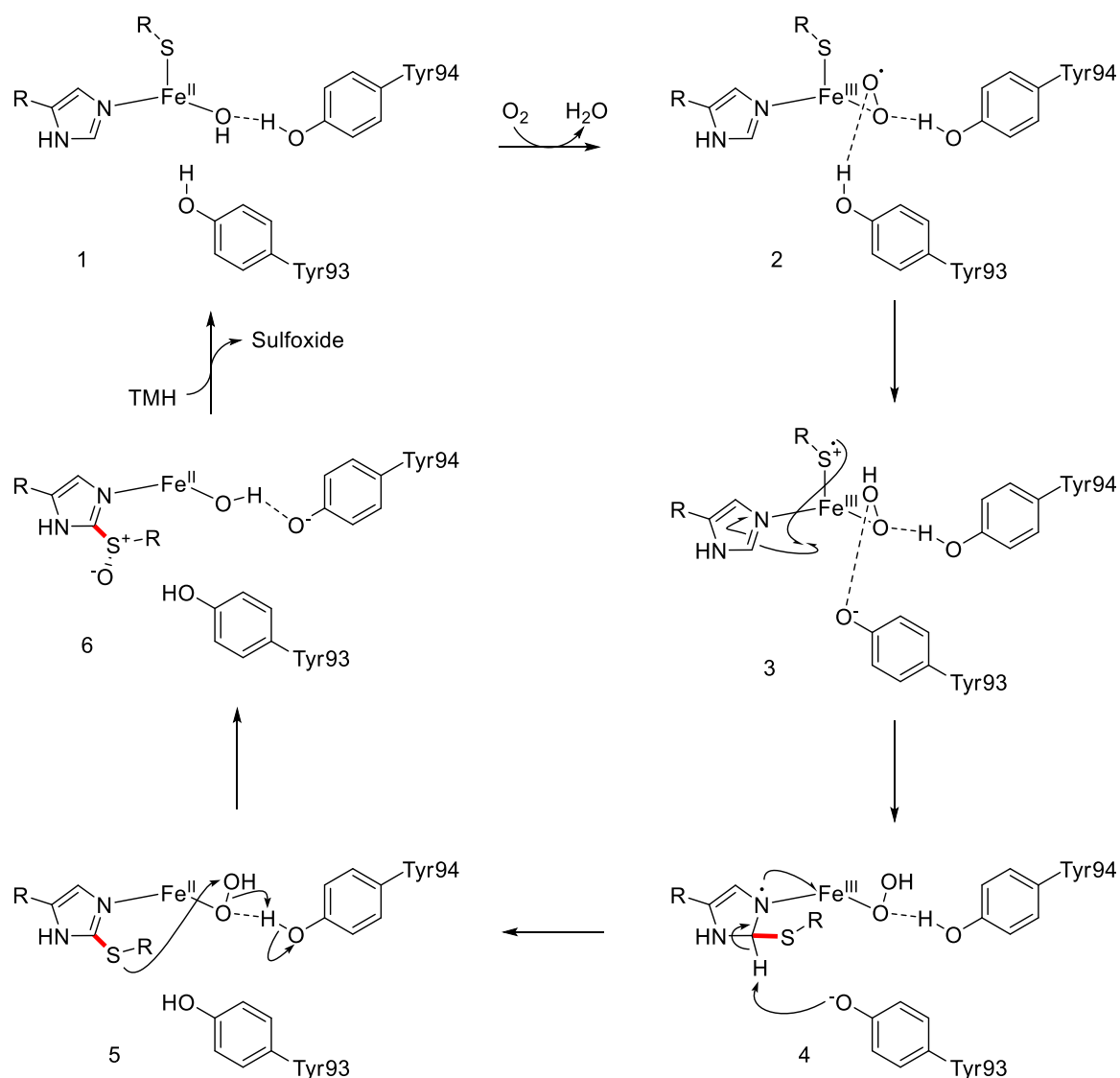


**Figure 18.** Mechanistic model for the C-S bond formation and sulfoxidation catalyzed by NHI enzyme EgtB (type II).

EgtB binds Fe(II) with a three-histidine facial triad in an octahedral geometry, leaving three coordination sites for the substrates. First *N*- $\alpha$ -trimethyl histidine (TMH) binds to the active site, coordinating with N1 to the iron center. Then, the cysteinyl substrate binds to the EgtB:TMH complex, coordinating with the thiolate to the iron ion (**1**, **figure 18**). Once the EgtB:TMH:Cys complex is formed, dioxygen replaces the bound water molecule at the iron center and forming an Fe(III)-superoxide species (**2**, **figure 18**). Tyr93 and Tyr94 both play catalytic important roles. Tyr94 is believed to hydrogen bond to the proximal oxygen atom of the iron bound superoxide and thereby make it more oxidative. Protonation of the distal superoxide oxygen by Tyr93 and coupled electron transfer from the thiolate generate a thiyl radical and hydroperoxide bound to Fe(III) (**3**, **figure 18**). The thiyl radical can form a C-S bond with C2 of the TMH imidazole ring thereby generating a N1-centered radical (**4**, **figure 18**). Proton abstraction and electron transfer from the imidazole ring to the Fe(III) results in the formation of the thioether intermediate (**5**, **figure 18**). The thioether then attacks the



---

distal oxygen of peroxide forming the sulfoxide and water. The iron is concomitantly reduced back to its ferrous state and the enzyme can go through a next catalytic cycle (**6, figure 18**). EgtB's also face the challenge that the cysteinyl substrate can be oxidized to the dioxide instead of undergoing C-S bond formation. Studies of different types of EgtB showed that protonation of the superoxide species is essential to channel the reaction towards C-S bond formation.<sup>85,87</sup> In the absence of the proton donor, the dioxygenation reaction is accelerated and the sulfoxidation almost ceases.

The examples of IPNS and EgtB show how nature can use the oxidative power of molecular oxygen to transform C-H bonds to C-S bonds. The activation of dioxygen generates a highly reactive species, which must be carefully controlled by the enzymes to prevent any undesired side reactions. How challenging this is can be seen in the case of EgtB. In chapter 5 of this thesis, the specific substrate-substrate interaction of type I and type II EgtBs and the role of precise substrate positioning are discussed in more detail.

---

## 1.6 Conclusion

In this overview, chemical and enzymatic methods to transform C-H bonds to C-S have been briefly described. All the reactions are considered as oxidative processes regarding the transformed C-H bond. Hence, many of the transformations work only in presence of an additional oxidant, such as dioxygen. However, some of the reactions have been developed in a way that the sulfur reactant itself serves as the oxidant and therefore the addition of an additional oxidant becomes obsolete. Interestingly, sulfur electrophiles are used for most of the ionic transformations.

Similar strategies to those found in chemical synthesis are also used in enzymatic catalysis. C-S bonds to carbons bearing acidic protons or electrophilic carbons are often formed in an ionic reaction. Non-activated C-H bonds are often activated by transition metals, other redox-active cofactors, such as FAD or NADH, or adenosyl radicals.<sup>70</sup> The high cost at which some of these reactions are run reflects the high difficulty of these transformations. Interestingly, even though the number of enzymes which can catalyze direct thio-functionalization of C-H bonds is quite limited, some transformations have been invented in different ways (see ergothioneine biosynthesis). The precise mechanisms are not understood for many of the above-mentioned transformations and it will be an important task for future research to gain a deeper understanding of these transformations.

As demonstrated above, the number of chemical and enzymatic methods to directly functionalize C-H bonds with sulfur compounds is quite limited. It appears that the introduction of sulfur atoms *via* chemically simpler reactions, such as substitutions or additions are favored.

There are common strategies applied by both chemists and nature, such as the radical pathways for C-S bond formation, and there are some methods restricted to either enzymatic or chemical transformations. Controlling the reactivity of persulfidic sulfur, for example, is difficult for chemists since they tend to react with each other, forming undefined mixtures of polysulfides and disulfides or they degrade by hydrolyse. Enzymes on the other hand can shield it off from water and other reactive sulfur species and specifically direct the persulfidic sulfur toward the substrate. On the other hand, transition metal-catalyzed C-S bond formation *via* C-H activation cannot be used by enzymes. The only transition metal involved in enzyme-catalyzed C-S bond forming reactions is iron. These enzymes generate reactive oxygen species, such as superoxide anions to abstract electrons and protons from substrates.

---

## 2 Aim of the Thesis

As this short overview on oxidative C-S bond forming reactions has shown, the field of direct C-H to C-S bond transformation is still growing. Many reactions are known, yet many are still to be discovered. Considering the importance of sulfur-containing molecules to nature and humankind, it is of high importance to find new ways to efficiently construct C-S bonds. In times of environmental concerns and an increasing interest in green alternatives to chemical transformations, biocatalysis becomes more and more important. Therefore, to discover new enzymes catalyzing unprecedented reactions and understand their catalytic mechanisms is still an important task.

In this thesis, a new class of enzymes is described which catalyzes a unprecedented oxidative C-S bond forming reaction between a cysteine persulfide and the non-activated imidazolyl C2 of histidine. It belongs to the class of oxidative ionic C-S bond forming reactions.

Furthermore, we aimed to deepen our insight into the binding mode of the substrates to EgtB.

---

---

---

### 3 Anaerobic Origin of Ergothioneine

Ergothioneine is a 2-thioimidazole and *N*- $\alpha$ -trimethylated derivative of histidine which is biosynthesized by various microorganisms.<sup>90</sup> However, it can also be found in plants and animals which take the compound up either from the soil or dietary sources.<sup>91</sup> The organic cation transporter OCTN1 is responsible for the uptake and distribution of dietary ergothioneine into animal tissues where it can accumulate to high concentrations.<sup>92</sup> Since the discovery of ergothioneine more than a century ago, many studies have been undertaken to understand its physiological role and the molecular mechanism of function in microorganisms and in humans.<sup>90,91,93,94</sup>

*In vitro* studies have revealed some interesting characteristics of ergothioneine and it has been suggested to play an antioxidant role *in vivo*.<sup>95</sup> The standard redox potential for the thiol-disulfide pair of ergothioneine is more electropositive (-60 mV) compared to the standard redox potential of other common thiols (between -200 mV and -320 mV).<sup>96</sup> The higher redox potential, and the fact that ergothioneine occurs mainly in its thione and not the thiol form, prevents ergothioneine from autooxidation.<sup>90</sup> Furthermore, it has been shown that ergothioneine readily scavenges hydroxyl radicals, hypochlorite, peroxynitrite and is superior to other thiols in deactivation of singlet oxygen.<sup>97</sup> Due to these antioxidant properties, ergothioneine was suspected to act as an antioxidant *in vivo*.

Studies on the role of ergothioneine in microorganisms have recently been reviewed by Cumming *et al.*<sup>90</sup> Many of these studies indicate that ergothioneine is somehow involved in protection against oxidative stress. Other functions that could be attributed to ergothioneine is protection against metal stress and alkylating agents, and it has been shown to increase the virulence of *Mycobacterium tuberculosis* in mice. Similar roles were attributed to ergothioneine in fungi. However, the molecular mechanism of action of ergothioneine has not been understood yet.

In 2010, Seebeck described the ergothioneine biosynthetic gene cluster (EgtA-E) and *in vitro* reconstitution of the ergothioneine biosynthesis was achieved.<sup>98</sup> Ergothioneine biosynthesis starts with the *N*- $\alpha$ -trimethylation of histidine by the SAM-dependent methyltransferase EgtD to yield *N*- $\alpha$ -trimethylhistidine (TMH). This is followed by oxidative C-S bond formation between a cysteinyl substrate, either cysteine or  $\gamma$ -GC, and the C2 of the histidyl imidazole ring by the non-heme iron dependent sulfoxide synthase, EgtB. Subsequent C-S bond cleavage by the PLP-dependent lyase, EgtE, removes the cysteinyl amino acid moiety thereby yielding ergothioneine. If  $\gamma$ -GC is the sulfur donor, the glutamyl moiety of  $\gamma$ -GC must be cleaved by the *N*-terminal nucleophile (NTN) amidohydrolase EgtC prior to the C-S bond cleavage.

---

Genome analysis suggested that EgtD and EgtB are gene signatures for ergothioneine biosynthesis.<sup>90</sup> The functions of the other ergothioneine biosynthetic enzymes can be covered by non-ergothioneine specific enzymes.

In a study performed during this thesis, we were able to show that ergothioneine can be biosynthesized in an oxygen-independent way by anaerobic organisms. This work was published in the following paper:

- Burn, R.; Misson, L.; Meury, M.; Seebeck, F. P. *Angew. Chemie Int. Ed.* **2017**, 56 (41), 12508.

Genome mining revealed that EgtD sometimes occurs in the absence of any other ergothioneine biosynthetic genes, and also in the absence of EgtB. Most of these EgtDs neighbor a gene which encodes for a rhodanese-like sulfurtransferase. This gene cluster was found mainly in anaerobic organisms, such as the green sulfur bacterium *Chlorobium limicola*. Methyl transferase activity of recombinant Clim\_1148, the EgtD homolog of *C. limicola*, was analyzed and shown to be specific for histidine with TMH as the main product.

Clim\_1149, a putative rhodanese-like sulfurtransferase, was also recombinantly produced in *E. coli* and tested for activity toward ergothioneine formation from TMH and a sulfur donor. Initial trials with sodium thiosulfate as sulfur donor resulted in very poor activity, but clearly showed ergothioneine formation. Therefore, the two enzymes were called ergothioneine anaerobic biosynthetic enzymes A and B (EanA and EanB).

We could show that EanB can be isolated in a persulfidated form from *E. coli*. This gives the opportunity to measure single turnover kinetics. The measured turnover rate for the single turnover reaction was 0.5 s<sup>-1</sup> and hence in a range with physiological relevance.

The fact that EanB can be isolated in its persulfide form means that EanB must be persulfidated by an enzyme in *E. coli*. The most prominent enzyme responsible for sulfur activation in *E. coli* is the PLP-dependent cysteine desulfurase, IscS. Indeed, the use of IscS and cysteine as a sulfur delivery system allowed us to develop a steady state system with a  $k_{cat}$  which matched the  $k_{turnover}$  obtained from the single turnover reaction. The steady state reaction conditions were used to determine *Michaelis-Menten* parameters of EanB.

To demonstrate that the reaction described *in vitro* is also relevant *in vivo*, *Salinibacter ruber* was cultivated and the ergothioneine concentration in the pellet was determined. *S. ruber* is an aerobic bacterium which contains the genes for EanA and EanB, but not for oxygen-dependent ergothioneine biosynthesis.

In this study, we could demonstrate that ergothioneine can be synthesized in an oxygen-independent way. The fact that ergothioneine can be produced by anaerobic organisms raises

---

the question of the role of ergothioneine under anaerobic conditions – i.e. whether the origin of ergothioneine lies back in times before antioxidants were required and that it was repurposed after the great oxygenation event. The mechanistic peculiarities of EanB are discussed in **Chapter 4**.

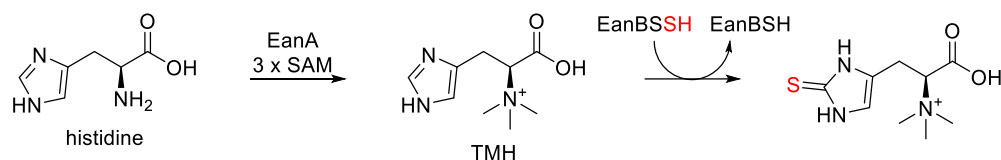


**Figure 19.** Anaerobic biosynthesis of ergothioneine.

**Author Contribution:**

- R. B. developed protocols for and performed the kinetic characterization of EanB and the isolation of ergothioneine from *S. ruber*.

## Anaerobic Origin of Ergothioneine

Reto Burn, Laëtitia Misson, Marcel Meury, and Florian P. Seebeck\*

**Abstract:** Ergothioneine is a sulfur metabolite that occurs in microorganisms, fungi, plants, and animals. The physiological function of ergothioneine is not clear. In recent years broad scientific consensus has formed around the idea that cellular ergothioneine primarily protects against reactive oxygen species. Herein we provide evidence that this focus on oxygen chemistry may be too narrow. We describe two enzymes from the strictly anaerobic green sulfur bacterium *Chlorobium limicola* that mediate oxygen-independent biosynthesis of ergothioneine. This anoxic origin suggests that ergothioneine is also important for oxygen-independent life. Furthermore, one of the discovered ergothioneine biosynthetic enzymes provides the first example of a rhodanese-like enzyme that transfers sulfur to non-activated carbon.

Ergothioneine (**1**, Figure 1) is a sulfur containing metabolite that occurs in many unicellular and multicellular organisms.<sup>[1]</sup> Bacteria and fungi produce ergothioneine.<sup>[2]</sup> Plants and animals depend on nutritional sources thereof.<sup>[3]</sup> Several lines of evidence suggest that active accumulation of ergothioneine in humans and other animals may be essential to mitigate inflammatory, cardiovascular, or infective disease, depression, dementia and other epiphenomena of aging.<sup>[1,3b,4]</sup> For pathogenic microorganisms ergothioneine may be essential to survive in host tissue.<sup>[5]</sup> Despite this medicinal relevance, the molecular functions of ergothioneine are still unclear. Model organisms that were made unable to either synthesize or to acquire ergothioneine are usually characterized by increased vulnerability to oxidative stress.<sup>[5,6]</sup> These findings, compounded with the unusual redox chemistry of ergothioneine,<sup>[7]</sup> have formed a broad consensus that this compound functions primarily as a protection against reactive oxygen species.<sup>[1,7c,8]</sup>

Biosynthesis of ergothioneine also includes remarkable oxidation chemistry. Numerous bacteria and most fungi make ergothioneine from *N*- $\alpha$  trimethylated histidine using either cysteine or  $\gamma$ -glutamyl cysteine as sulfur source (Figure 1). The corresponding enzymes from *M. smegmatis* and *Neurospora crassa* have been identified and characterized (Figure 1).<sup>[2c,9]</sup> The key steps in ergothioneine production are *N*- $\alpha$  trimethylation of histidine by the S-adenosylmethionine (SAM) dependent enzyme EgtD (Figure 1), and sulfurization of the imidazole ring of *N*- $\alpha$  trimethylhistidine (**2**, TMH). This second reaction is achieved by an iron-dependent

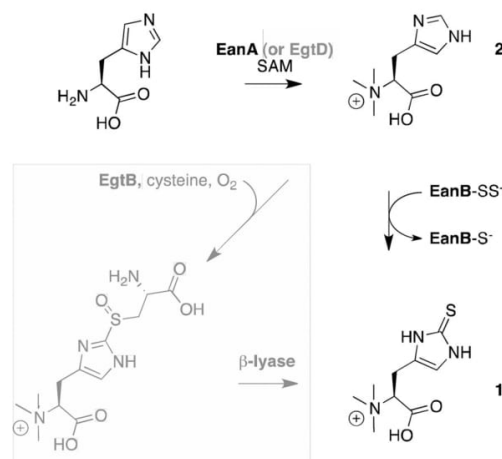


**Figure 1.** Oxygen-dependent (gray) and oxygen-independent (black) biosynthesis of ergothioneine (**1**). Mycobacterial EgtBs utilize  $\gamma$ -glutamyl cysteine as sulfur donor,<sup>[2c]</sup> fungal EgtBs directly utilize cysteine.<sup>[2b,9b,10]</sup>

sulfoxide synthase (EgtB).<sup>[9f]</sup> This enzyme catalyzes a four-electron oxidation reaction that forms a carbon–sulfur bond (C–S) to TMH and subsequently sulfoxidizes the resulting thioether. Although the catalytic mechanism of this enzyme is still controversial,<sup>[9f,11]</sup> all proposed models agree that molecular oxygen is the terminal electron acceptor in this reaction.

Herein we describe an entirely novel ergothioneine biosynthetic pathway. We demonstrate that the green-sulfur bacterium *Chlorobium limicola* (DSM 245) encodes a sulfur transferase that converts TMH into ergothioneine using oxygen-independent chemistry. This enzyme is the first known example of a rhodanese-like enzyme that transfers sulfur to non-activated carbon.<sup>[12]</sup> This discovery also suggests that ergothioneine may play a role in anoxic biochemistry and raises the possibility that the emergence of ergothioneine predates the rise of atmospheric oxygen 2.4 billion years ago.<sup>[13]</sup>

*C. limicola* grows in illuminated anoxic waters and conducts anaerobic photosynthesis using sulfides as electron donor for carbon dioxide fixation.<sup>[14]</sup> The genome of this strictly anaerobic organism encodes a protein (locus tag Clim\_1148) with 33% sequence identity to EgtD from *M. smegmatis*.<sup>[9d]</sup> Alignment of the sequences from Clim\_1148 and EgtD shows that the substrate recognition sites in the two enzymes are identical (Figure S1 in the Supporting Information). Consistently, recombinant Clim\_1148 showed histidine-specific methyltransferase activity and produced TMH as the main product. Other proteinogenic amino acids did not induce measurable consumption of

[\*] R. Burn, Dr. L. Misson, Dr. M. Meury, Prof. F. P. Seebeck  
Department for Chemistry, University of Basel  
St. Johannis-Ring 19, 4056 Basel (Switzerland)  
E-mail: florian.seebeck@unibas.ch

Supporting information and the ORCID identification number(s) for the author(s) of this article can be found under:  
<https://doi.org/10.1002/anie.201705932>.



**Table 1:** Kinetic parameters of ergothioneine biosynthetic enzymes.<sup>[a]</sup>

Enzyme	$k_{\text{cat}}$ [min <sup>-1</sup> ]	$K_{\text{M,HIS}}$ [μM]	$K_{\text{M,SAM}}$ [μM]	$K_{\text{M,TMH}}$ [μM]
EanA	3.8	110	270	n/a
EgtD	35	110	72	n/a
EanB	0.5	n/a	n/a	28
EgtB	72	n/a	n/a	42

[a] Data represent averages from multiple measurements. The standard error is less than 20% of the average value. Reaction conditions see Supporting Information.  $K_{\text{M,HIS}}$  and  $K_{\text{M,SAM}}$  were determined in the presence of 1 mM SAM and 0.5 mM His, respectively. Parameters for EgtD and EgtB from *M. smegmatis* are from references [9d] and [9f].

SAM. Clim\_1148 is characterized by a  $k_{\text{cat}}$  of 3.8 min<sup>-1</sup> and apparent  $K_{\text{M,SAM}}$  of 270 μM and  $K_{\text{M,HIS}}$  of 110 μM (Table 1, Figure S3). Given the similar substrate specificity as EgtD, we concluded that Clim\_1148 is a bona fide histidine *N*-α-methyltransferase (EC 2.1.1.44).

Despite this assignment it is clear that Clim\_1148 must contribute to a different pathway than EgtD in *M. smegmatis*. Most bacterial or fungal genomes that encode an EgtD homolog also encode an EgtB homologue, often at the same genomic loci or even as a EgtD/B fusion.<sup>[2c]</sup> The genome of *C. limicola* does not encode an EgtB homologue. Instead Clim\_1148 is co-encoded with a putative rhodanese-like sulfur transferase (Clim\_1149). Rhodanese, the namesake enzyme for this large enzyme family, catalyzes the transfer of sulfur from thiosulfate to cyanide in a two-step mechanism (Figure 2).<sup>[12a,c]</sup> In a first step, an active site cysteine accepts a sulfur atom from thiosulfate. This transfer forms the persulfide form of the enzyme. In the second step, cyanide attacks the persulfide and is oxidized to rhodanide. By

analogy, we surmised that Clim\_1149 may catalyze sulfur transfer to TMH. As the following data shows, this speculation turned out correct. Therefore we termed the methyltransferase and the sulfurtransferase from *Chlorobium limicola* ergothioneine anaerobic biosynthetic enzymes A and B (EanA and EanB; Figure 1). We found homologous enzyme pairs in at least 20 genomes from predominantly anaerobic bacteria and archaea (Table S1).

To examine the sulfurtransferase activity, we incubated 50 μM of recombinant EanB in the presence of 50 mM thiosulfate, and 1 mM TMH at 25 °C. Under these conditions EanB did indeed produce a small amount of ergothioneine. To facilitate detection and identification of this reaction product we treated the terminated reactions with 4-bromo-methyl-7-methoxycoumarin. The coumarin adduct of ergothioneine can be conveniently analyzed by RP-HPLC and detected by UV-spectroscopy. Using this assay we identified the coumarin-adduct of ergothioneine by ESI-HRMS, and by HPLC comparison with an authentic sample (Figure S4). Monitoring the reaction for hours showed steady but very slow turnover ( $k_{\text{product}} < 10^{-3}$  min<sup>-1</sup>; Figure S4). The reaction is not saturated even at a thiosulfate concentration of 200 mM (Figure S5), indicating that this may not be the ideal sulfur source. In contrast, TMH clearly saturates the enzyme at concentrations above 0.1 mM and inhibits turnover at higher concentrations (Figure S5).

To measure the rate of sulfur transfer from EanB to TMH directly, we exploited the fact that the recombinant protein can be isolated in the persulfide form, if reducing agents such as dithiothreitol (DTT) are avoided during purification. Incubation of this form of EanB with 1 mM TMH resulted in formation of  $0.9 \pm 0.05$  equivalents of ergothioneine (Fig-

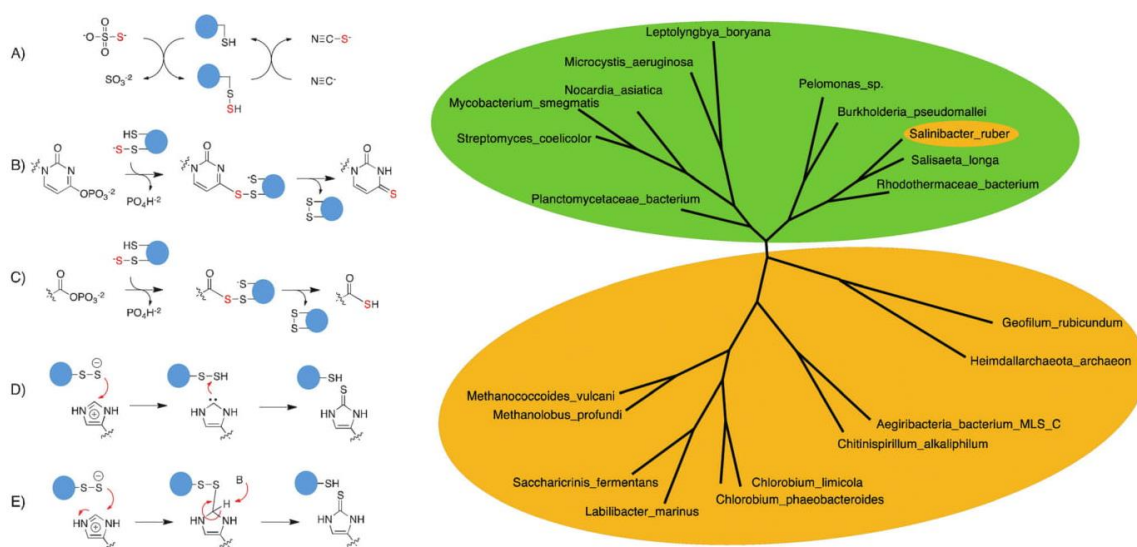


**Figure 2.** Left: Mechanisms of carbon-sulfur bond forming reactions catalyzed by rhodanese-like enzymes (blue). A) Rhodanese-catalyzed sulfuration of cyanide; B) Sulfur transfer from the sulfur-transferase Thil to phosphorylated uridine.<sup>[18]</sup> C) Sulfur transfer from the sulfur-transferase MOCS3 to the phosphorylated C-terminus of the sulfur carrier protein URM1.<sup>[12d]</sup> D) and E) possible mechanisms of EanB catalysis. Right: phylogenetic tree containing histidine-specific methyltransferases that participate in oxygen-dependent (green) or oxygen-independent (yellow) ergothioneine biosynthesis.

ure S6). Fitting the corresponding product versus time plot to a unimolecular rate law revealed a rate for C–S bond formation ( $k_{\text{C-S}}$ ) of  $0.5 \pm 0.1 \text{ min}^{-1}$ . Evidently, EanB can directly and efficiently convert TMH into ergothioneine.

Because recombinant EanB is nearly quantitatively sulfurized during recombinant production, we surmised that the cysteine desulfurase IscS from *E. coli* may serve as sulfur donor for EanB. Charging sulfurtransferases is indeed one of the main functions of IscS in *E. coli*.<sup>[12a,b,d]</sup> Addition of 30  $\mu\text{M}$  IscS to a reaction containing 4  $\mu\text{M}$  EanB, 1 mM TMH and 1 mM Cys as sulfur source resulted in steady production of ergothioneine at a rate ( $k_{\text{turnover}}$ ) of  $0.5 \pm 0.05 \text{ min}^{-1}$ . Given that  $k_{\text{turnover}}$  matches  $k_{\text{C-S}}$  indicates that formation of the persulfide form of EanB by IscS is no more rate limiting.

With this hybrid sulfurtransfer cascade we were able to determine the Michaelis–Menten parameters for EanB ( $k_{\text{cat}}$ ,  $K_{\text{M, TMH}}$ , Table 1, Figure S7). This analysis showed that  $k_{\text{cat}}$  for EanB catalyzed C–S bond formation is ten-fold slower than  $k_{\text{cat}}$  for EgtB catalyzed C–S bond formation (Table 1).<sup>[9]</sup> This difference may be due to incomplete in vitro reconstitution of EanB. Alternatively, this difference may also reflect that anaerobic oxidation of TMH is coupled to reduction of a persulfide, while aerobic C–S bond formation is driven by reduction of molecular oxygen. The aerobic C–S bond formation is a far more exothermic reaction. Hence, oxygen-independent ergothioneine biosynthesis may be simply less efficient than its oxygen-dependent counterpart.

To test whether EanA and EanB encoding species do produce ergothioneine, we cultivated the extremely halophilic and slow growing bacterium *Salinibacter ruber* (DSM 13855).<sup>[15]</sup> This species also encodes close EanA/B homologues (Table S1) but no discernable EgtB homolog. In contrast to *C. limicola* and most other EanA/B encoding species *S. ruber* grows aerobically and is relatively simple to cultivate. Using the same ESI-HRMS and HPLC methodology we identified the coumarin-adduct of ergothioneine in cell lysates from *S. ruber* (Figure S8). Calibration with authentic samples showed that lab-cultivated cells contain ergothioneine at a concentration of  $1.5 \pm 0.9 \text{ mM}$ . Similar levels have been found in cells that produce ergothioneine by the aerobic pathway.<sup>[6c,d]</sup> Evidently, the EanA/B couple is competent to facilitate significant accumulation of intracellular ergothioneine.

The discovery that EanA/B from *C. limicola* mediate oxygen-independent ergothioneine production has two major implications. First, EanB appears to employ a novel catalytic strategy from enzymatic C–S bond formation.<sup>[12a,b,16]</sup> In contrast to any other rhodanese-like enzyme with known function, EanB catalyzes sulfurtransfer to a carbon center without prior substrate activation. Rhodanese transfers sulfur to hydrogencyanide which is easily deprotonated ( $\text{p}K_{\text{a,HCN}} = 9.2$ ). The imidazole C<sub>2</sub>-H position is a much weaker carbon acid ( $\text{p}K_{\text{a}}: 24$ ).<sup>[17]</sup> and its conjugated base is a rather unstable imidazole-2-yl carbene (Figure 2D).<sup>[17]</sup> It is therefore questionable whether EanB could form a carbon nucleophile to induce C–S bond formation.

Other C–S bond forming rhodanese-like enzymes are involved in thiolation of nucleic acids<sup>[12d,f]</sup> and in the biosynthesis of thiamine,<sup>[12g]</sup> the molybdenum cofactor,<sup>[12d]</sup>

or thiosugars<sup>[19]</sup> (Figure 2). The persulfide sulfur of these enzymes attack highly electrophilic carbon on phosphorylated nucleobases, or the phosphorylated C-terminus of sulfur carrier proteins. These attacks lead to covalent enzyme:substrate complexes that decay because a second active site cysteine cleaves the intermolecular disulfide bond and releases the thiolated product (Figure 2B,C). Overall, these sulfur transfers are redox-neutral substitutions. EanB catalysis must follow a different mechanism because sulfurization of TMH is an oxidation reaction. In addition, an imidazole ring is far less electrophilic than phosphorylated carboxylates, isoureas, or amides. Also, EanB and its close homologs do not seem to contain a conserved second cysteine in the active site. A possible mechanism following an addition/elimination Scheme would start with the persulfide anion attacking the imidazolium ring of TMH, followed by deprotonation of the intermediate (Figure 2E). In-depth studies are clearly necessary to elucidate this catalytic mechanism, and to inquire whether this reaction type could also explain the assembly of other sulfur metabolites of unknown origin.<sup>[16]</sup>

The fact that ergothioneine biosynthesis can occur in the complete absence of oxygen also sheds light onto its evolutionary emergence. Both aerobic and anaerobic pathways share the same type of methyltransferase (EgtD/EanA) indicating that one pathway must have emerged as a modification of the other. A phylogenetic tree of EgtD and EanA homologs illustrates that the methyltransferases participating in either anaerobic or in aerobic ergothioneine biosynthesis clearly sort into two deep-rooting branches. Members of the EanA and the EgtD-like methyltransferases share no more than 40 % sequence similarity. *S. ruber* provides an exception to this rule. The methyltransferase of this organism belongs to the EgtD branch, yet cooperates in anaerobic ergothioneine production. Nevertheless, the overall pattern of this phylogenetic tree indicates that separation of the two groups cannot have been a recent event. On the other hand, this tree does not reveal whether the last common ancestor evolved in the presence or absence of oxygen.

Planetary life started as an anaerobic process about 3.4 billion years ago and evolved for one billion years before atmospheric oxygen became abundant during the great oxygenation event.<sup>[13]</sup> During this time ancient organisms presumably invented a full complement of defense mechanisms against physical and chemical stress associated with anaerobic life. Ergothioneine may have been one of these inventions, and may still be used in similar ways by extant anaerobes such as *C. limicola*. This view argues for an anaerobic origin of ergothioneine. With the rise of atmospheric oxygen ergothioneine may have been repurposed as a scavenger of reactive oxygen species due to its fortuitous redox capabilities.<sup>[13]</sup> In a way, ergothioneine may be an accidental antioxidant with equally important anoxic functions.

In conclusion, we have discovered an entirely novel biosynthetic pathway for ergothioneine production. The sulfurtransferase EanB from *C. limicola* is the first known rhodanese-like enzyme that transfers sulfur to unactivated carbon. This finding should facilitate the functional assignment of other members of the large class of rhodanese-like



sulfurtransferases. Phylogenetic comparison of the histidine-specific methyltransferases from aerobic and anaerobic organisms raises the possibility that the first ergothioneine producers were ancient anaerobic bacteria. Furthermore, production of ergothioneine in extant anaerobes confirms the idea that this metabolite serves important cellular function under anoxic conditions. So far, biomedical investigations on the physiological function of ergothioneine in humans and human pathogens has focused on oxygen-dependent processes. The anoxic biochemistry of ergothioneine has been largely neglected. This report opens a new perspective onto ergothioneine-mediated cellular processes and the possibilities to develop ergothioneine-related therapeutic approaches.

## Acknowledgements

We thank Alice Harnacke for ESI-HRMS measurements, the “Professur für Molekulare Bionik”, the Commission for Technology an Innovation, and the European Research Council (ErgOX) for financial support.

## Conflict of interest

The authors declare no conflict of interest.

**Keywords:** antioxidants · carbon–sulfur bonds · enzyme catalysis · ergothioneine · sulfur transferases

**How to cite:** *Angew. Chem. Int. Ed.* **2017**, *56*, 12508–12511  
*Angew. Chem.* **2017**, *129*, 12682–12685

- [1] B. Halliwell, I. K. Cheah, C. L. Drum, *Biochem. Biophys. Res. Commun.* **2016**, *470*, 245–250.
- [2] a) D. S. Genghof, E. Inamine, V. Kovalenko, D. B. Melville, *J. Biol. Chem.* **1956**, *223*, 9–17; b) A. Askari, D. B. Melville, *J. Biol. Chem.* **1962**, *237*, 1615–1618; c) F. P. Seebeck, *J. Am. Chem. Soc.* **2010**, *132*, 6632–6633.
- [3] a) D. Gründemann, S. Harlfinger, S. Golz, A. Geerts, A. Lazar, R. Berkels, N. Jung, A. Rubbert, E. Schoemig, *Proc. Natl. Acad. Sci. USA* **2005**, *102*, 5256–5261; b) J. Ey, E. Schomig, D. Taubert, *J. Agric. Food Chem.* **2007**, *55*, 6466–6474.
- [4] a) I. K. Cheah, R. Tang, P. Ye, T. S. Z. Yew, K. H. C. Lim, B. Halliwell, *Free Radical Res.* **2016**, *50*, 14–25; b) T. Y. Song, H. C. Lin, C. L. Chen, J. H. Wu, J. W. Liao, M. L. Hu, *Free Radical Res.* **2014**, *48*, 1049–1060; c) Y. Kato, Y. Kubo, D. Iwata, S. Kato, T. Sudo, T. Sugiura, T. Kagaya, T. Wakayama, A. Hirayama, M. Sugimoto, K. Sugihara, S. Kaneko, T. Soga, M. Asano, M. Tomita, T. Matsui, M. Wada, A. Tsuji, *Pharm. Res.* **2010**, *27*, 832–840; d) I. K. Cheah, L. Feng, R. M. Tang, K. H. Lim, B. Halliwell, *Biochem. Biophys. Res. Commun.* **2016**, *478*, 162–167; e) R. W. Li, C. Yang, A. S. Sit, Y. W. Kwan, S. M. Lee, M. P. Hoi, S. W. Chan, M. Hausman, P. M. Vanhoutte, G. P. Leung, *J. Pharmacol. Exp. Ther.* **2014**, *350*, 691–700.
- [5] H. S. Saini, B. M. Cumming, L. Guidry, D. A. Lamprecht, J. H. Adamson, V. P. Reddy, K. C. Chinta, J. H. Mazorodze, J. N. Glasgow, M. Richard-Greenblatt, A. Gomez-Velasco, H. Bach, Y. Av-Gay, H. Eoh, K. Rhee, A. J. C. Steyn, *Cell Rep.* **2016**, *14*, 572–585.
- [6] a) B. D. Paul, S. H. Snyder, *Cell Death Differ.* **2009**, *47*, S149–S149; b) C. Pfeiffer, M. Bach, T. Bauer, J. C. da Ponte, E. Schöming, D. Gründemann, *Free Radical Biol. Med.* **2015**, *83*, 178–185; c) C. Sao Emani, M. J. Williams, I. J. Wiid, N. F. Hiten, A. J. Viljoen, R.-D. D. Pietersen, P. D. van Helden, B. Baker, *Antimicrob. Agents Chemother.* **2013**, *57*, 3202–3207; d) M. H. Bello, V. Barrera-Perez, D. Morin, L. Epstein, *Fungal Genet. Biol.* **2012**, *49*, 160–172; e) S. Nakajima, Y. Satoh, K. Yanashima, T. Matsui, T. Dai, *J. Biosci. Bioeng.* **2015**, *120*, 294–298; f) K. J. Sheridan, B. E. Lechner, G. O. Keefe, M. A. Keller, E. R. Werner, H. Lindner, G. W. Jones, H. Haas, S. Doyle, *Sci. Rep.* **2016**, *6*, 35306.
- [7] a) K. D. Asmus, R. V. Bensasson, J. L. Bernier, R. Houssin, E. J. Land, *Biochem. J.* **1996**, *315*, 625–629; b) L. Servillo, D. Castaldo, R. Casale, N. D’Onofrio, A. Giovane, D. Cautela, M. L. Balestrieri, *Free Radical Biol. Med.* **2015**, *79*, 228–236; c) P. E. Hartman, *Methods Enzymol.* **1990**, *186*, 310–318.
- [8] a) L. Servillo, N. Donofrio, M. L. Balestrieri, *J. Cardiovasc. Pharmacol.* **2017**, *69*, 183–191; b) S. Yoshida, H. Shime, K. Funami, H. Takaki, M. Matsumoto, M. Kasahara, T. Seya, *PLoS One* **2017**, *12*, e0169360.
- [9] a) Y. Ishikawa, D. B. Melville, *J. Biol. Chem.* **1970**, *245*, 5967–5973; b) W. Hu, H. Song, A. Sae Her, D. W. Bak, N. Naowarojna, S. J. Elliot, L. Qin, X. Chen, P. Liu, *Org. Lett.* **2014**, *16*, 5382–5385; c) H. Song, W. Hu, N. Naowarojna, A. S. Her, S. G. Wang, R. Desai, L. Qin, X. Chen, P. Liu, *Sci. Rep.* **2015**, *5*, 11870; d) A. Vit, L. E. Misson, W. Blankenfeldt, F. P. Seebeck, *ChemBioChem* **2015**, *16*, 119–125; e) A. Vit, G. T. Mashabela, W. Blankenfeldt, F. P. Seebeck, *ChemBioChem* **2015**, *16*, 1490–1496; f) K. V. Goncharenko, A. Vit, W. Blankenfeldt, F. P. Seebeck, *Angew. Chem. Int. Ed.* **2015**, *54*, 2821–2824; *Angew. Chem.* **2015**, *127*, 2863–2866; g) J. H. Jeong, H. J. Cha, S. C. Ha, C. Rojviriya, Y. G. Kim, *Biochem. Biophys. Res. Commun.* **2014**, *452*, 1098–1103.
- [10] T. Pluskal, M. Ueno, M. Yanagida, *PLoS One* **2014**, *9*, e97774.
- [11] a) K. V. Goncharenko, F. P. Seebeck, *Chem. Commun.* **2016**, *52*, 1945–1948; b) G. T. Mashabela, F. P. Seebeck, *Chem. Commun.* **2013**, *49*, 7714–7716; c) E. A. Bushnell, G. B. Fortowsky, J. W. Gauld, *Inorg. Chem.* **2012**, *51*, 13351–13356; d) W. J. Wei, P. E. Siegbahn, R. Z. Liao, *Inorg. Chem.* **2017**, *56*, 3589–3599; e) A. S. Faponle, F. P. Seebeck, S. P. de Visser, *J. Am. Chem. Soc.* **2017**, *139*, 9259–9270.
- [12] a) E. G. Mueller, *Nat. Chem. Biol.* **2006**, *2*, 185–194; b) D. Kessler, *FEMS Microbiol. Rev.* **2006**, *30*, 825–840; c) R. Cipollone, P. Ascenzi, P. Visca, *IUBMB Life* **2007**, *59*, 51–59; d) S. Leimkühler, M. Bühning, L. Beilschmidt, *Biomolecules* **2017**, *7*, E5; e) J. Papenbrock, S. Guretzki, M. Henne, *Amino Acids* **2011**, *41*, 43–57; f) C. Zheng, K. A. Black, P. C. Dos Santos, *Biomolecules* **2017**, *7*, 0; g) C. T. Jurgenson, T. P. Begley, S. E. Ealick, *Annu. Rev. Biochem.* **2009**, *78*, 569–603.
- [13] W. W. Fischer, J. Hemp, J. S. Valentine, *Curr. Opin. Chem. Biol.* **2016**, *31*, 166–178.
- [14] B. B. Buchanan, D. I. Arnon, *Photosynth. Res.* **1990**, *24*, 47–53.
- [15] J. Antón, A. Oren, S. Benlloch, F. Rodríguez-Valera, R. Amann, R. Rosselló-Mora, *Int. J. Syst. Evol. Microbiol.* **2002**, *52*, 485–491.
- [16] K. L. Dunbar, D. H. Scharf, A. Litomska, C. Hertweck, *Chem. Rev.* **2017**, *117*, 5521–5577.
- [17] T. L. Amyes, S. T. Diver, J. P. Richard, F. M. Rivas, K. Toth, *J. Am. Chem. Soc.* **2004**, *126*, 4366–4374.
- [18] C. M. Wright, G. D. Christman, A. M. Snellinger, M. V. Johnston, E. G. Mueller, *Chem. Commun.* **2006**, 3104–3106.
- [19] E. Sasaki, X. Zhang, H. G. Sun, M. Y. Lu, M. Y. Liu, T. L. Liu, A. Ou, J. Y. Li, Y. H. Chen, S. E. Ealick, H. W. Liu, *Nature* **2014**, *510*, 427–431.

Manuscript received: June 11, 2017

Accepted manuscript online: August 8, 2017

Version of record online: September 1, 2017

---

---

---

## 4 Structural and mechanistic basis for anaerobic ergothioneine biosynthesis.

As described in **Chapter 1**, direct enzymatic C-H bond to C-S bond functionalizations are rather rare. In **Chapter 3**, the discovery of the ergothioneine anaerobic biosynthetic enzyme, EanB, was described. EanB does perform such a direct C-H to C-S bond functionalization in an unprecedented way. In a study performed during this thesis, the mechanistic proposal of the C-S bond forming reaction catalyzed by EanB has been elucidated based on kinetic and structural data. The study was described in the following publication:

- Leisinger, F.; Burn, R.; Meury, M.; Lukat, P.; Seebeck, F. P. *J. Am. Chem. Soc.* **2019**, *141* (17), 6906.

During this study, three different structures of EanB were solved. The first structure was the apo form of EanB, the second, EanB with TMH bound in the active site, and the third structure was EanB with a persulfide on the active site cysteine. These structures revealed ten residues that make up the active site surface. Three of them form an aromatic box for the binding of the trimethyl ammonium cation. Two tyrosines form hydrogen bonds to the carboxylate of TMH. Four of the others are involved in a hydrogen bonding network, which connects to the substrate through a water molecule. The active site cysteine and the proposed catalytic acid and base tyrosine are also part of this network.

All the kinetic characterizations were done with persulfidated EanB in a single turnover kinetic assay to assure that the observed perturbations result from the sulfur transfer reaction from EanB to TMH and from the EanB persulfidation reaction.

To study the hydrogen bonding interactions in the active site, kinetic characterization of four mutants, each lacking a hydroxyl group, was performed. This confirmed the role of the two tyrosines in substrate binding and revealed a threonine and a tyrosine residue important for catalysis.

To determine whether EanB binds the protonated or deprotonated form of TMH, a pH profile of the reaction was constructed. This revealed that EanB selectively binds the deprotonated form of TMH and hence protonation of TMH must be the first step during catalysis.

Substrate and solvent kinetic isotope effects were measured to determine the rate-limiting step of the reaction. The absence of a kinetic isotope effect, with 2-D-TMH as a substrate, ruled out that the C-H bond cleavage is rate-limiting. The presence of a significant inverse solvent kinetic isotope effect is a strong indication that no exchangeable proton is transferred during the rate-limiting step and therefore protonation of the imidazole  $N^{\pi}$  and attack of the

persulfide on the imidazole C<sub>2</sub> are not coupled. Based on the structural and kinetic data, a mechanistic model was elucidated (**figure 1**).

Additionally, a structural comparison with YnjE, the homolog of EanB found in *E. coli*, revealed that most active site residues involved in substrate binding and catalysis are conserved and that the active site architecture is mostly identical. The major difference between the two structures is the presence of an extra active site loop in EanB. This loop folds over the TMH binding site thereby closing the active site of EanB tightly. Due to the lack of this extra loop, the active site of YnjE is more open, and therefore could accommodate larger substrates. We are confident that our findings will assist in the assignment of functions to other sulfurtransferases homologous to EanB.

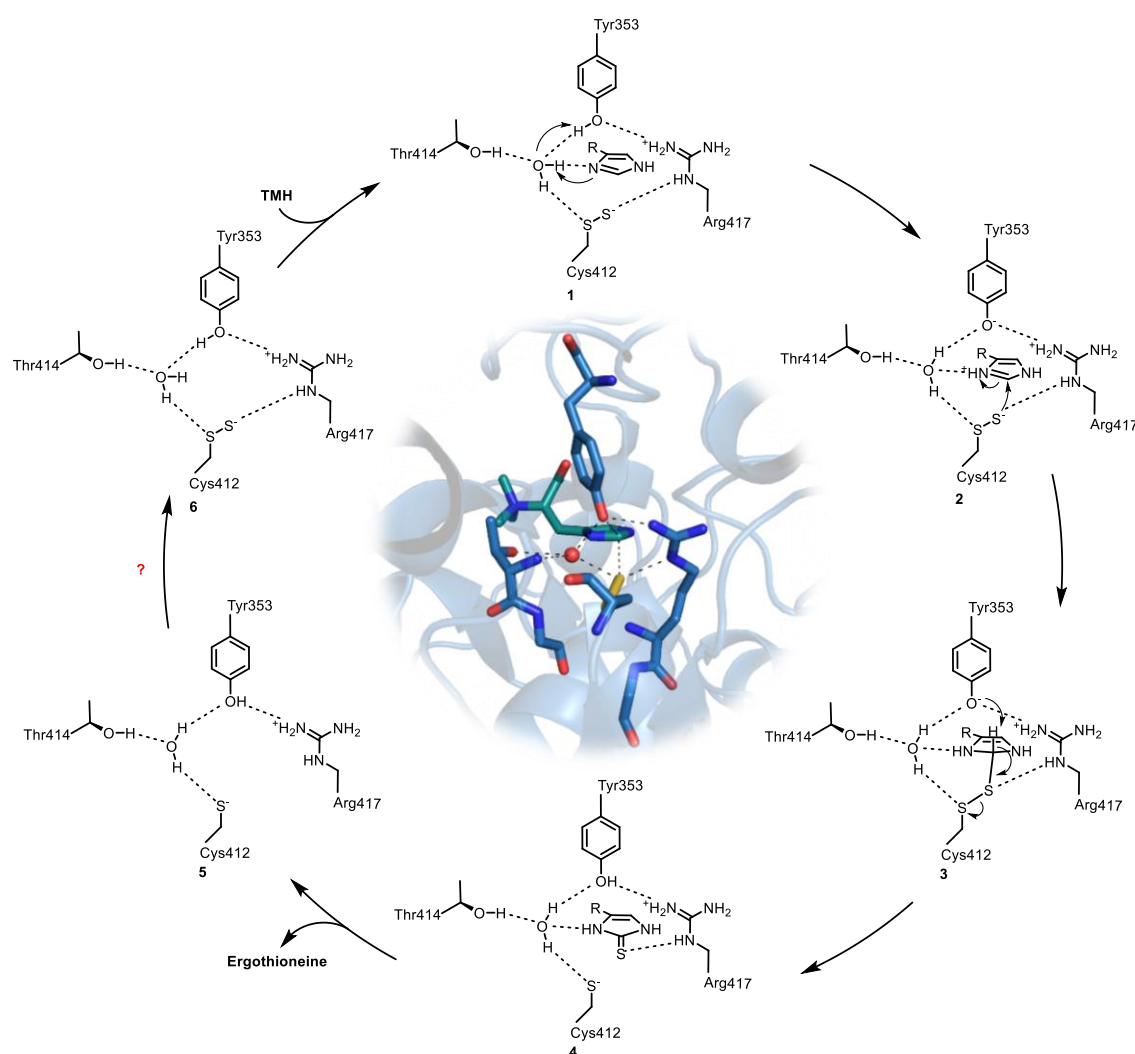



**Figure 20.** Mechanism for the EanB catalyzed C-S bond formation.

#### Author Contribution:

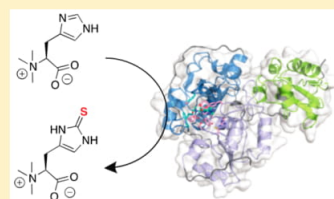
- R. B. designed kinetic experiments, developed protocols for and performed the kinetic characterization of EanB, data analysis



# Structural and Mechanistic Basis for Anaerobic Ergothioneine Biosynthesis

Florian Leisinger,<sup>†,§</sup> Reto Burn,<sup>†,§</sup> Marcel Meury,<sup>†</sup> Peer Lukat,<sup>‡</sup> and Florian P. Seebeck<sup>\*,†</sup><sup>†</sup>Department for Chemistry, University of Basel, Mattenstrasse 24a, BPR 1002, 4056, Basel, Switzerland<sup>‡</sup>Structure and Function of Proteins, Helmholtz Centre for Infection Research, Inhoffenstr. 7, 38124, Braunschweig, Germany Supporting Information

**ABSTRACT:** Ergothioneine is an emergent factor in cellular redox biochemistry in humans and pathogenic bacteria. Broad consensus has formed around the idea that ergothioneine protects cells against reactive oxygen species. The recent discovery that anaerobic microorganisms make the same metabolite using oxygen-independent chemistry indicates that ergothioneine also plays physiological roles under anoxic conditions. In this report, we describe the crystal structure of the anaerobic ergothioneine biosynthetic enzyme EanB from green sulfur bacterium *Chlorobium limicola*. This enzyme catalyzes the oxidative sulfurization of N- $\alpha$ -trimethyl histidine. On the basis of structural and kinetic evidence, we describe the catalytic mechanism of this unusual C–S bond-forming reaction. Significant active-site conservation among distant EanB homologues suggests that the oxidative sulfurization of heterocyclic substrates may occur in a broad range of bacteria.



## INTRODUCTION

Sulfur plays a central role in the primary and secondary metabolism of any organism. The availability of numerous redox states and the high polarizability enable sulfur to react as a nucleophile, an electrophile, or a radical and make this element an irreplaceable building block in many small and large biomolecules.<sup>1–5</sup> The malleability of sulfur is also reflected in the broad range of different enzymatic reactions that form carbon–sulfur (C–S) bonds.<sup>1</sup> Because of this diversity, it is not uncommon that natural products with similar sulfurous substructures emerge from entirely different chemistries. For example, the thiazolidine moiety of penicillin is formed in an oxygen-dependent reaction catalyzed by an iron-dependent oxidase,<sup>6</sup> whereas the thiophane ring in biotin is formed by an S-adenosyl methionine-dependent radical enzyme.<sup>7</sup>

Even more remarkable is the case of thiamine biosynthesis, where bacteria, archaea, and eukaryotes utilize different C–S bond-forming reactions to produce an identical product.<sup>8–10</sup>

Recently, we discovered that ergothioneine biosynthesis also emerged through multiple routes.<sup>11,15</sup> Actinobacteria, cyanobacteria, many proteobacteria, and most fungi synthesize ergothioneine by way of an iron-dependent sulfoxide synthase (EgtB, Figure 1). In cooperation with two additional enzymes, EgtB attaches a cysteine-derived sulfur atom to the imidazole ring of N- $\alpha$ -trimethyl histidine (TMH).<sup>16–18</sup> Although the mechanistic details of the EgtB reaction are controversial, the involvement of oxygen as an electron acceptor is undisputed.<sup>12,19,20</sup> In contrast, a group of mainly anaerobic bacteria and archaea recruited a rhodanese-like enzyme (EanB) to introduce sulfur into TMH.<sup>11</sup> Rhodanese-like enzymes are ubiquitous C–S bond-forming catalysts involved in the biosynthesis of cofactors, thiosugars, and thiolated nucleic acids.<sup>1,8,21–23</sup> Invariably, these enzymes bind their substrate in

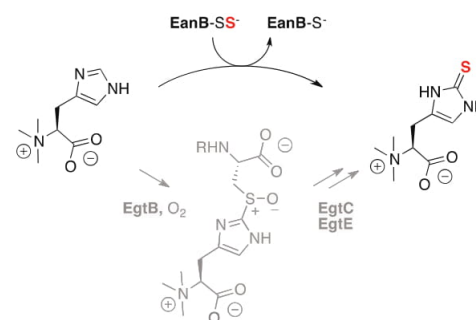


**Figure 1.** Rhodanese-like enzyme EanB from *Chlorobium limicola* catalyzes oxidative sulfur transfer to N- $\alpha$ -trimethylhistidine (TMH) in an oxygen-independent reaction.<sup>11</sup> Sulfoxide synthase EgtB from *Mycobacterium thermoresistibile* catalyzes the oxygen-dependent sulfurization of TMH.<sup>12</sup> This second pathway requires two additional enzymes (EgtC and E) to produce ergothioneine.<sup>13,14</sup>

activated form, after phosphorylation or adenylation, and mediate the nucleophilic substitution of the phosphate or the AMP leaving group with a sulfur atom. EanB does not follow this paradigm. This enzyme binds its substrate TMH without prior activation and attaches a sulfur atom in place of a proton. This combination of substrate activation with oxidative sulfurization is unprecedented in enzymology.<sup>1</sup>

To elucidate the catalytic mechanism of EanB, we solved the crystal structure and examined the catalytic activity of this enzyme and variants thereof. The described structural and

Received: November 23, 2018

Published: April 3, 2019

kinetic observations suggest that C–S bond formation occurs by the nucleophilic attack of an active-site persulfide anion onto the imidazolium ring of TMH. Significant active-site similarity among a large subclass of rhodanese-like enzymes with unknown functions indicates that this reaction type may apply to several different biosynthetic pathways occurring in proteobacteria, spirochaetes, and firmicutes.

## RESULTS

**Crystal Structure of Native EanB.** We produced EanB from *Chlorobium limicola* in *Escherichia coli* as previously described.<sup>11</sup> To optimize EanB for crystallization, we engineered a truncated version of this protein that lacks the first 34 residues. A homology model of EanB based on the crystal structure of rhodanese-like enzyme YnjE suggested that this N-terminal appendix is not part of the folded core and is located far away from the presumed active site.<sup>24</sup> In addition, we mutated three consecutive lysine residues on the protein surface to alanine (K357A, K358A and K359A) in order to reduce the surface entropy (Figure S1).<sup>25</sup> The resulting protein (EanB<sub>SER</sub>) is stable and active (Table 1) and formed diffracting crystals (Figure S2).

Table 1. Rate Constants for EanB Variants<sup>a,b</sup>

enzyme	$k_{\text{turnover}} [\text{s}^{-1}] \times 10^{-3}$	$k_{\text{cat}} [\text{s}^{-1}] \times 10^{-3}$	$K_{\text{M, TMH}} [\text{M}] \times 10^{-6}$	$k_{\text{turnover}}/K_{\text{M}} [\text{M}^{-1} \text{s}^{-1}]$
EanB <sub>wt</sub>	8.3 <sup>c</sup>	11	40	275
EanB <sub>SER</sub>	8.5	n.d.	n.d.	n.d.
EanB <sub>T414A</sub>	<0.1	n.d.	n.d.	n.d.
EanB <sub>Y353F</sub>	<0.1	n.d.	n.d.	n.d.
EanB <sub>Y355F</sub>	6.5	5.0	4900	1.0
EanB <sub>Y375F</sub>	5.5	2.5	1700	1.5

<sup>a</sup>All values represent averages of at least two independent measurements. The standard error on all kinetic parameters is  $\leq 20\%$  of the average value. <sup>b</sup>n.d. = not determined. <sup>c</sup>Data from ref 11.

One diffraction data set with a resolution of 1.8 Å was used to solve the structure of EanB by molecular replacement (Table S1).<sup>26</sup> The measured electron density revealed a continuous polypeptide chain from Glu35 to Pro456. The residue numbering was chosen in accord with gene locus Clm\_1149 in the genome of *Chlorobium limicola* DSM 245. EanB folds into three consecutive rhodanese-like domains (35–139, 160–291, and 319–445), which are connected by 19- and 26-residue-long linker regions (red, Figure 2A). The structure of EanB is remarkably similar to that of *E. coli* protein YnjE (Figure 3A).<sup>24</sup> A detailed description of the overall structure of EanB can be found in the Supporting Information (Figures S3 and S4). The central and C-terminal domains form a dimer with pseudo- $C_2$  symmetry (Figure 2C). The active site, as identified by the location of a conserved cysteine residue in the C-terminal domain,<sup>24</sup> maps to the dimer interface near the pseudo- $C_2$ -symmetry axis. The N terminus docks to this dimer far away from the active site and possibly serves as a stabilizing clamp. One conspicuous difference between EanB and YnjE occurs near the active site. EanB residues 245–260 and 348–360 form two loops that shape the active site into a deep, narrow tunnel with the catalytic cysteine on the bottom. YnjE lacks the first loop, leaving the active site as a large and water-exposed cleft (Figure 3).<sup>24</sup>

**Structure of EanB in Complex with TMH.** On the basis of a data set with a resolution of 2.8 Å (Table S1), we also obtained the structure of EanB in complex with substrate TMH. This

structure provides the first view at a triple-domain rhodanese-like enzyme bound to its genuine substrate (Figure 2B, Figure S5). TMH stacks on top of the indole ring of Trp416. N $\pi$  and N $\pi'$  of the imidazole ring hydrogen bond to the backbone carbonyl of Ala374 (2.8 Å, Figure S9) and to a water molecule (H<sub>2</sub>O\_1, 2.6 Å), respectively. This water molecule is immobilized by two additional hydrogen bonds to the side chains of Thr414 (2.5 Å) and Tyr353 (3.0 Å). The backbone amides of residues 414–416 point to three additional hydrogen bond donors toward H<sub>2</sub>O\_1 (3.0–3.5 Å). The carboxylate group of TMH is solvated by the phenol functions of Tyr375 and Tyr355 (Figure S6). The *N*- $\alpha$ -trimethylammonium moiety docks into an aromatic box formed by the side chains of Tyr188, Trp216, Trp416, and Tyr355. The side chain of Glu178 points toward this aromatic pocket and presumably neutralizes the positive charge of the ammonium ligand. In the apo structure, this ammonium binding pocket hosts a loosely coordinated magnesium cation, corroborating the cation-binding propensity of this site. It is unlikely that this cation plays any role in EanB catalysis. Similar aromatic boxes are typical for betaine binding proteins.<sup>27–29</sup>

**Structure of the Persulfide Form of EanB.** A third data set with a resolution of 1.6 Å revealed the structure of EanB with extra electron density around active-site cysteine Cys412 (Figure 2E). This protrusion fits well to a model with a sulfane sulfur attached to Cys412. A point atom refined model revealed a distance of the electron density peak centers between Cys-S<sub>y</sub> and the protrusion (point atom) of 2.04 Å. This distance is in good agreement with the expected length of an S–S bond (2.07 Å).<sup>30</sup> In contrast, the S–O bond of a cysteine sulfenic acid is much shorter (1.67 Å) and produced no acceptable fit upon model refinement (Figure S7). Further evidence for the presence of a persulfide function at Cys412 was gained from anomalous diffraction data sets. Restrained SAD data refinement revealed a peak in the anomalous sulfur electron density map corresponding to two sulfur atoms at this position (Figure 2E). The presence of the persulfide function is corroborated by the observation that recombinant EanB can convert up to 1 equiv of TMH to ergothioneine in the absence of an exogenous sulfur donor.<sup>11</sup> The persulfide is within hydrogen bonding distance to the guanidinium side chain of Arg417 (2.8 Å, Figure 2F). The sulfane sulfur atom approaches Arg417 in the plane of the guanidinium function (dihedral angle NCNS,  $-8.6^\circ$ ; bond angle CNS,  $120^\circ$ ). This geometry is suggestive of hydrogen bonding. The entire persulfide is placed in the positive electrostatic field generated by the dipole moment of one of the two symmetry-related  $\alpha$ -helices (residues 415–429). In the absence of the sulfane sulfur atom, the side chain of Cys412 adopts an identical conformation, placing the side chain within hydrogen bonding distance of Gly415 (3.2 Å) and H<sub>2</sub>O\_1 (3.3 Å).

**Model of the Reactive Complex.** Comparison of the native structure of EanB, the persulfide form, and the complex with TMH shows that substrate binding induces almost no conformational change in the active site (Figure S8, Table S2). Therefore, we concluded that the superposition of the persulfide form and the TMH complex should provide a relevant model for the reactive complex of EanB (Figure 2F). In this model, the sulfane sulfur on Cys412 approaches TMH from below the imidazole plane to a near van der Waals distance ( $S_{\text{Cys412}} - C_{2\text{-TMH}}$ , 3.4 Å). The phenol ring of Tyr353 hovers on the other side of the imidazole plane in contact with Arg417 (2.8 Å), H<sub>2</sub>O\_1 (3.0 Å), and the backbone of Gly413 (3.3 Å).

**Mutagenesis of Active Site Residues.** The surface of the active site is formed by 10 residues. Although 6 out of the 10



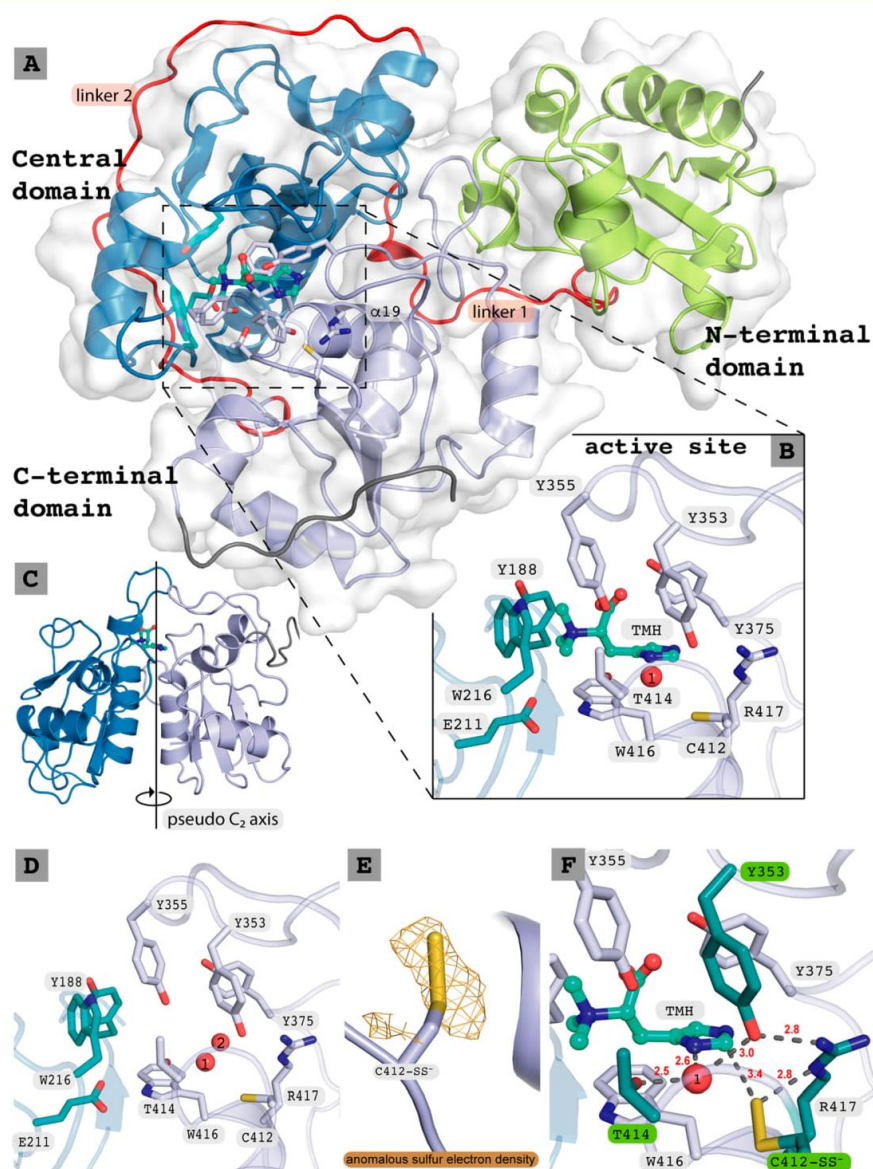


**Figure 2.** (A) Overall view of EanB in complex with TMH (turquoise). Active site residues are shown in lilac and turquoise blue; the N-terminal domain, in green; the central domain, in blue; the C-terminal domain, in violet; the linker regions, in red. (B) Active site of the TMH-complexed EanB structure with residues represented as sticks, where H<sub>2</sub>O<sub>1</sub> is shown as a red sphere. (C) Pseudo-C<sub>2</sub> symmetry axis between the central and C-terminal domains. (D) Active site of apo-EanB. H<sub>2</sub>O<sub>1</sub> hydrogen bonds to a second water molecule instead of TMH. (E) Anomalous sulfur electron density map at catalytic cysteine persulfide (Cys412-SS) revealing the presence of two sulfur atoms. (F) Active-site model of the reactive complex with TMH and Cys-SS<sup>-</sup>. Distances are indicated in red.

residues are aromatic, polar interactions are clearly most important for binding and catalysis. To examine these interactions, we constructed four EanB variants that each lack one hydroxyl group by mutating Thr414 to Ala and Tyr353 to Tyr 355 or Tyr375 to Phe (Table 1).

We excluded Arg417 from this study because the mutagenesis of active-site arginines to any other proteinogenic amino acid is usually too disruptive to give interpretable results.

The catalytic activities of these variants (EanB<sub>T414A</sub>, EanB<sub>Y353F</sub>, EanB<sub>Y355F</sub>, and EanB<sub>Y375F</sub>) were assessed by measuring the rate of ergothioneine production in single turnover reactions. For this characterization, we exploited the fact that EanB can be isolated partially in persulfide form from *E. coli* lysates.<sup>11</sup> The persulfide content of the EanB variants was also determined by the colorimetric quantification of thiocyanide formed when the proteins were incubated with

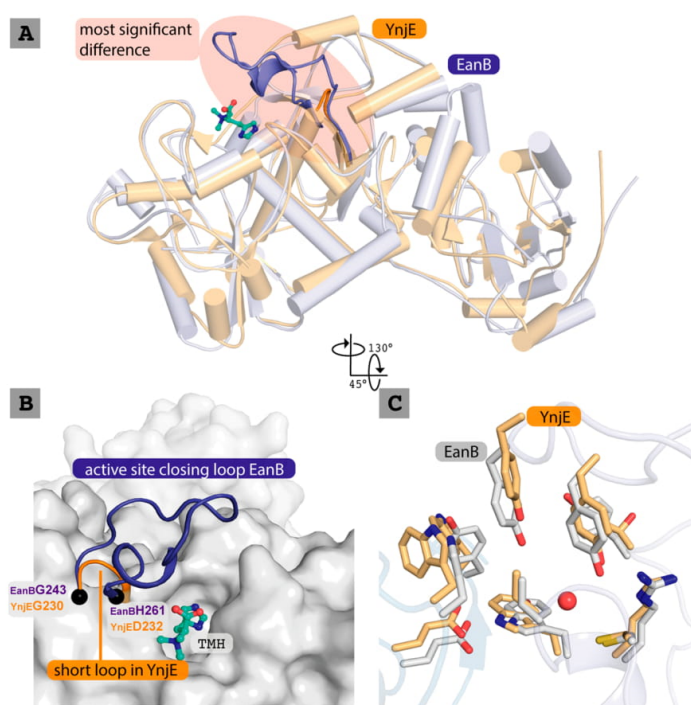


**Figure 3.** (A) Superposition of EanB structure with the YnjE structure (PDB code 3IPO, RMSD: 2.64 Å over 400 residues).<sup>24</sup> (B) The extra active-site loop in EanB is shown in dark blue (residues 245–260). The much shorter turn in YnjE is shown in orange. (C) Superposition of active-site residues of EanB with YnjE.

cyanide (Table S3). This analysis showed that all isolated EanB variants contained between 0.2 and 0.5 equiv of sulfane sulfur.

To determine single-turnover rates ( $k_{\text{turnover}}$ ), we incubated the enzymes with a saturating concentration of TMH and monitored product formation by HPLC. In this assay, EanB<sub>wt</sub>, EanB<sub>SER</sub>, EanB<sub>Y355</sub>, and EanB<sub>Y375</sub> catalyzed sulfur transfer to TMH at similar rates (Table 1, Figure S10). In contrast, no product formation was observed for EanB<sub>T414A</sub> and EanB<sub>Y353F</sub>, suggesting that their activity is less than 1% of the wild type activity. This dramatic effect establishes Thr414 and Tyr353 as essential catalytic residues. The available kinetic data does not allow a judgment as to whether the mutations predominantly affected substrate binding or turnover. However, because these residues undergo only indirect or weak interactions with TMH, it is safe to assume that the mutations predominantly affected turnover.

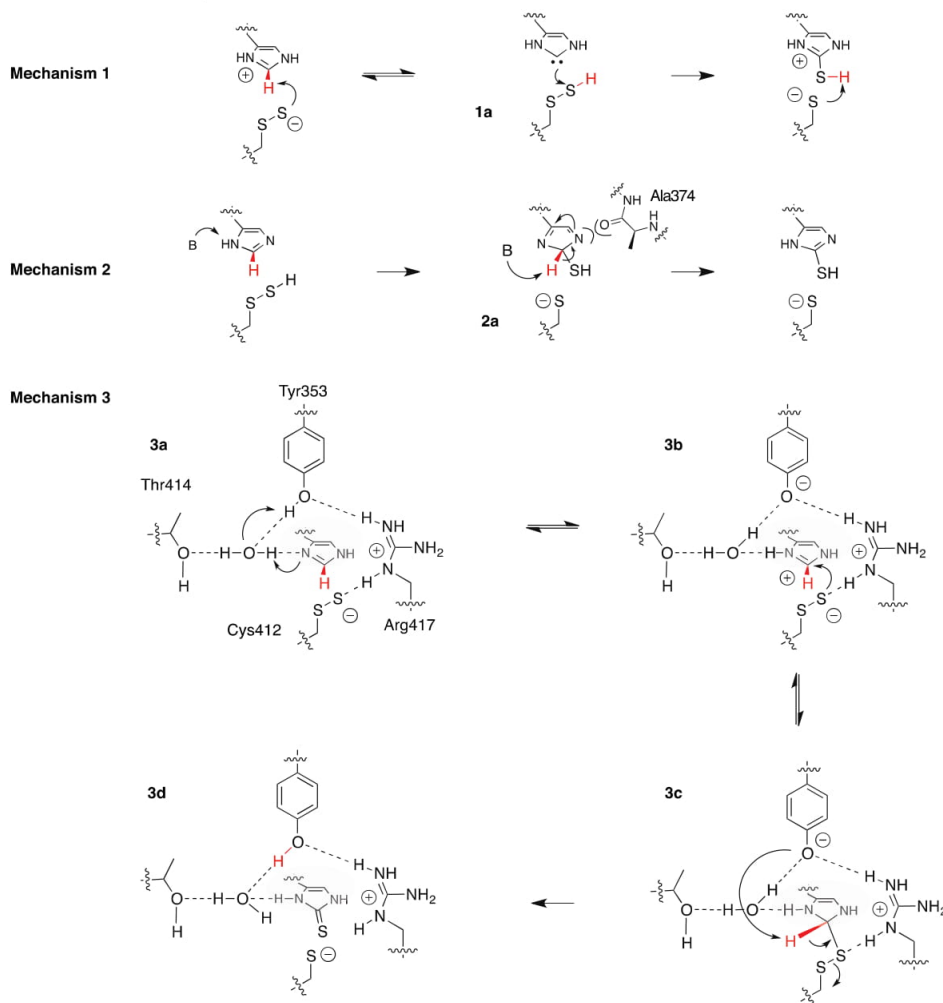
To interrogate the functions of Tyr355 and Tyr375 in more detail, we determined the Michaelis–Menten parameters for EanB<sub>wt</sub>, EanB<sub>Y355F</sub>, and EanB<sub>Y375F</sub> by measuring  $k_{\text{turnover}}$  as a function of the TMH concentration (Figures S11 and S12). This experiment showed that EanB<sub>Y355</sub> and EanB<sub>Y375</sub> are characterized by  $K_M$  values that are 170- and 60-fold higher than that determined for wild type. Meanwhile, the catalytic constant ( $k_{\text{cat}}$ ) remained largely unaffected by either mutation. These observations suggest that Tyr355 and Tyr375 are mainly important for substrate recognition.

**pH Dependence of Catalysis.** The active site of EanB and the substrate TMH contain several ionizable groups with  $pK_a$ s close to the reaction pH (8.0). Therefore, we found it important to determine the pH-dependence of EanB (Figure S12). This

experiment showed that increasing the reaction pH from 5 to 9 reduced the  $K_M$  by 20-fold and  $k_{\text{turnover}}$  by only 1.3-fold. Plotting the catalytic efficiency against pH revealed that the change in activity is related to a single protonation event characterized with a kinetic  $pK_a$  of  $6.1 \pm 0.1$ . Because  $k_{\text{turnover}}$  is not affected, it is clear that this protonation affects an equilibrium reaction before the rate-limiting step. Because the imidazole  $pK_a$  of TMH as inferred by NMR titration to be  $6.0 \pm 0.1$  (Figure S13), we interpret the pH dependence as evidence that EanB binds TMH only in its neutral (deprotonated) form. Hence, lowering the reaction pH reduces the effective substrate concentration and in turn increases the observed  $K_M$ . The absence of additional kinetically relevant protonation equilibria suggests that catalytic residues such as Tyr353 and Cys412 do not change their protonation states between pH 5 and 9.

**Kinetic Isotope Effects.** To probe which elementary step in the catalytic cycle of EanB may be rate-limiting, we measured substrate and solvent kinetic isotope effects (KIE). We showed earlier that the rate-limiting step must occur during sulfur transfer from EanB to TMH rather than during sulfur transfer to EanB.<sup>11</sup> To examine whether the abstraction of the proton from the TMH imidazole ring at C<sub>2</sub> (C<sub>2</sub>–H) may be rate-limiting, we determined the substrate KIE on  $k_{\text{turnover}}$  using C<sub>2</sub>-deuterated TMH as a substrate (Figure S14). This experiment revealed a KIE of  $1.1 \pm 0.3$ , suggesting that the deprotonation of C<sub>2</sub> is not rate-limiting. Proton exchange at the C<sub>2</sub> center of imidazole rings at pH 8.0 is slow enough that we can exclude nonenzymatic wash-out of the deuterium label from TMH as an explanation of the observed KIE.<sup>31</sup>

Scheme 1. Three Possible Catalytic Mechanisms of EanB.



In contrast, we observed a significant inverse solvent KIE effect on  $k_{\text{turnover}}$  ( $s\text{KIE} = 0.8 \pm 0.04$ , Figure S15). The observation that the  $s\text{KIE}$  is not larger than unity provides evidence against a mechanism in which an exchangeable proton is being transferred during the rate-limiting step.

## DISCUSSION

EanB-catalyzed sulfur transfer to TMH is formally an oxidation reaction that couples C–S bond formation with S–S bond reduction. This reaction type is also interesting because both the imidazole ring of TMH and cysteine persulfide can in principle act as nucleophile or as electrophile, depending on their protonation state. In the following section, we will match structural and kinetic evidence with different mechanistic proposals. As a result, we find that the EanB-catalyzed sulfurization of TMH most likely occurs via nucleophilic attack of a persulfide anion on the imidazolium ring of TMH. Subsequently, we will summarize the indications that this reaction type may be catalyzed by many YnjE-like rhodanases.<sup>24</sup>

**Catalytic Mechanism.** Rhodanase and most rhodanase-like enzymes can transfer sulfur to cyanide to form thiocyanide.<sup>32</sup> This reaction is facilitated by the considerable nucleophilicity of the cyanide anion and the acidity of hydrogen cyanide ( $\text{p}K_{\text{a}} = 9$ ).<sup>33</sup> By analogy, we surmised that EanB could deprotonate TMH at C<sub>2</sub> to form the corresponding carbene which may attack the Cys412 persulfide (1a, Scheme 1). This scheme would require deprotonation of the imidazole or imidazolium ring of TMH. Although C<sub>2</sub> protons in imidazolium rings are not particularly acidic ( $\text{p}K_{\text{a}} = 24$ ),<sup>31</sup> the conjugated base, the imidazole-2-yl carbene, does occur as an intermediate during proton exchange in water.<sup>31</sup> The involvement of carbene intermediates in enzyme catalysis is also preceded by the cofactor chemistry of thiamine pyrophosphate.<sup>34,35</sup> However, the formation of a TMH carbene in the EanB reaction is unlikely. Proton abstraction would require a strong base positioned in the plane with the imidazole ring, juxtaposed to the scissile C<sub>2</sub>–H. The two candidate bases, Tyr353 and the persulfide anion of Cys412, are both located out of the plane (Figure 2F). In



addition, both moieties are weak bases (Tyr,  $pK_a = 10$ ; persulfide,  $pK_a = 6-7$ ),<sup>33</sup> and both make direct hydrogen bonding contact with the cationic side chain of Arg417. This interaction likely reduces rather than increases the basicity of Tyr353 and Cys412. As discussed below, the pH dependence of EanB indicates that Tyr353 is protonated at physiological pH and is therefore not available as a base. The persulfide function of Cys412 is likely anionic. However, in a hypothetical equilibrium where TMH and the active-site persulfide anion share a proton ( $C_2-H$ ), only 1 out of  $10^{17}$  enzymes would be in the carbene state ( $1a$ ,  $K_{a, TMH}/K_{a, persulfide} = 10^{-24} M/10^{-7} M = 10^{-17}$ ). Because the enzyme turns over at a rate of  $10^{-2} s^{-1}$  (Table 1), carbene species  $1a$  would have to react forward at a rate equal to or faster than  $10^{15} s^{-1}$ . This frequency is 3 orders of magnitude higher than that of many bond vibrations. Therefore, we conclude that  $1a$  is not kinetically competent. We have no evidence that the acidities of TMH or the persulfide are perturbed to the extent that this conclusion would not hold.

A second possible mechanism could be nucleophilic attack at the sulfane sulfur of Cys412 by the neutral imidazole ring of TMH ( $2a$ ). Precedence for nucleophilic attack by an imidazole ring can be found in the mechanism of urocanases.<sup>36</sup> In this reaction, the imidazole ring of urocanic acid attacks the nicotinamide ring of  $NAD^+$ . In EanB, nucleophilic attack by TMH is unlikely for the following reasons: The persulfide function of Cys412 is not protonated at physiological pH. The low intrinsic  $pK_a$  of persulfides ( $pK_a = 6.2$ ),<sup>33</sup> the close interaction between Cys412 and Arg417, and the pH dependence of EanB all point to an anionic persulfide function. We note that proton transfer from Tyr353 (Figure 2F) could provide a mechanism to activate the persulfide as an electrophile.

An even more severe problem of mechanism 2 is that intermediate  $2a$  would require coordination by two hydrogen bond donors. Although the backbone carbonyl of Ala374 is in hydrogen-bonding distance of  $N\tau$  (2.8 Å), this residue can hardly serve as a proton donor (Scheme 1, Figure S9). The remaining surface around  $N\tau$  is composed of hydrophobic moieties of Ile262, Ala259, Trp416, Arg417, and Tyr375, suggesting that this pocket is poorly equipped to stabilize intermediate  $2a$ .

The third model suggests that the nucleophilic persulfide anion attacks TMH ( $3b$ ) to form  $3c$ . Tyr353-mediated  $C_2-H$  cleavage from intermediate  $3c$  leads to aromatization of the mercaptoimidazole ring and S-S bond cleavage ( $3d$ ). The crystal structure of EanB, showing the suggested nucleophile and base positioned on opposite sides of the imidazole plane (Figure 2F), is consistent with this mechanism. The observed pH dependence and kinetic isotope effects of EanB allow us to add further details to this mechanistic picture. The  $K_M$  of EanB is characterized by a kinetic  $pK_a$  that is identical to the thermodynamic  $pK_a$  of TMH. This dependence shows that EanB binds its substrate only in neutral form. There is no evidence for additional kinetically relevant protonation equilibria, suggesting that the protonation states in the active site, specifically those of Tyr353 and Cys412, remain unchanged between pH 5 and 9. Therefore, we conclude that species  $3a$  is the dominant first intermediate. The direct formation of  $3b$ , by an encounter of cationic TMH and EanB with an anionic Tyr353, may be possible but is rare.

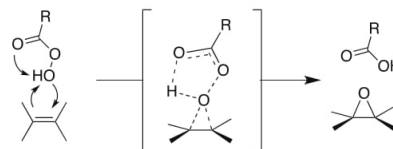
The proposition that Tyr353 is the proton donor to TMH is supported by the following considerations. Because an imidazolium ring is significantly more electrophilic than an imidazole ring, protonation would activate TMH for C-S bond

formation. This proton must be donated by  $H_2O\_1$  (Figure 2F) because this is the only possible hydrogen bond donor in direct contact with the imidazole ring of TMH. Because water has a much higher  $pK_a$  than an imidazolium cation, the formation of a hydroxide/imidazolium ion pair would produce a very unstable intermediate. Alternatively,  $H_2O\_1$  could relay a proton from a secondary proton donor. Possible candidates are Thr414 and Tyr353. The latter is certainly more acidic. Proton transfer from Tyr353 to TMH would also activate Tyr353 as a base for subsequent  $C_2-H$  cleavage. Hence, the most likely interpretation of the structure and pH-dependence of EanB is that TMH and Tyr353 share a proton via  $H_2O\_1$  in the reactive complex.

A second interesting question is whether the protonation of TMH occurs in an equilibrium between  $3a$  and  $3b$  or whether  $3a$  reacts directly to  $3c$  via proton transfer coupled with C-S bond formation. The KIE substrate is close to unity, suggesting that proton abstraction from species  $3c$  is not rate-limiting. Because  $k_{turnover}$  was measured in a single-turnover assay, we can exclude product release as a rate-limiting step. Because EanB turns over less than once every minute, substrate binding is also unlikely to be rate-limiting. The remaining candidate for the rate-limiting step is C-S bond formation. If this step is coupled to proton transfer from Tyr353 to TMH, then one might predict a solvent KIE that is significantly larger than 1. In contrast, we found a slightly inverse KIE. This behavior does not provide evidence for coupled proton transfer and C-S bond formation, but we cannot definitively exclude this mechanism either. An alternative interpretation is that proton transfer between TMH and Tyr353 occurs as an equilibrium connecting species  $3a$  with  $3b$ . Because the  $pK_a$  of the TMH imidazole ring is lower than that of Tyr353, even in the enzyme complex, species  $3a$  is likely more stable than  $3b$ . Because  $3b$  is immediately connected to the rate-limiting step, the position of this internal equilibrium would directly factor into the rate of catalysis. This interpretation can also accommodate the observed inverse KIE. It is possible that solvent deuteration affects the equilibrium between  $3a$  and  $3b$ , causing faster turnover in  $D_2O$  than in water.

The reaction according to mechanism 3 is deceptively similar to that of nucleophilic aromatic substitution. Examples of proteins that attack electron-deficient heterocycles with S-nucleophiles include glutathione-S-transferases,<sup>37</sup> dimethyl-arginine dimethylaminohydrolase,<sup>38</sup> inosine 5'-monophosphate dehydrogenase,<sup>39</sup> and numerous nucleobase sulfurizing enzymes.<sup>21</sup> In these cases, C-S bond formation is followed by the elimination of a halide, a phosphate, or a hydride from the ipso position.<sup>39</sup> In contrast, EanB removes a proton, resulting in oxidative sulfur transfer. We are unaware of any precedence for this reaction type in enzymology.<sup>1</sup> On the other hand, the EanB-catalyzed reaction is somewhat reminiscent of the peracid-mediated epoxidation of olefins (Scheme 2).<sup>40</sup> This reaction mediates oxidative C-O bond formation with reductive O-O bond cleavage. However, because of the high  $pK_a$  of peracids and

Scheme 2



because isolated olefins are electron-rich, the reaction is believed to occur via nucleophilic attack by the  $sp^2$  carbon.

#### Active-Site Conservation among YnjE Rhodanases.

The structure of EanB provides indications that many rhodanese-like enzymes with currently unknown function might catalyze related reactions. EanB belongs to a large group of enzymes termed the YnjE rhodanases group because YnjE from *E. coli* was the first structurally characterized representative of this family.<sup>24</sup> Members of this class occur in several bacterial phyla (proteobacteria, spirochaetes, fusobacteria, and firmicutes) and several archaeal species. YnjE rhodanases are characterized by a highly conserved six-residue active-site motif (CG[T/S]GWR, Cys412–Arg417 in EanB).<sup>24</sup> On the basis of structural evidence, we can now attribute specific roles to each of these residues (Figure 4). Cys412 is responsible

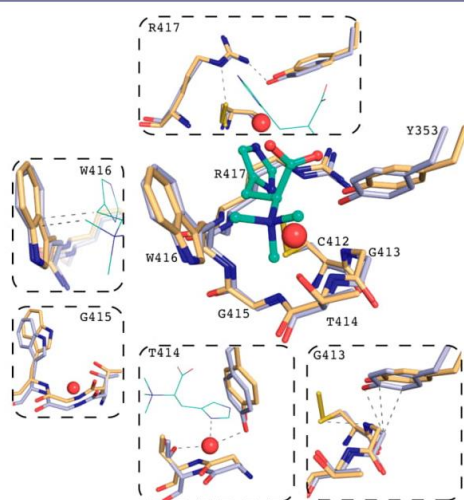


**Figure 4.** Overlay of the conserved active-site motifs (CG[T/S]GWR) in EanB (pale blue) and YnjE (pale orange). The residue numbering is according to EanB from *C. limicola*.

for presenting the sulfane sulfur in the active site. The backbone of Gly413 hydrogen bonds to the thiolate side chain of Cys412 in the apo form. The  $\alpha$  atom of Gly413 packs so tightly to Tyr353 that any other residue in this position would cause the displacement of the catalytic base. Hence, Gly is conserved at this position. The essential catalytic role of Thr414 has been discussed above. Gly415 adopts a backbone conformation ( $\varphi = 134^\circ$ ,  $\psi = -14^\circ$ ) that is difficult to attain for any other residue. The indole ring of Trp416 contributes a large hydrophobic patch to the substrate binding pocket, interacting with the imidazole ring, the  $\beta$ -carbon, and one of the  $N$ - $\alpha$ -methyl groups.

Finally, Arg417 hydrogen bonds to Tyr353 and the persulfide anion on Cys412. Strict conservation of a Thr or Ser at position 414 is particularly interesting because this residue makes no direct contact with the substrate or catalytic residues. Instead, the  $\beta$ -hydroxy side chain of Thr414 forms a strong hydrogen bond to  $H_2O_1$ , which in turn also forms hydrogen bonds to Tyr353 and TMH. The observation that EanB<sub>T414A</sub> is at least 2 orders of magnitude less active than wild type demonstrates that  $H_2O_1$  is crucial for catalysis. As described above, the most likely role of  $H_2O_1$  is to mediate proton transfer between

Tyr353 and TMH (3a  $\rightarrow$  3b, Scheme 1). In this way, Thr414 and  $H_2O_1$  contribute to substrate activation.

In addition to the conserved active-site motif (CG[T/S]GWR), YnjE rhodanases also share other active-site features that are essential for EanB activity. Tyr353 and Tyr355 are both strictly conserved. The mutation of Tyr353 produced a completely inactive EanB variant, corroborating the key role of this residue in catalysis. The mutation of Tyr355 predominantly affected substrate binding, which is consistent with the observed contact of this residue with the carboxylate of TMH. Finally, the ammonium binding pocket formed by Tyr188, Trp216, Trp416, Tyr355, and Glu211 is also largely conserved.

On the other hand, EanB also contains features that are exclusive to homologues that are involved in ergothioneine biosynthesis.<sup>11</sup> The most important distinction from other YnjE rhodanases is an extra active-site loop in EanB that folds over the TMH binding pocket (Figure 3B, residues 245–260). Second, Tyr375 is strictly conserved among EanB homologues but is absent in several subgroups of YnjE rhodanases. The mutation of this residue in EanB reduced the substrate affinity dramatically, suggesting that Tyr375 is a determinant for substrate specificity.

This analysis shows that most active-site residues with a role in substrate-binding and catalysis by EanB are conserved in all YnjE rhodanases. Therefore, we predict that most YnjE rhodanases catalyze the oxidative sulfurization of heterocycles with a quaternary ammonium moiety. However, we should note that YnjE from *E. coli* has already functioned as a sulfur transferase in molypterin biosynthesis.<sup>41</sup> This activity does not involve oxidative C–S bond formation and may therefore be a secondary function of YnjE.

## CONCLUSIONS

In this report, we describe the crystal structure of rhodanese-like enzyme EanB. This enzyme catalyzes the oxidative sulfurization of TMH as the second step in oxygen-independent ergothioneine biosynthesis in *C. limicola*. Structural and kinetic evidence suggest that this reaction occurs via nucleophilic attack of an active-site cysteine persulfide anion on the imidazolium ring of TMH. This rate-limiting step is followed by base-catalyzed deprotonation and rearomatization of the mercaptoimidazole side chain of the product ergothioneine. The conservation of key active-site residues across all members of the YnjE rhodanese enzyme family suggests that this novel reaction type may apply to several other biosynthetic pathways of heretofore unknown sulfur metabolites.

## ASSOCIATED CONTENT

### Supporting Information

The Supporting Information is available free of charge on the ACS Publications website at DOI: 10.1021/jacs.8b12596.

Detailed descriptions of all experiments, with supporting figures and tables (PDF)

## AUTHOR INFORMATION

### Corresponding Author

\*florian.seebeck@unibas.ch

### ORCID

Florian P. Seebeck: 0000-0003-4625-1369

### Author Contributions

<sup>§</sup>These authors contributed equally.



## Notes

The authors declare no competing financial interest.

## ■ ACKNOWLEDGMENTS

We thank Alice Maurer for HR ESI MS measurements. This project was supported by the Swiss National Science Foundation, the University of Basel, the Commission for Technology and Innovation, "Professur für Molekulare Bionik", and a starting grant from the European Research Council (ERC-2013-StG 336559). We thank the DESY PETRAIII (Hamburg, Germany) p11 and the SLS (Villigen, Switzerland) X06DA for access to facilities and the beamline.

## ■ REFERENCES

- (1) Dunbar, K. L.; Scharf, D. H.; Litomska, A.; Hertweck, C. Enzymatic Carbon-Sulfur Bond Formation in Natural Product Biosynthesis. *Chem. Rev.* **2017**, *117* (8), 5521–5577.
- (2) Schöneich, C. Sulfur Radical-Induced Redox Modifications in Proteins: Analysis and Mechanistic Aspects. *Antioxid. Redox Signaling* **2017**, *26* (8), 388–405.
- (3) Bonfio, C.; Valer, L.; Scintilla, S.; Shah, S.; Evans, D. J.; Jin, L.; Szostak, J. W.; Sasselov, D. D.; Sutherland, J. D.; Mansy, S. S. UV-light-driven prebiotic synthesis of iron-sulfur clusters. *Nat. Chem.* **2017**, *9* (12), 1229–1234.
- (4) Filipovic, M. R.; Zivanovic, J.; Alvarez, B.; Banerjee, R. Chemical Biology of H<sub>2</sub>S Signaling through Persulfidation. *Chem. Rev.* **2018**, *118* (3), 1253–1337.
- (5) Fass, D.; Thorpe, C. Chemistry and Enzymology of Disulfide Cross-Linking in Proteins. *Chem. Rev.* **2018**, *118* (3), 1169–1198.
- (6) Baldwin, J. E.; Bradley, M. *Chem. Rev.* **1990**, *90*, 1079–1088.
- (7) Jarrett, J. T. The biosynthesis of thiol- and thioether-containing cofactors and secondary metabolites catalyzed by radical S-adenosylmethionine enzymes. *J. Biol. Chem.* **2015**, *290* (7), 3972–3979.
- (8) Jurgenson, C. T.; Begley, T. P.; Ealick, S. E. The Structural and Biochemical Foundations of Thiamin Biosynthesis. *Annu. Rev. Biochem.* **2009**, *78*, 569–603.
- (9) Chatterjee, A.; Abeydeera, N. D.; Bale, S.; Pai, P.-J.; Dorrestein, P. C.; Russell, D. H.; Ealick, S. E.; Begley, T. P. *Saccharomyces cerevisiae* THI4p is a suicide thiamine thiazole synthase. *Nature* **2011**, *478* (7370), 542–U146.
- (10) Eser, B. E.; Zhang, X.; Chanan, P. K.; Begley, T. P. From Suicide Enzyme to Catalyst: The Iron-Dependent Sulfide Transfer in *Methanococcus jannaschii* Thiamine Thiazole Biosynthesis. *J. Am. Chem. Soc.* **2016**, *138* (11), 3639–3642.
- (11) Burn, R.; Misson, L. E.; Meury, M.; Seebeck, F. P. Anaerobic Origin of Ergothioneine. *Angew. Chem., Int. Ed.* **2017**, *56* (41), 12508–12511.
- (12) Goncharenko, K. V.; Vit, A.; Blankenfeldt, W.; Seebeck, F. P. Structure of the Sulfoxide Synthase EgtB from the Ergothioneine Biosynthetic Pathway. *Angew. Chem., Int. Ed.* **2015**, *54* (9), 2821–2824.
- (13) Vit, A.; Mashabela, G. T.; Blankenfeldt, W.; Seebeck, F. P. Structure of the Ergothioneine-Biosynthesis Amidohydrolase EgtC. *ChemBioChem* **2015**, *16* (10), 1490–1496.
- (14) Song, H.; Hu, W.; Naowarajina, N.; Her, A. S.; Wang, S. G.; Desai, R.; Qin, L.; Chen, X.; Liu, P. Mechanistic studies of a novel C-S lyase in ergothioneine biosynthesis: the involvement of a sulfenic acid intermediate. *Sci. Rep.* **2015**, *5*, 11870.
- (15) Liao, C.; Seebeck, F. P. Convergent Evolution of Ergothioneine Biosynthesis in Cyanobacteria. *ChemBioChem* **2017**, *18* (21), 2115–2118.
- (16) Seebeck, F. P. In vitro reconstitution of Mycobacterial ergothioneine biosynthesis. *J. Am. Chem. Soc.* **2010**, *132*, 6632–6633.
- (17) Naowarajina, N.; Cheng, R.; Chen, L.; Quill, M.; Xu, M.; Zhao, C.; Liu, P. Mini-Review: Ergothioneine and Ovothiol Biosyntheses, an Unprecedented Trans-Sulfur Strategy in Natural Product Biosynthesis. *Biochemistry* **2018**, *57* (24), 3309–3325.
- (18) Peck, S. C.; van der Donk, W. A. Go It Alone: Four Electron Oxidations by Mononuclear Non-heme Iron Enzymes. *JBC, J. Biol. Inorg. Chem.* **2017**, *22* (2–3), 381–394.
- (19) Faponle, A. S.; Seebeck, F. P.; de Visser, S. P. Sulfoxide Synthase versus Cysteine Dioxygenase Reactivity in a Nonheme Iron Enzyme. *J. Am. Chem. Soc.* **2017**, *139* (27), 9259–9270.
- (20) Wei, W. J.; Siegbahn, P. E.; Liao, R. Z. Theoretical Study of the Mechanism of the Nonheme Iron Enzyme EgtB. *Inorg. Chem.* **2017**, *56* (6), 3589–3599.
- (21) Leimkühler, S.; Böhning, M.; Beilschmidt, L. Shared Sulfur Mobilization Routes for tRNA Thiolation and Molybdenum Cofactor Biosynthesis in Prokaryotes and Eukaryotes. *Biomolecules* **2017**, *7* (1), E5.
- (22) Sasaki, E.; Zhang, X.; Sun, H. G.; Lu, M. Y.; Liu, M. Y.; Liu, T. L.; Ou, A.; Li, J. Y.; Chen, Y. H.; Ealick, S. E.; Liu, H. W. Co-opting sulphur-carrier proteins from primary metabolic pathways for 2-thiosugar biosynthesis. *Nature* **2014**, *510* (7505), 427–431.
- (23) Wright, C. M.; Christman, G. D.; Snellinger, A. M.; Johnston, M. V.; Mueller, E. G. Direct evidence for enzyme persulfide and disulfide intermediates during 4-thiouridine biosynthesis. *Chem. Commun.* **2006**, *29*, 3104–3106.
- (24) Hänzelmann, P.; Dahl, J. U.; Kuper, J.; Urban, A.; Müller-Theissen, U.; Leimkühler, S.; Schindelin, H. Crystal structure of YnjE from *Escherichia coli*, a sulfurtransferase with three rhodanese domains. *Protein Sci.* **2009**, *18* (12), 2480–2491.
- (25) Goldschmidt, L.; Cooper, D. R.; Derewenda, Z. S.; D, E. Toward rational protein crystallization: A Web server for the design of crystallizable protein variants. *Protein Sci.* **2007**, *16* (8), 1569–1576.
- (26) Long, F.; Vagin, A. A.; Young, P.; Murshudov, G. N. BALBES: a molecular-replacement pipeline. *Acta Crystallogr., Sect. D: Biol. Crystallogr.* **2008**, *64*, 125–132.
- (27) Dougherty, D. A. The Cation  $\pi$  Interaction. *Acc. Chem. Res.* **2013**, *46* (4), 885–893.
- (28) Mahadevi, A. S.; Sastry, G. N. Cation  $\pi$  Interaction: Its Role and Relevance in Chemistry, Biology, and Material Science. *Chem. Rev.* **2013**, *113* (3), 2100–2138.
- (29) Ziegler, C.; Bremer, E.; Krämer, R. The BCCT family of carriers: from physiology to crystal structure. *Mol. Microbiol.* **2010**, *78* (1), 13–34.
- (30) Steudel, R.; Steudel, Y. Derivatives of cysteine related to the thiosulfate metabolism of sulfur bacteria by the multi-enzyme complex "Sox"-studied by B3LYP-PCM and G3X(MP2) calculations. *Phys. Chem. Chem. Phys.* **2010**, *12* (3), 630–644.
- (31) Amyes, T. L.; Diver, S. T.; Richard, J. P.; Rivas, F. M.; Toth, K. Formation and Stability of N-Heterocyclic Carbenes in Water: The Carbon Acid pK<sub>a</sub> of Imidazolium Cations in Aqueous Solution. *J. Am. Chem. Soc.* **2004**, *126* (13), 4366–4374.
- (32) Cipollone, R.; Ascenzi, P.; Visca, P. Common Themes and Variations in the Rhodanese Superfamily. *IUBMB Life* **2007**, *59* (2), 51–59.
- (33) Park, C. M.; Weerasinghe, L.; Day, J. J.; Fukuto, J. M.; Xian, M. Persulfides: current knowledge and challenges in chemistry and chemical biology. *Mol. Biosyst.* **2015**, *11* (7), 1775–1785.
- (34) Breslow, R. On the Mechanism of Thiamine Action. Evidence from Studies on Model Systems. *J. Am. Chem. Soc.* **1958**, *80* (14), 3719–3726.
- (35) Meyer, D.; Neumann, P.; Ficner, R.; Tittmann, K. Observation of a stable carbene at the active site of a thiamin enzyme. *Nat. Chem. Biol.* **2013**, *9*, 488–490.
- (36) Retey, J. The urocanase story: a novel role of NAD<sup>+</sup> as electrophile. *Arch. Biochem. Biophys.* **1994**, *314* (1), 1–16.
- (37) Graminski, G. F.; Zhang, P. H.; Sesay, M. A.; Ammon, H. L.; Armstrong, R. N. Formation of the 1-(S-glutathionyl)-2,4,6-trinitrocyclohexadienolate anion at the active site of glutathione S-transferase: evidence for enzymic stabilization of sigma-complex intermediates in nucleophilic aromatic substitution reactions. *Biochemistry* **1989**, *28* (15), 6252–6258.
- (38) Johnson, C. M.; Monzingo, A. F.; Ke, Z.; Yoon, D. W.; Linsky, T. W.; Guo, H.; Robertus, J. D.; Fast, W. On the mechanism of

dimethylarginine dimethylaminohydrolase inactivation by 4-halopyridines. *J. Am. Chem. Soc.* **2011**, *133* (28), 10951–10959.

(39) Hedstrom, L. IMP Dehydrogenase: Structure, Mechanism, and Inhibition. *Chem. Rev.* **2009**, *109*, 2903–2928.

(40) Clayden, J.; Greeves, N.; Warren, S. *Organic Chemistry*, 2nd ed.; Oxford University Press Inc.: Oxford, U.K., 2012.

(41) Dahl, J. U.; Urban, A.; Bolte, A.; Sriyabhaya, P.; Donahue, J. L.; Nimtz, M.; Larson, T. J.; Leimkühler, S. The identification of a novel protein involved in molybdenum cofactor biosynthesis in *Escherichia coli*. *J. Biol. Chem.* **2011**, *286* (41), 35801–35812.

---

---



## 5 Probing the Substrate-Substrate Interaction in Type I and Type II EgtB Catalysis

### 5.1 Introduction

The ergothioneine biosynthetic enzyme EgtB catalyzes oxidative carbon-sulfur bond formation between *N*- $\alpha$ -trimethyl histidine (TMH) and a cysteinyl substrate in aerobic ergothioneine biosynthesis (**figure 21**).<sup>84,87,98</sup> Ergothioneine (**1**) is a 2-thioimidazole and *N*- $\alpha$ -trimethylated derivative of histidine with antioxidant properties synthesized by a myriad of microorganisms.<sup>90,99</sup> Although Ergothioneine's antioxidant properties have been demonstrated *in vitro*, the precise mechanism of action *in vivo* is still not fully understood.<sup>99</sup> However, various studies indicate that ergothioneine has a cytoprotective role, while disruption of the ergothioneine biosynthetic pathway leads to an increased vulnerability toward oxidative stress.<sup>90,91</sup>

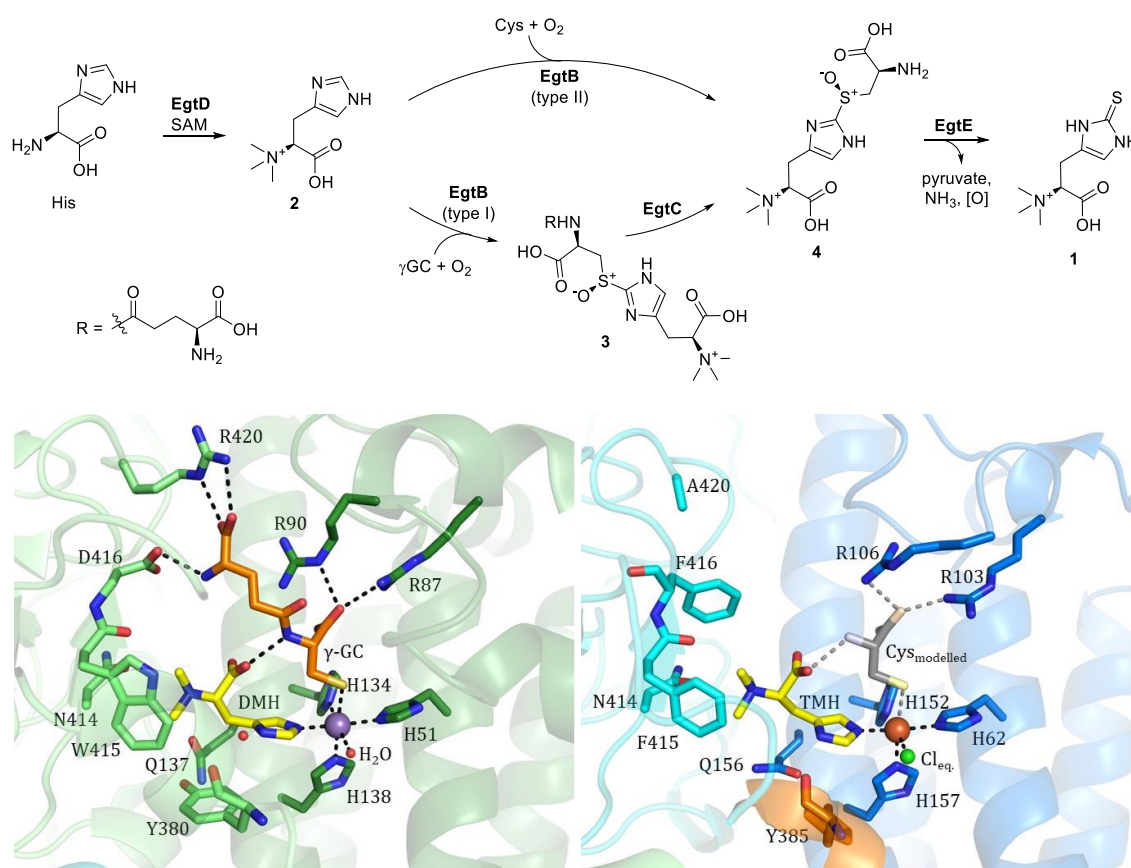


**Figure 21. Top:** Aerobic biosynthesis of ergothioneine. Trimethylation of histidine by EgtD is the first step and common for all pathways. Type I EgtBs catalyze the C-S bond formation between TMH (**2**) and  $\gamma$ GC and the subsequent sulfoxidation to form sulfoxide **3**. The glutamyl moiety is cleaved by the NTN-hydrolase EgtC to form sulfoxide **4**. Type II EgtBs catalyze the C-S bond formation between TMH (**2**) and cysteine and the subsequent sulfoxidation to produce sulfoxide **4**. The amino acid moiety is eliminated in the final step by the PLP dependent lyase EgtE to form ergothioneine (**1**). **Bottom left:** Crystal structure of MthEgtB with bound DMH,  $\gamma$ -GC and manganese (4X8D). (Adapted from Stampfli et al.<sup>87</sup>). **Bottom right:** Crystal structure of CthEgtB with bound TMH (4QKJ). Cysteine is model into the structure based on the structure of MthEgtB with bound  $\gamma$ -GC and DMH (Adapted from Stampfli et al.<sup>87</sup>).

---

EgtB is a member of a new class of nonheme iron-dependent enzymes. Considering that catalyzed C-S bond formation and simultaneous sulfoxidation was unprecedented and that direct C-H to C-S bond transformations are not common, a special interest arose to understand the catalytic mechanism of EgtB. Different studies investigated the mechanistic peculiarity through the use of kinetic, structural and computational methods.<sup>84–86,100,101</sup> Recent efforts by Stampfli *et al.*<sup>87</sup> in understanding the catalytic mechanism of EgtB and its evolutionary origin resulted into the classification of EgtBs into five types. All types are expected to use TMH as the histidyl substrate. The main differences between the different types of EgtB are the primary structure, the cysteinyl substrate and the cysteinyl substrate binding mode. Type I EgtBs use  $\gamma$ -glutamyl cysteine ( $\gamma$ GC) as a sulfur donor, type II-IV use cysteine and type V EgtBs use a currently unknown sulfur donor. The variability in substrates and their binding mode is interesting as enzymes with the same catalytic activity often share similar active site architectures and substrate binding modes.<sup>102</sup> As suggested by Stampfli *et al.*<sup>87</sup>, the diversity indicates that the ancestral enzyme (type 0 EgtB) used a different sulfur donor. Perhaps when this substrate became scarce, enzymes had to adapt to use other available sulfur donors.

Crystal structures of a type I EgtB from *Mycobacterium thermoresistibile* (*MthEgtB*) could be solved in the presence of *N*- $\alpha$ -dimethyl histidine (DMH) and  $\gamma$ GC (*bottom left, figure 21*). The protein was crystallized with manganese in absence of iron to obtain an unreactive EgtB:Mn:DMH: $\gamma$ -GC complex. In combination with kinetic experiments, this structure gave insight into the catalytic mechanism and binding mode of the substrates of *MthEgtB*.<sup>84</sup> The structure suggested various important interactions between  $\gamma$ -GC and the EgtB:Mn:DMH complex. The cysteinyl moiety of  $\gamma$ -GC makes three interactions: (i) ion pairing of the carboxylate to R87 and R90, (ii) coordination of the thiolate to the active site Mn(Fe)-ion, and (iii) a hydrogen bond of the  $\alpha$ -amino group to the carboxylate of DMH. In addition to that, there are two interactions from the glutamyl moiety: (i) a salt bridge of the  $\alpha$ -aminogroup to D416 and (ii) a salt bridge of the carboxylate to R420. The importance of the interaction of the glutamyl  $\alpha$ -amino group to D416 has been demonstrated in a previous publication by Goncharenko *et al.*<sup>84</sup> Both, the use of a substrate analog missing the glutamyl amino group, *N*-glutaryl cysteine (NGC), and the use of a *MthEgtB*<sub>D416N</sub> mutant lead to a more than 100-fold increase of cysteinyl  $K_M$ . NGC, on the other hand, had the higher affinity to the mutant than  $\gamma$ GC.

Recently, a structure of a type II EgtB from *Chloracidobacterium thermophilum* (*CthEgtB*) could be solved in presence of TMH (*bottom right, figure 21*).<sup>87</sup> Unfortunately, no structure with cysteine bound could be solved. Cysteine was modeled into the *CthEgtB*:TMH complex based on the structure of *MthEgtB*:DMH: $\gamma$ -GC. According to this model, cysteine is expected to make three interactions with the EgtB:TMH complex: (i) ion bonding of the carboxylate to

R106 and R103, (ii) coordination of the thiolate to the active site Fe-ion, and (iii) a salt bridge of the  $\alpha$ -amino group to the carboxylate of TMH (*bottom right, figure 21*). However, no experimental data has been obtained to support this binding model yet.

In this study we designed a series of substrate analogs to probe the role of the substrate-substrate interaction for binding of the cysteinyl substrates to type I and type II EgtBs. Furthermore, we designed bisubstrates to demonstrate the central role of this interaction for binding and catalysis. These substrate analogs revealed that precise substrate positioning is essential for the sulfoxide synthase activity but less for the dioxygenase activity.

## 5.2 Results

### 5.2.1 Probing the Substrate-Substrate Interaction for Binding and Catalysis

An analog of each substrate was designed to probe the substrate-substrate interaction (top, **figure 22**). An amide derivative of TMH (TMHA, **figure 22**), an  $\alpha$ -hydroxy derivative of cysteine (CysOH, **figure 22**) and an ester derivative of  $\gamma$ -GC ( $\gamma$ -GC-ester, **figure 22**) were synthesized. Turning the carboxylate of TMH into an amide turns a good hydrogen bond acceptor into a good hydrogen bond donor and acceptor. Since the negative charge carboxylate is removed, TMHA cannot form a salt bridge with cysteinyl carboxylate. Replacing the amino group of cysteine with a hydroxy group basically leads to the same result. The hydroxy group is a hydrogen bond donor and acceptor but cannot form a salt bridge. On the other hand, replacing the amide of  $\gamma$ -GC with an ester turns a good hydrogen bond donor into a poor hydrogen bond acceptor.<sup>103</sup>

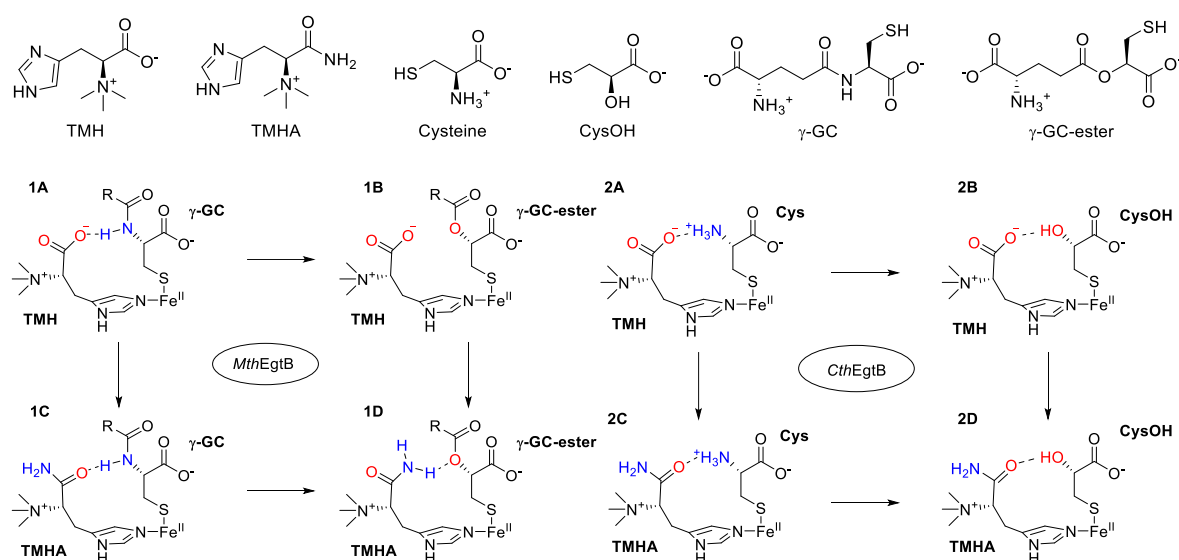


**Figure 22.** Top: Substrates analogs used for probing the substrate-substrate interactions of MthEgtB and CthEgtB. Bottom left: Substrate pairs for MthEgtB. Bottom right: Substrate pairs for CthEgtB.

**Table 1.** Michaelis-Menten parameters for CthEgtB and MthEgtB with natural substrates and analogues.

Complex	Enzyme	Donor	Acceptor	$K_M, \text{donor}$ [ $\times 10^{-6}$ M]	$k_{cat, \text{sulfoxide}}$ [ $\text{s}^{-1}$ ]	$k_{cat}/K_M$ [ $\text{s}^{-1}\text{M}^{-1}$ ]
<b>1A</b>	<i>MthEgtB</i>	$\gamma$ GC	TMH	$32 \pm 2$	$0.63 \pm 0.014$	$19000 \pm 1500$
<b>1B</b>	<i>MthEgtB</i>	$\gamma$ GOC	TMH	$2400 \pm 300$	$0.34 \pm 0.024$	$140 \pm 30$
<b>1C</b>	<i>MthEgtB</i>	$\gamma$ GC	TMHA	$5400 \pm 1300$	$0.1 \pm 0.01$	$19 \pm 5$
<b>1D</b>	<i>MthEgtB</i>	$\gamma$ GOC	TMHA	-	-	$29 \pm 1$
<b>2A</b>	<i>CthEgtB</i>	Cysteine	TMH	$40 \pm 3$	$0.057 \pm 0.001$	$1400 \pm 110$
<b>2B</b>	<i>CthEgtB</i>	CysOH	TMH	$680 \pm 70$	$0.0099 \pm 0.0003$	$15 \pm 2$
<b>2C</b>	<i>CthEgtB</i>	Cysteine	TMHA	$1200 \pm 200$	$0.0056 \pm 0.0004$	$4.7 \pm 0.9$
<b>2D</b>	<i>CthEgtB</i>	CysOH	TMHA	$79 \pm 34$	$0.024 \pm 0.04$	$310 \pm 140$

The different substrate combinations result in the formation of different types of substrate-substrate interactions. The substrate pairs for *MthEgtB* are depicted in **figure 22**, bottom left. **1A** (*MthEgtB*:TMH: $\gamma$ -GC) is the native substrate pair with an expected strong inter-substrate hydrogen bond. No hydrogen bonding is possible in **1B** (*MthEgtB*:TMH: $\gamma$ -GC-ester) as there is no hydrogen bond donor for this substrate combination. In contrast, a hydrogen bond between the two substrates is possible in **1C** (*MthEgtB*:TMHA: $\gamma$ -GC) and **1D** (*MthEgtB*:TMHA: $\gamma$ -GC-ester). In **1C** a strong hydrogen bond could be formed, while only a very weak hydrogen bond is expected for **1D**, as the single bonded oxygen of  $\gamma$ -GC-ester is a poor hydrogen bond acceptor.

The substrate pairs for *CthEgtB* are depicted in **figure 22**, bottom right. Again, **2A** (*CthEgtB*:TMH:Cysteine) is the native substrate pair with an expected strong salt bridge. In all other cases (**2B-2D**), the salt bridge is turned into a hydrogen bond.

The catalytic activity of all the different substrate pairs was characterized using the established HPLC-based kinetic assay described in previous publications (**table 1**).<sup>84,87,104</sup> Reaction products were analyzed by IE-HPLC, NMR and HRMS. The  $k_{cat}$  for sulfoxide production and the  $K_M$  for the cysteinyl substrate were determined at saturating concentration of the histidyl substrate and varying concentrations of the cysteinyl substrate.

Michaelis-Menten kinetics were measured to probe the role of the substrate-substrate hydrogen bond in *MthEgtB* (**table 1**). The kinetic parameters for the native substrate pair (**1A**) were measured first and are in agreement with previously measured data.<sup>84</sup> The  $K_M$  for the thiol substrates increases 100-fold when the  $\gamma$ -GC-ester was used in combination with TMH (**1B**). This effect was expected as the substrate pair is missing a hydrogen bond donor. When TMHA was used in combination with  $\gamma$ -GC (**1C**) a similar change in  $K_M$  (200-fold) was observed. In fact, a hydrogen bond between these two substrates is possible and the 200-fold increase in  $K_M$  is higher than expected. A hydrogen bond between the amide of TMHA and the oxygen of the ester can be formed when the two substrate analogs are paired (**1D**). This hydrogen bond is expected to be weaker than the original amide to carboxylate hydrogen

bond, as the lone pairs of the ester oxygen are delocalized into the carbonyl oxygen. No full catalytic characterization could be obtained for this substrate pair as inhibition by the  $\gamma$ -GC-ester was observed at high concentrations. Nevertheless, the catalytic efficiency ( $k_{cat}/K_M$ ) was determined to be in the same range as the catalytic efficiency for the other two non-native substrate pairs.

*Michaelis-Menten* parameters were also determined for the different substrate pairs of *CthEgtB* (**table 1**). As for *MthEgtB*, the native substrate pair was measured first (**2A**) and the obtained data is in good agreement with previously measured data.<sup>87</sup> A more than tenfold increase in  $K_M$  was observed when CysOH was used in combination with TMH (**2B**). An even larger increase of  $K_M$  (30-fold) was observed when TMHA was used in combination with cysteine (**2C**). The combination of the two substrate analogs (**2D**) resulted in a two-fold increase of  $K_M$  for CysOH compared to cysteine in the natural substrate pair.

For *CthEgtB*, an effect on  $k_{cat}$  could be observed in a similar range as the effect on  $K_M$ , indicating that the strength of the bond between the two substrates has an influence on catalysis. A possible explanation is that salt bridges are generally shorter than hydrogen bonds and therefore the ternary complex might be perturbed.<sup>105</sup> A decrease of  $k_{cat}$  was observed to a smaller extent for *MthEgtB*. The glutamyl moiety of the  $\gamma$ -GC substrates could lock the substrate tighter into the active site. Even if the substrate-substrate interaction is weakened, the position of the thiolate might not change.

EgtBs produce cysteine dioxide as a side product. The dioxygenation reaction is assumed to be more facile than the sulfoxide synthase reaction and only a specific active site configuration can channel the reaction towards the sulfoxide formation.<sup>87</sup> Perturbing the active site can result in derailing the reaction towards dioxide formation.<sup>85,87</sup> Hence, the ratio between the two products is an important parameter to judge if *Michaelis-Menten* complex is impaired. Therefore, the product distributions were assessed by <sup>1</sup>H NMR for the native substrate pair (**2A**, **figure 22**) and the two substrate analog pair of *CthEgtB* (**2D**, **figure 22**). Indeed, the product distribution is unaffected in the *CthEgtB*:TMHA:CysOH complex (**2D**).

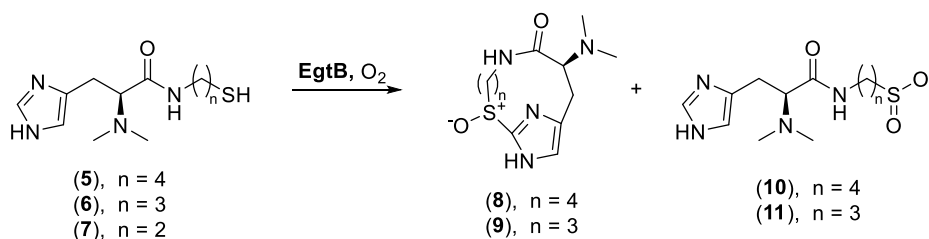


**Figure 23.** Reaction scheme with the linked substrates. The imidazole moiety and the thiolate were separated by different length alkyl chains (2-4 carbons). For the shortest substrate (2 carbons, **7**) no reaction was observed for either enzyme.

**Table 2.** Michaelis-Menten parameters for *CthEgtB* and *MthEgtB* with the linked substrates.

Enzyme	Substrate	$K_M$ [ $\times 10^{-6}$ M]	$k_{cat, \text{ sulfoxide}}$ [ $s^{-1}$ ]	$k_{cat, \text{ sulfinic acid}}$ [ $s^{-1}$ ]	$k_{cat}/K_M$ [ $s^{-1}M^{-1}$ ]	Sulfoxide/ $Product_{total}$
<i>CthEgtB</i>	<b>5</b>	$75 \pm 3$	$0.13 \pm 0.002$	$0.03^a$	$1700 \pm 100$	0.8
<i>CthEgtB</i>	<b>6</b>	12	$0.0021 \pm 0.0001$	$0.01^a$	$670 \pm 200$	0.2
<i>CthEgtB</i>	<b>7</b>	no reaction observed				
<i>MthEgtB</i>	<b>5</b>	$240 \pm 20$	$0.0005^b$	$0.020 \pm 0.001$	$83 \pm 12$	0.03
<i>MthEgtB</i>	<b>6</b>	$180 \pm 10$	$0.019 \pm 0.002$	$0.08^a$	$100 \pm 3$	0.2
<i>MthEgtB</i>	<b>7</b>	no reaction observed				

<sup>a</sup> Values were estimated from the measured rate of sulfoxide production and the observed product distribution. <sup>b</sup> Value was estimated from the measured rate of sulfinic acid production and the observed product distribution.

### 5.2.2 Bisubstrate analogs as substrates for EgtB

Bisubstrates are conjugated fragments making interactions between two binding sites of a multisubstrate enzyme.<sup>106</sup> Bisubstrate compounds are often used as enzyme inhibitors, having the advantage to make more interactions than a single site inhibitor. Additionally, the entropic penalty for binding a single substrate is smaller than the penalty for binding two substrates. Motivated by the finding that good binding and proper catalysis can be achieved with different types of substrate-substrate interactions we hypothesized that the non-covalent substrate interaction could be converted to a covalent bond, creating a bisubstrate analog, without perturbing binding and catalysis. The simplest bisubstrates are aminoalkylthiols linked through an amide bond to the carboxylate of TMH. The crystal structure of *MthEgtB* with bound substrates reveals a distance between the carbonyl carbon of TMH and the thiolate of cysteine which corresponds to the length which can be spanned by four methylene groups (**5**, **figure 23**). Additionally, two shorter bisubstrates were synthesized, one linked through three methylene groups (**6**) and one linked through two methylene groups (**7**). The shorter linker should increase the strain on the bicyclic system formed during catalysis, thereby perturbing the reaction. Kinetic parameters for the bisubstrates were determined for both EgtB variants by the same HPLC-kinetic assay previously described. Product distributions were determined by <sup>1</sup>H NMR (**table 2**).

The four-carbon linked substrate (**5**) is a good substrate for *CthEgtB* with a  $k_{cat}$  ( $0.13 s^{-1}$ ) similar to the genuine substrates. The  $K_M$  increases only two-fold (to  $75 \mu M$ ) compared to the  $K_M$  of cysteine and TMH. Furthermore, the product distribution is identical, judging by NMR and HPLC. The reaction becomes strongly perturbed when the linker is one methylene group shorter (three-carbon linked substrate, **6**). Both, the  $k_{cat, \text{ sulfoxide}}$  ( $0.003 s^{-1}$ ) and the product distribution (20% sulfoxide) are affected. In contrast the  $K_M$  is decreased six-fold ( $12 \mu M$ ). No reaction could be observed when the two-carbon linked substrate (**7**) was used.

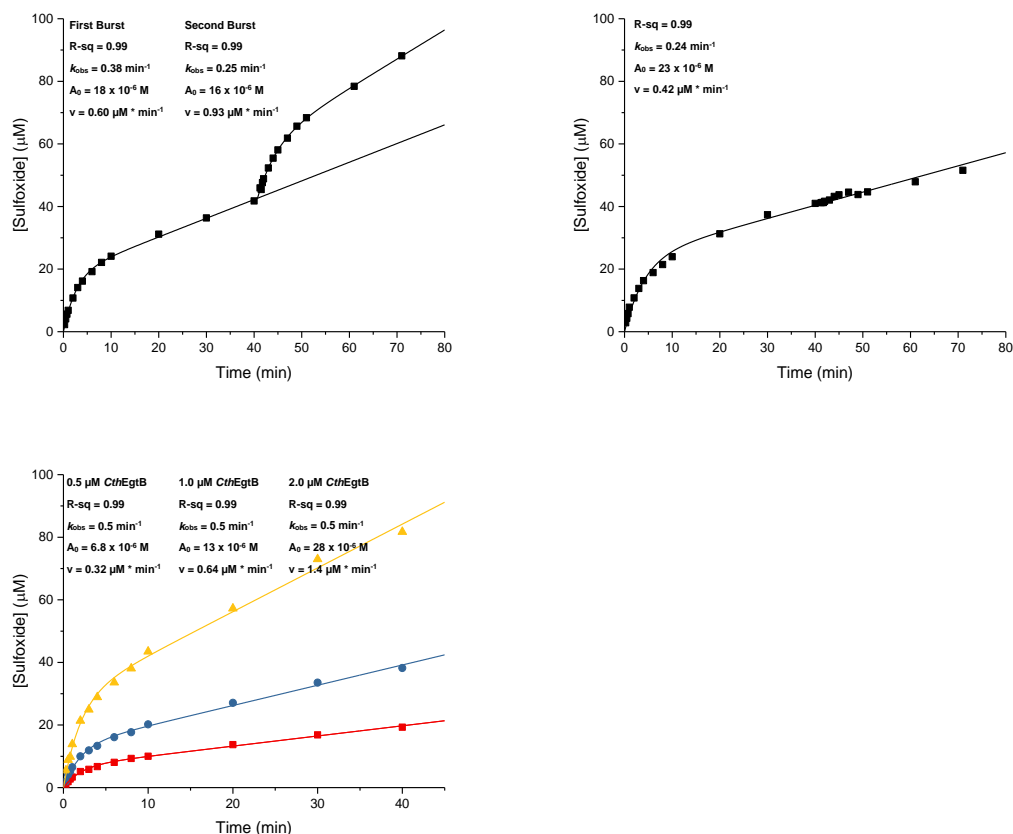


**Figure 24.** Top left: Pre steady state kinetics with 1 μM CthEgtB and 1 mM bisubstrate 5. Addition of 1 eq. of CthEgtB after 41 min. Top right: control, water added after 41 min. Bottom: Pre steady state kinetics with different concentrations of CthEgtB and 1 mM bisubstrate 5, [CthEgtB] = 0.5 μM, 1 μM or 2 μM.

The same reactions were performed with *MthEgtB*. The four-carbon (5) and the three-carbon linked (6) analogs are substrates. The  $K_M$ 's are five-fold larger than for the genuine substrates, which is reasonable as the whole glutamyl moiety is missing, which makes several important interactions to the enzyme for γ-GC.<sup>84</sup> Furthermore, the  $k_{\text{cat, sulfoxide}}$  for both substrates are 30-1000-fold lower than observed for the *MthEgtB*:TMH:γ-GC complex and the product distribution is shifted towards the sulfinic acid for both substrates (3% sulfoxide for 5, 20% sulfoxide for 6). Again, no reaction was observed for the two-carbon linked analog (7).

As described above, the four-methylene group linked substrate (5) is a good substrate for *CthEgtB*. However, a burst phase was observed at the beginning of the reaction, during which approximately 15 equivalents of sulfoxide, relative to the enzyme concentration, are formed. The reaction rate is reduced by ten-fold after this burst phase. To test whether the inactivation is due to product inhibition, fresh enzyme was added to the reaction after 40 minutes. A second burst could be observed with almost identical parameters as the initial burst (top, figure 24). Hence, product inhibition can be ruled out. Additionally, the reaction was run with different enzyme concentrations to see if inactivation is dependent on the enzyme concentration (bottom, figure 24). The inactivation rate is independent of the enzyme concentration. One

---

reason for the inactivation could be that the enzyme gets modified during catalysis. To test this hypothesis the enzyme was incubated with and without substrate **5** and analyzed by HRMS in attempts to detect any covalent modifications on the protein. However, no modifications could be observed, ruling out an irreversible modification of the enzyme.

## 5.3 Discussion

### 5.3.1 Substrate-substrate interaction

The kinetic data for *MthEgtB* with the substrate analogs revealed some important points. As expected, the  $\gamma$ -GC-ester has a low affinity for both the EgtB:TMH and EgtB:TMHA complexes. This strongly supports the idea that the intersubstrate hydrogen bond is important for the binding of  $\gamma$ -GC. The absence of a hydrogen bond donor or acceptor cannot be compensated by the other interactions between the substrate and the enzyme. More surprising was the low affinity of  $\gamma$ -GC for the EgtB:TMHA complex as amides are in general excellent hydrogen bond acceptors. Amide-amide hydrogen bonds are common and essential for defining protein secondary and tertiary structure.<sup>107</sup> An explanation for the low affinity of  $\gamma$ -GC to the EgtB:TMHA complex could be that TMHA tries to align the dipole of the amide functional group with the trimethyl ammonium group thereby forming a polar interaction between the polarized methyl group of the trimethylammonium and the amide carbonyl (**A, figure 25**). This would lead to a EgtB:TMHA complex in which the amide NH<sub>2</sub> would point toward the cysteinyl binding sight so that the two hydrogen bond donors would face each other.

In contrast, kinetic data for *CthEgtB* is more surprising. As previously mentioned, all the different substrate pairs can form intersubstrate hydrogen bonds. Generally, it is not trivial to predict hydrogen bond strength, but it is expected that a salt bridge is strong.<sup>105</sup> The fact that a similar binding affinity has been observed for a normal hydrogen bond between an alcohol and an amide as for the native salt bridge and a lower affinity was observed for the two pairs where a charged to polar residue hydrogen bond can be formed could be explained in two ways. A similar explanation as for *MthEgtB* could be used. The TMHA might prefer a conformation in which the negatively polarized carbonyl interacts with the polarized hydrogen of the trimethyl ammonium group and the hydrogen bond donor would point toward the cysteine binding site. Hence, no interaction with the cysteine ammonium group would be possible (**B, figure 25**). In the *CthEgtB*:TMH:CysOH complex, CysOH should be the hydrogen bond donor. The hydrogen of the alcohol is expected to interact with the carboxylate forming a five membered ring (**C, figure 25**). The intramolecular hydrogen bond should become stronger when CysOH enters the active site and thereby is desolvated. This leaves no hydrogen bond donor for the substrate-substrate hydrogen bond and therefore the increase



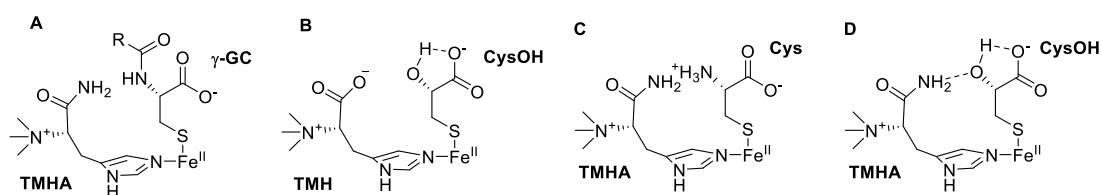


**Figure 25.** Possible interactions of TMHA and CysOH substrate analogs that could explain the lower affinities.

of  $K_M$  could be explained. The EgtB:TMHA:CysOH complex could still form a substrate-substrate interaction (**D, figure 26**), with the hydrogen bond donor and acceptor swapped.

Another possible explanation for higher affinity of the cysteinyl substrate in the EgtB:TMHA:CysOH complex comparing to the affinity in the EgtB:TMH:CysOH and EgtB:TMHA:Cys complexes is that the penalty for burying a charge in the hydrophobic environment of a protein is usually large and hence the pairing of two opposite charges is advantageous and results in strong interactions. Removing the charge completely removes the energetic penalty and a stronger bonding is achieved (**D, figure 25**).<sup>107,108</sup>

The data indicates that the interaction between the two substrates contributes an important part to the binding of the cysteinyl substrate for both enzymes. Perturbing this interaction increases the  $K_m$  of the cysteinyl substrate to physiologically irrelevant concentrations and thereby contributes to prevent binding of the cysteinyl substrate prior to TMH binding, which would lead to substrate inhibition.

The fact that replacement of the salt bridge by a covalent bond can almost compensate for the lack of the other interactions underlines the importance of this bond. *CthEgtB* does not require any additional ion pairing of the cysteine carboxylate to R103 and R106 to form a productive complex. On the other hand, the covalent bond cannot fully compensate for the loss of the whole glutamyl moiety. Both, the  $k_{cat, sulfoxide}$  and the  $K_M$  are worse than for the native substrates. Considering that the addition of these interaction could increase the affinity of the bisubstrates by an order of magnitude or more, the bisubstrates are a good template for the design of potent inhibitors of EgtB. Such inhibitors could be used for co-crystallization with *CthEgtB*.

### 5.3.2 Precise substrate positioning is essential for sulfoxide synthase activity

The mutation of the catalytic tyrosine (Y377) of *MthEgtB* to a phenylalanine lead to inactivation of the sulfoxide synthase activity with concomitant acceleration of the dioxygenase activity.<sup>85</sup> The same was observed when catalytic tyrosine (Y93) of *CthEgtB* was mutated to a phenylalanine. This effect is attributed to the changed polarity around the oxygen binding site and the absence of the catalytic acid which is responsible for protonation of the superoxide.<sup>87,104</sup> Another study investigated the cysteine dioxygenase activity with histidyl substrates which are blocked at the 2-position (2-amino or 2-methylhistidine).<sup>109</sup> This study shows that the shutdown of the sulfoxide synthase pathway does not lead to an increase of the

---

dioxygenase activity. The linked substrates provide another system which perturbs the sulfoxide synthase activity more than the dioxygenase activity. The system is especially interesting since the enzyme and the reactive moieties (thiol and imidazole) are unchanged.

The formation of an initial reactive enzyme/substrate complex (EgtB:Fe:TMH:cysteiny substrate:O<sub>2</sub>) and the formation of a superoxide radical is the basis of all current mechanistic proposals. In the catalytic model proposed for *CthEgtB* by Stampfli *et al.*<sup>87</sup>, a preequilibrium between the superoxide radical (**1, figure 26**) and the hydroperoxyl anion/thiyl radical (**2, figure 26**) exists. The subsequent C-S bond formation to produce a thioether intermediate (**3, figure 26**) is assumed to be irreversible. A proton transfer (PT) from the imidazole C2 to the tyrosine (**4, figure 26**) and subsequent oxygen atom transfer (OAT) lead to the product sulfoxide (**5, figure 26**). Direct oxygen atom transfer (**6, figure 26**) from the superoxide radical complex (**1, figure 26**) leads to dioxygenation *via* the CDO pathway.<sup>86</sup>

A change in the bisubstrate linker length perturbed the sulfoxidation reaction much stronger than the dioxygenation reaction. This indicates that the decrease of  $k_{cat, sulfoxide}$  does not result from a perturbation of the formation reactive complex and oxygen activation, otherwise both reactions should be affected identical. Furthermore, the ratio between the two products is defined by the equilibria before the first irreversible steps after bifurcation of the pathway and the rates of these first irreversible steps. Everything which happens after these first irreversible steps cannot influence the product ratio and therefore must influence both pathway identically.<sup>109</sup> Assuming that C-S bond formation is the first irreversible step after bifurcation of the pathways, a decreased rate of the steps which follow later should decrease the rate of both reactions, the sulfoxidation and the dioxygenation. Hence, the only way to observe a much stronger decrease in the sulfoxidation rate compared to the dioxygenation rate is to perturb the first irreversible step after bifurcation, which is assumed to be the C-S bond formation. The perturbation of this step could result from the unprecise positioning of the thiyl radical and the imidazol ring. The C-S bond can only be formed when the sulfur and the imidazol C2 are proper aligned. Changing the linker length would lead to different binding angles which could result in less efficient C-S bond formation.

In *MthEgtB* C-S bond formation is more efficient if the linker is shorter. This might be due to the loss of flexibility. The lack of the glutamyl moiety introduced more flexibility to the substrate which might lead to difficulties for precise substrate positioning. The shorter the linker, the more strained is the system and the lower the flexibility. The initial hypothesis was that increasing strain in the formed bicyclic intermediate increases the energy for the proton abstraction, since proton abstraction leads to aromatization and should increase the ring strain even further. This is rather unlikely, as an increase of  $k_{cat, sulfoxide}$  was observed for *MthEgtB* when the linker length was decreased.

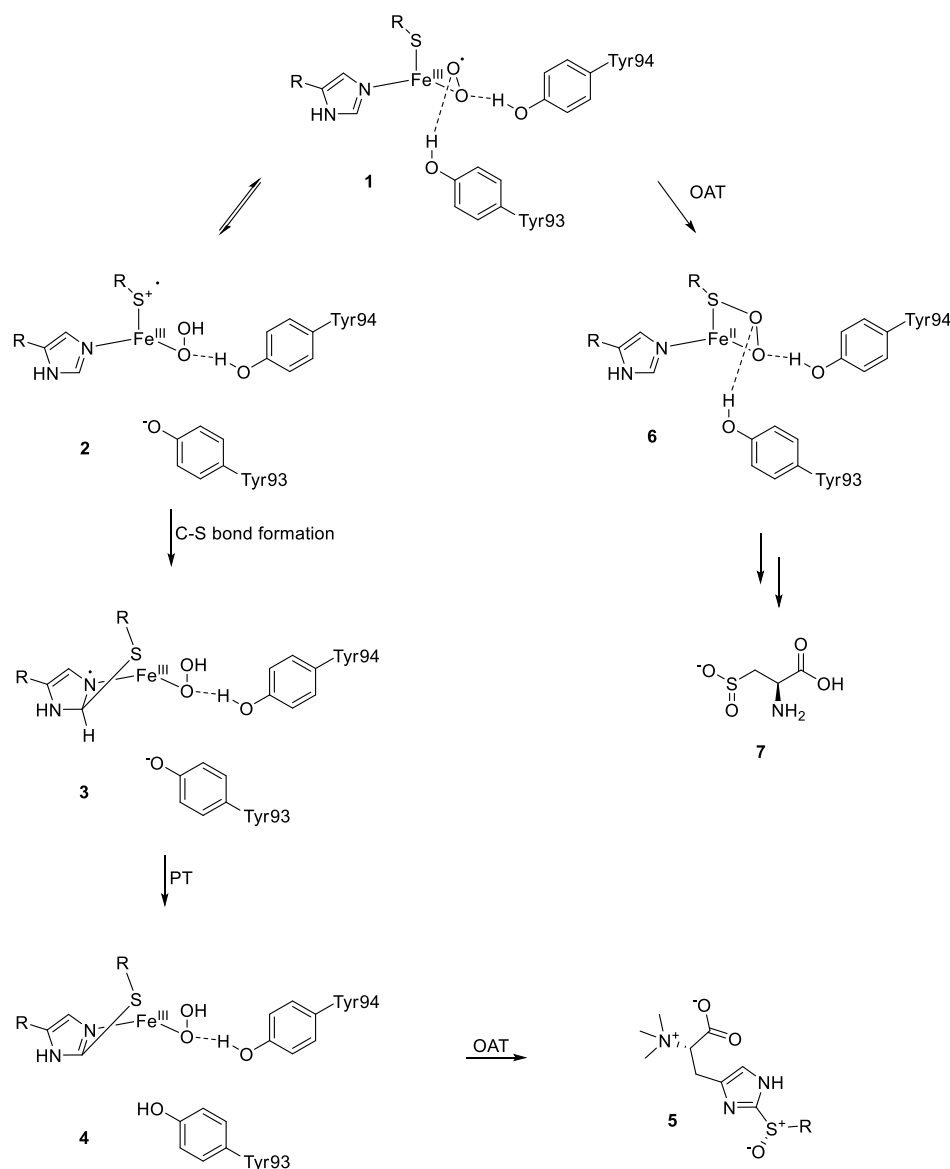


**Figure 26.** Suggested model for the bifurcation of the reactions catalyzed by EgtB. A small effect on the rate of dioxide formation was observed compared to the effect on the rate of the *sulfoxide* formation. This indicates that the pre-equilibrium is hardly changed, however the irreversible C-S bond formation is slowed down. A possible explanation for this is that even though the thiyl radical is formed, the C-S bond cannot be formed due to unprecise positioning sulfur atom relative to the C2 of the imidazole ring.

### 5.3.3 Inactivation of *CthEgtB* by the linked substrate

The observed inactivation of the enzyme is an interesting aspect and reflects the complexity of EgtB catalysis. The simplest explanation for a burst phase is slow product release. This is visualized on the kinetic mechanism of an enzyme with one substrate and two products (**figure 27**). The product ratio **P/Q** is determined by the microscopic rate constants  $k_3$ - $k_8$ . The microscopic rate constants  $k_9$ - $k_{12}$  influence the overall rate of both reactions. A burst phase for **P** can be observed if  $k_{10}$ - $k_{12}$  are rate limiting. If  $k_{10}$  is rate limiting, a lag phase for **Q** is observed while the burst phase of **P** has the magnitude of  $\mathbf{P/Q} \cdot \mathbf{E_{tot}}$ . If  $k_{12}$  is rate limiting, there is a burst phase for both products. During the burst phase **Q** accumulates to the concentration  $\mathbf{E_{tot}}$  and **P** to  $\mathbf{P/Q} \cdot \mathbf{E_{tot}}$ . There is also a burst phase for both products if  $k_{11}$  is rate limiting, however, the



## 5.5 Experimental Part

### Synthesis

**General.** All reagents used were purchased from commercial sources and used without further purification. All solvents used in reactions were purchased in HPLC-grade quality and used as such. Dry solvents were purchased in HPLC-grade quality and used as such. Chromatographic purifications (flash) were performed with SiliaFlash P60 from Silicycle (40-63  $\mu\text{m}$ ; (230-400) mesh). NMR spectra were acquired on a Bruker 400 MHz or a Bruker 500 MHz instrument.  $^1\text{H}$  and  $^{13}\text{C}$  chemical shifts are quoted relative to solvent signals unless for  $^{13}\text{C}$  NMRs in  $\text{D}_2\text{O}$  *t*-butanol was added as internal standard. ESI-MS spectra were obtained were obtained on a Bruker Esquire3000plus spectrometer by direct injection in positive polarity of the ion trap detector.

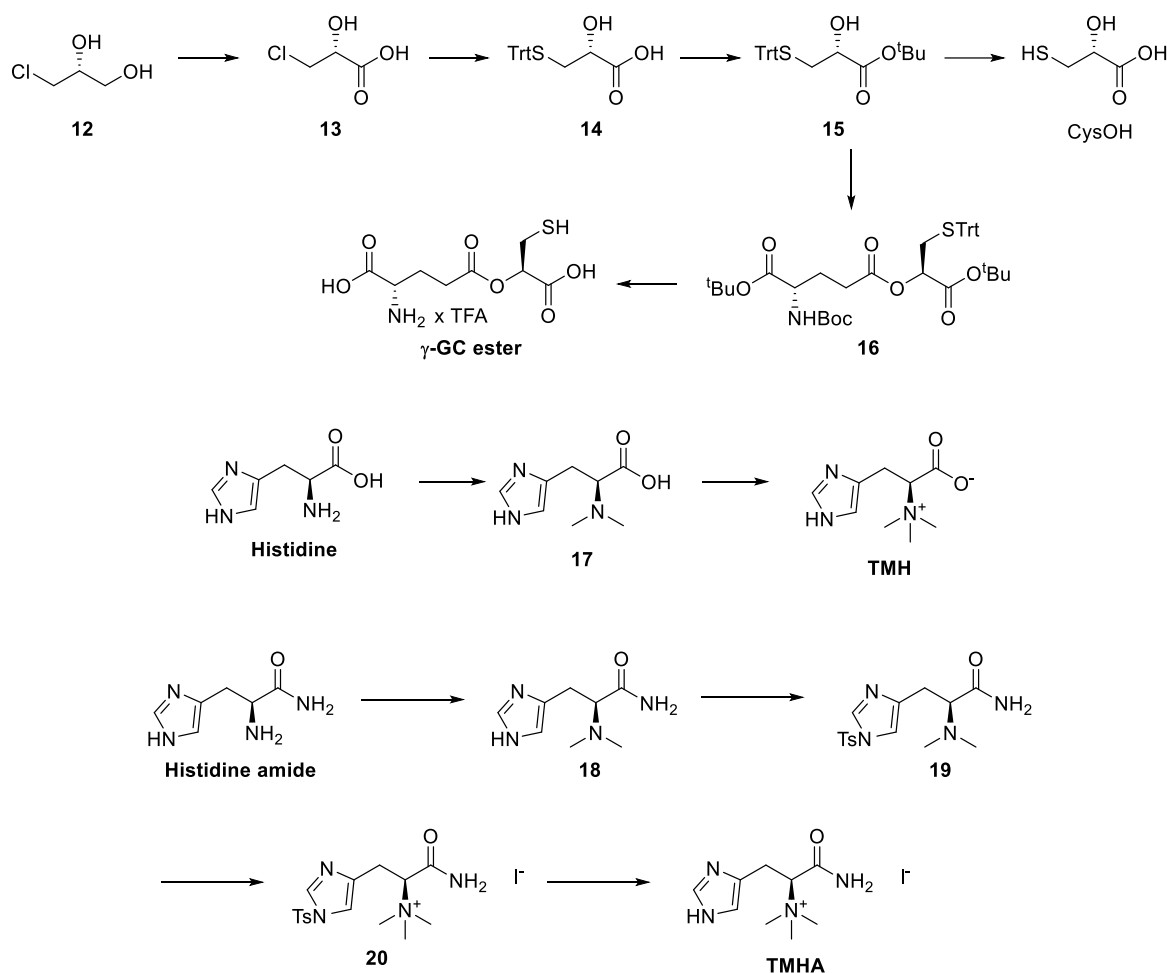


**Figure 28.** Synthesis of  $\gamma$ GC-ester, CysOH, TMH and TMHA.

**(R)-3-chloro-2-hydroxypropanoic acid (13).** The procedure was adopted from the one published by Gerfaud *et al.*<sup>111</sup> A two necked round bottom flask equipped with a magnetic stirring bar, a reflux condenser, and an addition funnel was charged with 3-chloro-1,2-

---

propanediol (5.00 g, 45.2 mmol, 1.0 eq.). The top of the condenser was fitted with a vacuum adapter which was connected to two washing bottles, the first empty to prevent the washing solution from being sucked into the reaction mixture, second with 100 ml 3 M NaOH aqueous solution cooled to 0°C to quench the acidic vapors. The addition funnel was charged with nitric acid (15.0 ml, 70% aqueous solution) and sealed with a septum. The flask and its content was heated to 80°C and some drops of nitric acid were added to initiate the reaction. After a few minutes dark orange-brown vapor arose. The remaining nitric acid was added over 10 min. Then the temperature of the oil bath was increased to 105 °C and the mixture was stirred for additional 3 hours at reflux. During this time, nitrogen was flushed through the apparatus *via* a needle through the septum of the addition funnel to ensure that all acidic vapors are bubbled through the NaOH solution. Then the oil bath was removed and when the mixture reached room temperature sodium bicarbonate (3.15 g) dissolved in water (18.0 ml) was added slowly to partially neutralize the nitric acid. The aqueous layer was saturated with NaCl and extracted with ethyl acetate (7 x 30 ml). The combined organic layers were dried over sodium sulfate. The solvent was evaporated by rotary evaporation (60 °C water bath temperature) and under high vacuum. The crude was recrystallized from boiling chloroform (70 ml). Crystals were collected by filtration to obtain the title compound as white, bright solid (2.57 g, 20.6 mmol, 46%). **<sup>1</sup>H NMR (400 MHz, methanol-d<sub>4</sub>, δ/ppm)** 4.43 (t, J = 4.2 Hz, 1H), 3.82 (dd, J = 4.2, 0.6 Hz, 2H).

**(R)-2-hydroxy-3-(tritylthio)propanoic acid (14).** The procedure was adopted from the one published by Wisniewski *et al.*<sup>112</sup> To a stirred solution of **13** (500 mg, 4.02 mmol, 1 eq.) dissolved in dry tetrahydrofuran (15 ml) sodium hydride (338 mg, 8.44 mmol, 2.1 eq.) was added portion wise at 0 °C. The mixture was stirred 5 minutes and then triphenylmethanethiol (1220 mg, 4.42 mmol, 1.1 eq.) was added portion wise. The cooling bath was removed, and the mixture was stirred overnight at room temperature. Then the solvent was removed *in vacuo* and the residue was 62ichlorom between water (25 ml) and ether (25 ml). The aqueous phase was washed with ether (2 x 25 ml), acidified with 1 M HCl and extracted with ethyl acetate (3 x 75 ml). The combined organic layers were dried over sodium sulfate. The solvent was evaporated *in vacuo* to yield the title compound as a white solid (1.38 g, 3.77 mmol, 93%). **<sup>1</sup>H NMR (400 MHz, CDCl<sub>3</sub>, δ/ppm)** 7.70 – 6.94 (m, 15H), 3.83 (dd, J = 7.3, 4.2 Hz, 1H), 2.77 (dd, J = 13.2, 4.2 Hz, 1H), 2.68 (dd, J = 13.2, 7.4 Hz, 1H). **ESI MS:** expected mass: [M-H]<sup>-</sup>=363.1, found: [M-H]<sup>-</sup>=363.0

***tert*-butyl (R)-2-hydroxy-3-(tritylthio)propanoate (15).** To a stirred solution of **14** (1.30 g, 3.57 mmol, 1.0 eq.) in ethyl acetate (18 ml) was added *tert*-butyl 2,2,2-trichloroacetimidate

---

(1.30 ml, 7.14 mmol, 2.0 eq) in cyclohexane (7.0 ml). The mixture was stirred overnight then the mixture was diluted with ethyl acetate and washed with sat. sodium bicarbonate (aq.), water and brine. The organic layer was dried over sodium sulfate and the solvent was removed *in vacuo*. The crude was purified by column chromatography (cyclohexane/ethyl acetate 9:1) to yield the title compound as white solid (590 mg, 1.40 mmol, 39%). **<sup>1</sup>H NMR (400 MHz, DMSO-d<sub>6</sub>, δ/ppm)** 7.46 – 7.14 (m, 16H), 5.57 (d, J = 6.0 Hz, 1H), 3.84 – 3.61 (m, 1H), 2.37 – 2.23 (m, 2H), 1.33 (s, 9H). **<sup>13</sup>C NMR (126 MHz, MeOD, δ/ppm)** 173.4, 146.1, 130.8, 128.9, 127.8, 82.8, 71.4, 67.7, 37.5, 28.2. **ESI MS:** [M+Na]<sup>+</sup> calculated: 443.17, found: 443.11.

**Synthesis of compound 16.**<sup>113</sup> To a stirred solution of **15** (50 mg, 0.119 mmol, 1.3 eq.) and Boc-Glu-*t*-Bu (28 mg, 0.092 mmol, 1.0 eq.) in dry dichloromethane (0.55 ml) was added DCC (20 mg, 0.096 mmol, 1.05 eq.) and DMAP (a tip of a spatula). After 3 hours the precipitate was filtered off and the filtrate was diluted with dichloromethane (10 ml), washed with sodium hydrogen sulfate (1 M, aq.) and dried over sodium sulfate. The solvent was removed *in vacuo*. The crude was purified by column chromatography (cyclohexane/ethyl acetate 9:1) to yield the product as a colorless oil (32.0 mg, 0.045 mmol, 50%). **<sup>1</sup>H NMR (400 MHz, CDCl<sub>3</sub>, δ/ppm)** 7.53 – 6.95 (m, 15H), 5.09 (d, J = 8.5 Hz, 1H), 4.61 (dd, J = 8.7, 3.9 Hz, 1H), 4.25 – 4.16 (m, 1H), 2.69 (dd, J = 13.1, 8.7 Hz, 1H), 2.57 – 2.37 (m, 3H), 2.24 – 2.09 (m, 1H), 1.91 (dddd, J = 14.1, 9.8, 8.4, 5.8 Hz, 1H), 1.45 (s, 9H), 1.43 (s, 9H), 1.37 (s, 9H). **<sup>13</sup>C NMR (126 MHz, MeOD, δ/ppm)** 173.3, 173.0, 169.1, 158.0, 145.7, 130.7, 129.1, 128.0, 83.8, 82.8, 80.5, 73.1, 68.2, 54.9, 34.1, 31.0, 28.8, 28.2, 27.8. **ESI MS:** [M+Na]<sup>+</sup> calculated: 728.32, found: 728.26

**Synthesis of γ-glutamyl cysteine ester derivative (γ-GC ester).**<sup>114</sup> A round bottom flask was charged with **16** (649 mg, 0.919 mmol, 1.0 eq.) under nitrogen atmosphere. To this solution was added propanethiol (2.0 ml), triethylsilane (0.3 ml) and trifluoroacetic acid (2.0 ml). The mixture was stirred overnight at room temperature. The solvent was removed under reduced pressure and co-evaporated with toluene (3 x 2.0 ml). The residual was suspended in water (5.0 ml) and washed with dichloromethane (3 x 5.0 ml). Then the aqueous phase was lyophilized. The product was isolated as white solid (332 mg, 0.91 mmol, 99%). **<sup>1</sup>H NMR (400 MHz, D<sub>2</sub>O, δ/ppm)** 5.01 (dd, J = 5.9, 4.3 Hz, 1H), 3.82 (dd, J = 6.9, 5.9 Hz, 1H), 2.99 – 2.87 (m, 2H), 2.72 – 2.51 (m, 2H), 2.33 – 1.97 (m, 2H). **<sup>13</sup>C NMR (101 MHz, D<sub>2</sub>O, *tert*-BuOH as internal standard, δ/ppm)** 175.6, 174.6, 174.4, 76.82, 54.5, 30.6, 26.1, 26.0. **ESI MS:** [M+H]<sup>+</sup> calculated: 252.05, found: 251.92

**Synthesis of α-hydroxycysteine.**<sup>114</sup> A round bottom flask was charged with **15** (300 mg, 0.713 mmol, 1.0 eq.) under nitrogen atmosphere. Thereto was added propanethiol (1.0 ml),

---

triethylsilane (0.1 ml) and TFA (1.0 ml). The mixture was stirred overnight at room temperature. The solvent was removed under reduced pressure and co-evaporated with toluene (3 x 2.0 ml). The residual was washed with dichloromethane. Then the aqueous phase was removed *in vacuo*. The product was isolated as white solid (16 mg, 0.07 mmol, 10%). **<sup>1</sup>H NMR (400 MHz, D<sub>2</sub>O, δ/ppm)** 4.47 (dd, J = 5.4, 4.2 Hz, 1H), 3.00 – 2.82 (m, 2H). **<sup>13</sup>C NMR (126 MHz, MeOD, δ/ppm)** 175.6, 72.6, 29.3. **ESI MS:** [M-H]<sup>-</sup> calculated: 121.00, found: 121.03

**Synthesis of N-α-dimethylhistidine (17):** To a stirred solution of histidine (1000 mg, 6.44 mmol, 1.0 eq.) dissolved in 500 mM acetate buffer pH 5 (40 ml) was added formaldehyde (37%, 2.42 ml, 32.2 mmol, 5.0 eq.). The mixture was cooled to 4°C. Then sodium cyanoborohydride (1210 mg, 19.3 mmol, 3.0 eq.) was added portion wise. The mixture was stirred for 1 hour at room temperature then the mixture was acidified to pH 1 by addition of 2 M HCl. The mixture was loaded on an ion exchange resin (DowX50RW50-100), washed with water and eluted with 100-1000 mM NH<sub>4</sub>OH. The water was evaporated under reduced pressure to yield **17** as white solid (1180 mg, 6.44 mmol, 100%). **<sup>1</sup>H NMR (400 MHz, Deuterium Oxide, δ/ppm)** 7.69 (d, J = 1.2 Hz, 1H), 7.00 (s, 1H), 3.79 (t, J = 6.5 Hz, 1H), 3.20 (dd, J = 6.5, 0.8 Hz, 2H), 2.83 (s, 6H).

**Synthesis of TMH: 17** (710 mg, 3.88 mmol, 1.0 eq.) was dissolved in methanol (16 ml). The pH was adjusted to 9 by addition of ammonium hydroxide. Then iodomethane (0.34 ml, 5.43 mmol, 1.4 eq.) was added. The reaction was stirred over night at room temperature. Then the solvent was evaporated. The crude was dissolved in water and run through an anion exchange column to remove the iodine. The solid residue was recrystallized from ethanol after evaporation of the solvent to yield **TMH** as a white solid (220 mg, 3.88 mmol, 29%). **<sup>1</sup>H NMR (400 MHz, Deuterium Oxide, δ/ppm)** 7.87 (d, J = 1.3 Hz, 1H), 7.04 (d, J = 1.0 Hz, 1H), 3.90 (dd, J = 11.1, 4.4 Hz, 1H), 3.41 – 3.19 (m, 11H).

**Synthesis of N-α-dimethyl histidine amide (18):** To a stirred solution of histidine amide dihydrochloride (5.00 g, 22.5 mmol, 1.0 eq.) dissolved in 500 mM acetate buffer pH 5 (100 ml) was added formaldehyde (37%, 8.45 ml, 112 mmol, 5.0 eq.). The mixture was cooled to 0 °C and sodium cyanoborohydride (4.24 g, 67.5 mmol, 3.0 eq.) was added portionwise. The mixture was stirred for 2 hours at room temperature then the mixture was acidified to pH 1 by addition of 2 M HCl. The mixture was then loaded on an cation exchange resin (DowX50RW50-100), washed with water and eluted with 100 mM NH<sub>4</sub>OH. The water was evaporated under reduced pressure to yield **18** as white solid (3.30 g, 18.1 mmol, 80%). **<sup>1</sup>H NMR (400 MHz, Deuterium Oxide, δ/ppm)** 7.64 (d, J = 1.2 Hz, 1H), 6.89 (s, 1H), 3.35 (dd, J =



---

10.0, 5.6 Hz, 1H), 2.96 (dd,  $J = 15.0, 10.0$  Hz, 1H), 2.90 (ddd,  $J = 15.0, 5.6, 0.9$  Hz, 1H), 2.32 (s, 6H). **ESI MS:**  $[M+H]^+$  calculated: 183.12, found: 183.0

**Synthesis of *N*<sup>r</sup>-tosyl-*N*- $\alpha$ -dimethyl histidine amide (**19**):** To a stirred suspension of **18** (3300 mg, 18.1 mmol, 1.0 eq.) in chloroform (100 ml) was added triethylamine (10.2 ml, 72.4 mmol, 4.0 eq.) and TsCl (6900 mg, 36.2 mmol, 2.0 eq.). The mixture was stirred until clear (0.5 h) and then the solvent was evaporated under reduced pressure. The solid residue was suspended in water and acidified with 2 M HCl. The aqueous phase was washed with dichloromethane, then basified with sodium hydrogen carbonate and extracted with dichloromethane. The solvent was removed under reduced pressure. Pure **19** was obtained without further purification (5000 mg, 18.1 mmol, 82%). **<sup>1</sup>H NMR (400 MHz, Chloroform-*d*,  $\delta$ /ppm)**  $\delta$  7.90 (d,  $J = 1.4$  Hz, 1H), 7.82 – 7.77 (m, 2H), 7.38 – 7.31 (m, 2H), 7.12 (q,  $J = 1.0$  Hz, 1H), 6.74 (s, 1H), 5.26 (s, 1H), 3.38 (dd,  $J = 7.5, 5.5$  Hz, 1H), 3.03 (dd,  $J = 15.1, 7.5$  Hz, 1H), 2.82 (dd,  $J = 15.1, 5.5$  Hz, 1H), 2.43 (s, 3H), 2.30 (s, 6H). **<sup>13</sup>C NMR (126 MHz, DMSO,  $\delta$ /ppm)** 175.3, 148.0, 142.5, 138.0, 136.3, 131.6, 128.6, 116.3, 68.6, 42.3, 28.0, 21.6. **ESI MS:**  $[M+H]^+$  calculated: 337.13, found: 336.98

**Synthesis of *N*<sup>r</sup>-tosyl-*N*- $\alpha$ -trimethyl histidine amide (**20**):** To a stirred suspension of **19** (5000 mg, 14.9 mmol, 1.0 eq.) in methanol (30 ml) was added methyl iodide (1.21 ml, 19.4 mmol, 1.3 eq.). The reaction was stirred at room temperature for 14 hours, then the solvent was evaporated to yield the **20** as yellowish solid (7127 mg, 14.9 mmol, 100%). **<sup>1</sup>H NMR (400 MHz, Deuterium Oxide)  $\delta$**  8.27 (d,  $J = 1.4$  Hz, 1H), 7.93 – 7.85 (m, 2H), 7.52 – 7.42 (m, 3H), 4.05 (dd,  $J = 11.3, 4.0$  Hz, 1H), 3.31 (m, 11H), 2.41 (s, 3H). **<sup>13</sup>C NMR (126 MHz, MeOD,  $\delta$ /ppm)** 168.6, 148.3, 138.8, 138.3, 136.0, 131.7, 128.7, 117.8, 74.8, 53.3, 26.7, 21.7. **ESI MS:**  $[M+H]^+$  calculated: 351.15, found: 351.0

**Synthesis of TMHA:** To a stirred solution of **20** (670 mg, 1.4 mmol, 1.0 eq.) in methanol (9 ml) was added HOBT (330 mg, 2.1 mmol, 1.5 eq.). The solvent was removed under reduced pressure after 45 minutes. The residue was suspended in 2 M HCl and filtered, the solid was washed with water. The solvent was removed under reduced pressure and the residue was suspended in acetone. The product was collected by filtration and washed with acetone to yield **TMHA** as white solid (245 mg, 0.91 mmol, 65%). **<sup>1</sup>H NMR (400 MHz, Deuterium Oxide,  $\delta$ /ppm)** 8.72 (d,  $J = 1.3$  Hz, 1H), 7.45 (s, 1H), 4.25 (dd,  $J = 11.3, 4.4$  Hz, 1H), 3.71 – 3.55 (m, 2H), 3.39 (s, 9H). **<sup>13</sup>C NMR (101 MHz, D<sub>2</sub>O,  $\delta$ /ppm)** 167.8, 135.0, 125.9, 119.1, 73.1, 53.4, 22.7. **ESI MS:**  $[M+H]^+$  calculated: 197.14, found: 197.03

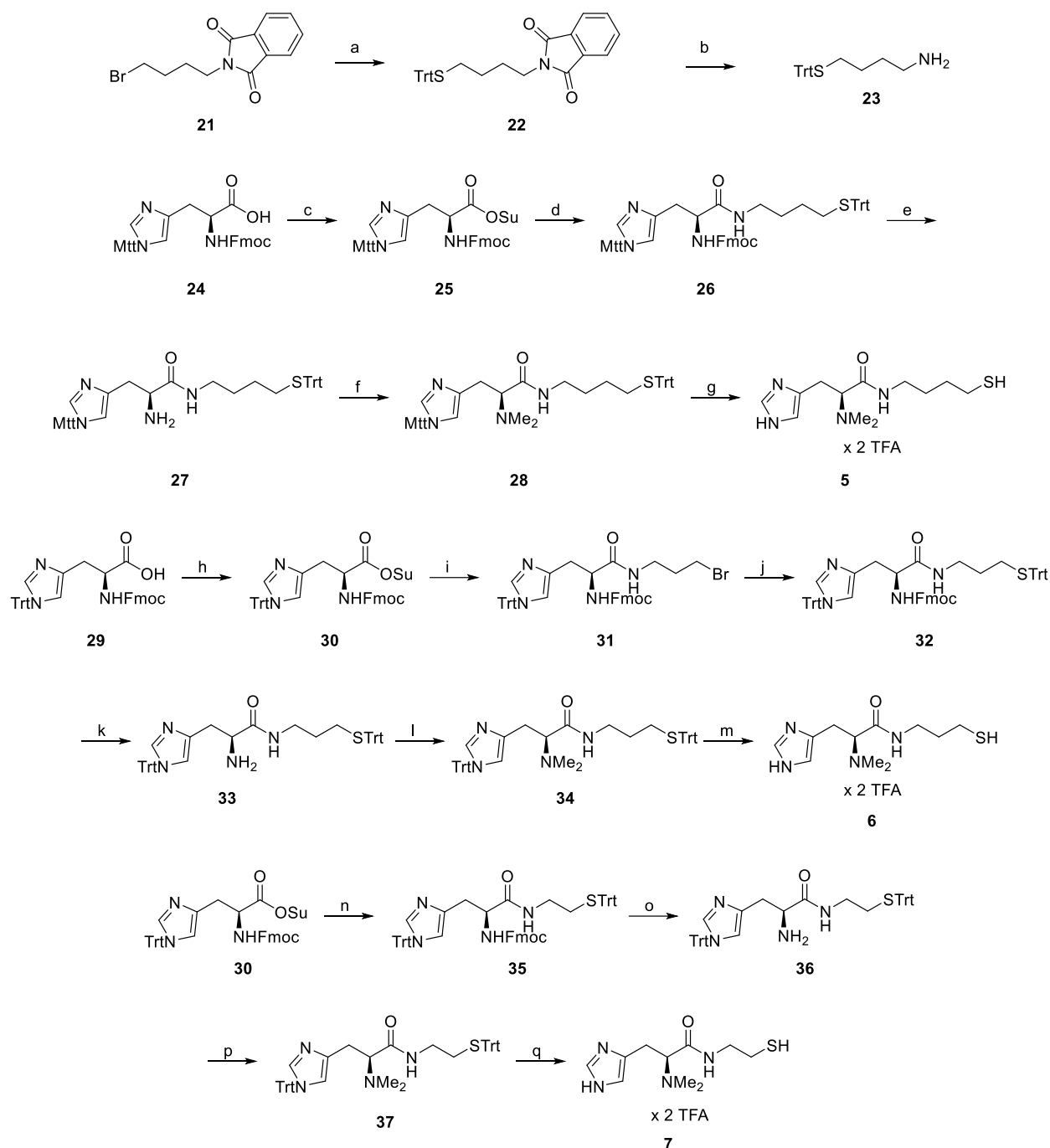


**Figure 29.** Overview for the bisubstrate synthesis.

**Synthesis of 2-(4-(tritylthio)butyl)isoindoline-1,3-dione (**22**):** The procedure was adopted from the one published by Jagadish *et al.*<sup>115</sup> Sodium hydride 60% mineral oil dispersion (0.745 g, 18.6 mmol, 1.03 eq.) was suspended in dimethylformamide (25 ml) under argon atmosphere and cooled to 0 °C. Then triphenylmethanethiol (4.95 g, 17.9 mmol, 1.0 eq.) was added portion wise to the mixture. The mixture was stirred for 5 min at 0°C and then allowed to reach room temperature. Then 2-(4-bromobutyl)isoindoline-1,3-dione (**21**) (5.2 g, 18.4 mmol, 1.03 eq.) dissolved in dimethylformamide (20 ml) was added to the mixture and stirred at room temperature for 1 hour. The reaction was diluted with ethyl acetate (150 ml)

---

and washed with water (3 x 200 ml), and brine (2 x 50 ml) and dried over sodium sulfate. The solvent was removed under reduced pressure and the crude was purified by column chromatography (cyclohexane/ethyl acetate 96:4 to 7:3) to give the product as beige solid (6.79 g, 14.2 mmol, 79%). **<sup>1</sup>H NMR (400 MHz, Chloroform-d,  $\delta$ /ppm)** 7.87 – 7.78 (m, 2H), 7.73 – 7.68 (m, 2H), 7.42 – 7.37 (m, 6H), 7.26 (s, 6H), 7.17 (tt,  $J$  = 7.3, 1.3 Hz, 3H), 3.56 (t,  $J$  = 7.1 Hz, 2H), 2.17 (t,  $J$  = 7.3 Hz, 2H), 1.69 – 1.57 (m, 2H), 1.44 – 1.34 (m, 2H).

**Synthesis of 4-(tritylthio)butan-1-amine (23):** The procedure was adopted from the one published by Jagadish *et al.*<sup>115</sup> To a suspension of **22** (2.00 g, 4.19 mmol, 1.0 eq.) in ethanol (25 ml) was added hydrazine hydrate (1.00 ml, 21.0 mmol, 5.0 eq.) and the mixture was heated to reflux. After a few minutes, a white precipitate formed which covered the whole reaction. After 5 hours at reflux, the reaction was cooled to room temperature, the precipitate was filtered off and the solvent evaporated to yield the product (1.00 g, 4.19 mmol, 69%). The product was used without further purification. **<sup>1</sup>H NMR (400 MHz, Chloroform-d,  $\delta$ /ppm)** 7.45 – 7.38 (m, 6H), 7.31 – 7.25 (m, 9H), 7.20 (tt,  $J$  = 7.1, 1.3 Hz, 3H), 2.58 – 2.53 (m, 2H), 2.19 – 2.13 (m, 2H), 1.43 – 1.36 (m, 4H).

**Synthesis of Fmoc-His(1-Mtt)-Osu (25):** Fmoc-His(1-Mtt)-OH (4.25 g, 6.71 mmol, 1.0 eq.) was dissolved in tetrahydrofuran (30 ml) and cooled to 0°C. *N*-hydroxysuccinimide (0.08 g, 6.98 mmol, 1.04 eq.) was added followed by DCC (1.52 g, 7.38 mmol, 1.1 eq.). The mixture was then stirred for 18 hours at room temperature. The precipitate was filtered off and the solvent was removed under reduced pressure. The crude was suspended in dichloromethane (10 ml) and filtered. The solvent was removed *in vacuo* to yield the product (**25**) (4.74 g, 6.49 mmol, 96%) as a white solid. **<sup>1</sup>H NMR (400 MHz, Chloroform-d,  $\delta$ /ppm)** 7.75 (d,  $J$  = 7.5 Hz, 2H), 7.62 (t,  $J$  = 7.5 Hz, 2H), 7.47 – 7.22 (m, 9H), 7.15 – 7.05 (m, 5H), 7.07 – 6.96 (m, 3H), 6.88 (s, 1H), 5.01 – 4.86 (m, 1H), 4.45 – 4.11 (m, 3H), 3.24 (d,  $J$  = 5.0 Hz, 2H), 2.71 (s, 4H), 2.35 (s, 3H).

**Synthesis of Fmoc-His(1-Mtt)-N-(4-tritylthiobutyl) amide (26):** Fmoc-His(1-Mtt)-Osu (4.50 g, 6.16 mmol, 1.0 eq., **25**) and **23** (2.14 g, 6.16 mmol, 1.0 eq.) were dissolved in dichloromethane (60 ml). DIPEA (2.1 ml, 12.3 mmol, 2.0 eq.) was added. The solvent was evaporated after 28 hours. The crude was dissolved in dichloromethane (200 ml) and washed with sat. ammonium chloride (aq.) (3 x 75 ml), and brine (1 x 75 ml) and dried over sodium sulfate. The solvent was removed *in vacuo* to yield **26** as a white powder (5.05 g, 5.24 mmol, 85%). **<sup>1</sup>H NMR (400 MHz, Chloroform-d,  $\delta$ /ppm)** 7.75 (d,  $J$  = 7.6 Hz, 2H), 7.59 (d,  $J$  = 7.4 Hz, 2H), 7.42 – 7.22 (m, 24H), 7.18 (tt,  $J$  = 7.2, 1.2 Hz, 3H), 7.08 (s, 6H), 6.96 (d,  $J$  = 8.0 Hz, 2H), 6.76 – 6.66 (m, 1H), 6.64 (s, 1H), 4.41 (q,  $J$  = 6.1 Hz, 1H), 4.37 – 4.28 (m, 2), 4.21 (t,  $J$  = 8.0, 6.4 Hz,

---

1H), 3.11 – 3.01 (m, 3H), 2.91 (dd, J = 14.9, 6.6 Hz, 1H), 2.33 (s, 3H), 2.11 (t, J = 6.0, 4.0 Hz, 2H), 1.43 – 1.30 (m, 4H).

**Synthesis of H-His(1-Mtt)-N-(4-tritylthiobutyl) amide (27):** **26** (4.5 g, 4.67 mmol, 1.0 eq.) was dissolved in dichloromethane (7 ml). Piperidine (4.6 ml, 46.7 mmol, 10 eq.) was added. The mixture was stirred for 2 h, then dichloromethane (200 ml) was added and the mixture was washed with half concentrated NaCl (aq) (3 x 75 ml). The organic layer was dried over sodium sulfate and the solvent was removed *in vacuo*. The crude was purified by silica gel column chromatography (dichloromethane/methanol 97:3->90:10) to yield **11** as a white solid (2.10 g, 2.83 mmol, 60%). **<sup>1</sup>H NMR (400 MHz, Chloroform-*d*, δ/ppm)** 7.50 – 6.78 (m, 31H), 6.54 (d, J = 1.4 Hz, 1H), 3.48 (dd, J = 8.3, 4.1 Hz, 1H), 3.08 – 2.86 (m, 3H), 2.62 (dd, J = 14.5, 8.2 Hz, 1H), 2.28 (s, 3H), 2.07 (t, J = 6.8 Hz, 2H), 1.40 – 1.17 (m, 4H).

**Synthesis Me<sub>2</sub>-His(1-Mtt)-N-(4-tritylthiobutyl) amide (28):** **27** (2.10 g, 2.83 mmol, 1.0 eq.) was dissolved in methanol (30 ml) and 1 M acetate buffer pH 5 (10 ml, 1 M) was added. Additional methanol was added until everything was dissolved. The mixture was cooled to 0°C, then formaldehyde (37% aq. Solution, 1.30 ml, 14.2 mmol, 5.0 eq.) was added followed by sodium cyanoborohydride (535 mg, 8.49 mmol, 3.0 eq.). The mixture was stirred overnight at room temperature and then methanol was removed under reduced pressure. The obtained aqueous layer was diluted with water and extracted with dichloromethane. The combined organic layer was washed with water, and brine and dried over sodium sulfate. The solvent was removed under reduced pressure. The crude was purified by silica gel column chromatography (dichloromethane/methanol 98:2 -> 90:10). The product was obtained as a white solid (1.79 g, 2.26 mmol, 80%). **<sup>1</sup>H NMR (400 MHz, Chloroform-*d*, δ/ppm)** 7.55 – 6.83 (m, 31H), 6.59 (d, J = 1.4 Hz, 1H), 3.30 (t, J = 6.4 Hz, 1H), 3.08 – 2.96 (m, 3H), 2.85 (dd, J = 14.9, 6.0 Hz, 1H), 2.34 (s, 3H), 2.30 (s, 6H), 2.12 (t, J = 8.9, 7.0 Hz, 2H), 1.41 – 1.24 (m, 4H).

**Synthesis of Me<sub>2</sub>-His-N-(4-mercaptobutyl) amide (5):** **28** (1.548 g, 1.95 mmol, 1.0 eq.) was dissolved in dichloromethane (5.0 ml). Propanethiol (0.46 ml, 5.0 mmol, 2.5 eq.) and triethylsilane (0.80 ml, 5.0 mmol, 2.5 eq.) were added. The mixture was stirred for 2 min, then TFA (5.0 ml) was added slowly. The mixture turned yellow for 15 min, then colorless again. After 1 hour, the volatiles were removed under reduced pressure. The residue was three times co-evaporated with toluene to remove all TFA. Then the residue was suspended in water (200 ml) and washed with diethyl ether (3 x 75 ml). The water was removed under reduced pressure to yield the product as colorless oil. **<sup>1</sup>H NMR (400 MHz, DMSO-*d*<sub>6</sub>, δ/ppm)** 9.00 (d, J = 1.3 Hz, 1H), 8.71 (t, J = 5.7 Hz, 1H), 7.45 (d, J = 1.3 Hz, 1H), 4.01 (dd, J = 10.1, 4.4 Hz, 1H),

---

3.38 (dd,  $J = 14.6, 4.3$  Hz, 1H), 3.19 (dd,  $J = 14.7, 10.1$  Hz, 1H), 3.13 – 2.93 (m, 2H), 2.83 (s, 7H), 2.46 – 2.38 (m, 2H), 2.23 (t,  $J = 7.8$  Hz, 1H), 1.41 – 1.30 (m, 4H).  **$^{13}\text{C}$  NMR (126 MHz, D<sub>2</sub>O,  $\delta$ /ppm)** 166.4, 135.0, 126.4, 119.1, 68.0, 42.5, 39.7, 31.0, 27.3, 24.4, 23.8. **ESI MS:**  $[\text{M}+\text{H}]^+$  calculated: 271.16, found: 271.15.

**Synthesis of Fmoc-His (1-Trt)-Osu (30):** Fmoc-His (1-Trt)-OH (25.0 g, 40.3 mmol, 1.0 eq, **28**) was dissolved in tetrahydrofuran (150 ml) and cooled to 0°C. *N*-hydroxysuccinimide (4.86 g, 42.3 mmol, 1.05 eq.) was added followed by DCC (9.10 g, 44.3 mmol, 1.1 eq.). The ice bath was removed, and the reaction was stirred for 18 hours at room temperature. The solid precipitate was filtered off and the solvent was removed under reduced pressure to yield activated ester **30** as a white solid (28.0 g, 90% w/w (contains tetrahydrofuran even after extensive drying) 35.1 mmol, 87%).  **$^1\text{H}$  NMR (400 MHz, DMSO- $d_6$ ,  $\delta$ /ppm)** 8.08 (d,  $J = 8.1$  Hz, 1H), 7.90 (d,  $J = 7.6$  Hz, 2H), 7.65 (d,  $J = 7.5$  Hz, 2H), 7.49 – 7.19 (m, 15H), 7.10 – 6.97 (m, 5H), 6.79 (s, 1H), 4.76 – 4.66 (m, 1H), 4.38 – 4.21 (m, 2H), 4.18 (t,  $J = 7.0$  Hz, 1H), 3.07 (dd,  $J = 14.6, 5.1$  Hz, 1H), 2.96 (dd,  $J = 14.4, 9.0$  Hz, 1H), 2.80 (s, 4H).

**Synthesis of compound Fmoc-His (1-Trt)-*N*-(3-bromopropyl) amide (31):** Activated ester **30** (4.00 g, 5.58 mmol, 1.0 eq.) was dissolved in dichloromethane (50 ml). 3-Bromopropanamine hydrobromide (1.31 g, 6.00 mmol, 1.1 eq.) was added followed by DIPEA (1.87 ml, 11.0 mmol, 2.0 eq.). The reaction mixture was diluted with dichloromethane (50 ml) after 1 h, washed with sat. ammonium chloride (aq.) and sat. sodium chloride solution. The organic layer was dried over sodium sulfate and the concentrated under reduced pressure. The crude product was purified by silica gel column chromatography (dichloromethane/methanol 97:3) to yield the product as white solid (3.42 g, 4.63 mmol, 83%).  **$^1\text{H}$  NMR (400 MHz, DMSO- $d_6$ ,  $\delta$ /ppm)** 8.00 (t,  $J = 5.7$  Hz, 1H), 7.89 (d,  $J = 7.5$  Hz, 2H), 7.68 (t,  $J = 7.4$  Hz, 2H), 7.48 (d,  $J = 8.3$  Hz, 1H), 7.45 – 7.23 (m, 14H), 7.04 (dt,  $J = 7.2, 2.2$  Hz, 6H), 6.70 (s, 1H), 4.26 – 4.08 (m, 4H), 3.46 (t,  $J = 6.7$  Hz, 2H), 3.12 (q,  $J = 6.2, 5.7$  Hz, 2H), 2.85 (dd,  $J = 14.5, 5.6$  Hz, 1H), 2.73 (dd,  $J = 14.5, 8.5$  Hz, 1H), 1.87 (p,  $J = 6.7$  Hz, 2H).  **$^{13}\text{C}$  NMR (126 MHz, DMSO,  $\delta$ /ppm)** 171.0, 155.7, 143.7, 141.9, 140.7, 137.4, 135.8, 129.2, 128.2, 128.1, 127.6, 127.0, 125.3, 120.1, 119.2, 74.9, 65.7, 54.9, 46.6, 46.6, 39.0, 37.2, 33.3, 32.3, 32.2. **ESI MS:**  $[\text{M}+\text{H}]^+$  calculated: 739.23, found: 739.30.

**Synthesis of Fmoc-His (1-Trt)-*N*-(3-tritylthiopropyl) amide (32):** Tritylthiol (0.760 g, 2.75 mmol, 1.0 eq.) was dissolved in tetrahydrofuran (27 ml) and cooled to 0°C. sodium hydride (60% dispersion in mineral oil, 110 mg, 2.75 mmol, 1.0 eq.) was added. The mixture was stirred at 0 °C for 30 min. The color turned red. **31** (2.00 g, 2.70 mmol, 1.0 eq.) was added.

---

The solvent was removed *in vacuo* after 16 h. The solid residue was dissolved in dichloromethane and washed with water. The organic layer was dried over sodium sulfate and concentrated under reduced pressure. The crude product was purified by silica gel column chromatography (dichloromethane/methanol 97:3). To yield the product as a white solid (1.52 g, 1.62 mmol, 60%). The product contains traces of methanol even after extensive drying (over night at the HV). **<sup>1</sup>H NMR (400 MHz, DMSO-d<sub>6</sub>, δ/ppm)** 7.89 (d, J = 7.6 Hz, 2H), 7.83 (t, J = 5.6 Hz, 1H), 7.67 (t, J = 6.9 Hz, 2H), 7.47 – 7.14 (m, 30H), 7.07 – 6.98 (m, 6H), 6.63 (d, J = 1.3 Hz, 1H), 4.21 – 4.08 (m, 4H), 2.91 (p, J = 6.6 Hz, 2H), 2.79 – 2.70 (m, 1H), 2.64 (dd, J = 14.5, 8.6 Hz, 1H), 2.03 (t, J = 7.4 Hz, 2H), 1.43 – 1.28 (m, 2H). **<sup>13</sup>C NMR (126 MHz, DMSO, δ/ppm)** 171.1, 155.7, 144.5, 143.7, 142.2, 140.7, 137.5, 136.9, 129.2, 129.0, 128.1, 127.9, 127.9, 127.6, 127.0, 126.6, 125.3, 120.1, 118.8, 74.4, 65.9, 46.6, 37.9, 31.1, 30.0, 28.9, 28.0. **ESI MS:** [M+H]<sup>+</sup> calculated: 935.40, found: 935.35.

**Synthesis of H-His (1-Trt)-N-(3-tritylthiopropyl) amide (33):** To a stirred solution of **32** (1.50 g, 1.60 mmol, 1.0 eq.) in dichloromethane (5.0 ml) was added piperidine (1.6 ml, 16.0 mmol, 10 eq.) and stirred overnight. The reaction was diluted with dichloromethane (200 ml) and washed with half concentrated sodium bicarbonate solution (3 x 100 ml). The organic layer was dried over sodium sulfate and the solvent was concentrated under reduced pressure. The crude product was dried on the HV overnight to remove the piperidine. The crude was purified by silica gel column chromatography (dichloromethane/methanol/triethylamine 970:30:1). The product was obtained as a white solid (950 mg, 1.33 mmol, 83%). The product contains traces of methanol even after extensive drying (over night at the HV). **<sup>1</sup>H NMR (400 MHz, DMSO-d<sub>6</sub>, δ/ppm)** 7.75 (t, J = 5.8 Hz, 1H), 7.49 – 7.17 (m, 25H), 7.14 – 7.00 (m, 6H), 6.57 (d, J = 1.4 Hz, 1H), 3.29 (dd, J = 7.8, 4.9 Hz, 1H), 2.91 (q, J = 6.6 Hz, 2H), 2.65 (dd, J = 14.2, 4.8 Hz, 1H), 2.43 (dd, J = 14.2, 7.8 Hz, 1H), 2.02 (t, J = 7.4 Hz, 2H), 1.88 (s, 2H), 1.47 – 1.30 (m, 2H). **<sup>13</sup>C NMR (126 MHz, MeOD, δ/ppm)** 176.3, 146.3, 143.6, 139.6, 138.0, 130.9, 130.7, 129.3, 129.3, 128.9, 127.7, 121.1, 76.8, 67.7, 56.2, 39.6, 34.8, 30.4, 29.4. **ESI MS:** [M+Na]<sup>+</sup> calculated: 735.31, found: 735.40.

**Synthesis of Me<sub>2</sub>-His (1-Trt)-N-(3-tritylthiopropyl) amide (34):** To a stirred suspension of **33** (900 mg, 1.26 mmol, 1.0 eq.) in a mixture of acetate buffer (1 M, pH 5) methanol and acetonitrile (1:4:4) was added formaldehyde (35 wt. %, 0.28 ml, 3.75 mmol, 3.0 eq.). The mixture was cooled to 0 °C. Sodium cyanoborohydride (392 mg, 6.25 mmol, 5.0 eq.) was added. The mixture was stirred for 15 min at 0 °C, then for 1 h at room temperature. The reaction was diluted with water and extracted with dichloromethane. The organic layer was washed with sodium bicarbonate and brine, then dried over sodium sulfate. The organic layer

---

was concentrated under reduced pressure. The crude product was purified by silica gel column chromatography (dichloromethane/methanol/triethylamine 950:50:1) to yield the product as white solid (674 mg, 0.969 mmol, 72%). The product contains traces of methanol even after extensive drying (over night at the HV). **<sup>1</sup>H NMR (400 MHz, DMSO-d<sub>6</sub>, δ/ppm)** 7.69 (t, J = 5.7 Hz, 1H), 7.44 – 7.14 (m, 25H), 7.10 – 6.97 (m, 6H), 6.46 (d, J = 1.4 Hz, 1H), 3.11 (dd, J = 9.4, 5.0 Hz, 1H), 2.95 (dq, J = 13.1, 6.6 Hz, 1H), 2.85 – 2.67 (m, 2H), 2.53 (dd, J = 14.2, 4.8 Hz, 1H), 2.11 (s, 6H), 2.02 (t, J = 7.5 Hz, 2H), 1.36 (p, J = 7.0 Hz, 2H). **<sup>13</sup>C NMR (126 MHz, DMSO, δ/ppm)** 169.9, 144.5, 142.3, 138.0, 137.2, 129.2, 129.0, 128.1, 128.0, 127.9, 126.6, 118.4, 74.3, 67.5, 65.9, 41.7, 37.6, 29.0, 28.1, 27.9. **ESI MS:** [M+H]<sup>+</sup> calculated: 741.36, found: 741.45.

**Synthesis of Me<sub>2</sub>-His-*N*-(3-mercaptopropyl) amide (6):** To a stirred solution of **34** (500 mg, 0.67 mmol, 1.0 eq.) in dichloromethane (1.0 ml) was added propanethiol (0.16 ml, 1.69 mmol, 2.5 eq.) and triethylsilane (0.27 ml, 1.69 mmol, 2.5 eq.). The mixture was cooled to 0 °C. TFA (1.0 ml) was added slowly. The mixture turned yellow and a precipitate formed. The volatiles were removed under reduced pressure, the residue was suspended in water and washed with ether. The aqueous phase was lyophilized to yield the product as a colorless solid (324 mg, 0.67 mmol, 100%). **<sup>1</sup>H NMR (400 MHz, DMSO-d<sub>6</sub>, δ/ppm)** 9.05 – 8.95 (m, 1H), 8.71 (d, J = 4.6 Hz, 1H), 7.45 (d, J = 1.2 Hz, 1H), 3.98 (dd, J = 9.7, 4.7 Hz, 1H), 3.45 – 3.32 (m, 1H), 3.26 – 3.04 (m, 3H), 2.83 (s, 6H), 2.37 – 2.22 (m, 3H), 1.65 – 1.47 (m, 2H). **<sup>13</sup>C NMR (126 MHz, MeOD, δ/ppm)** 166.8, 135.8, 128.2, 119.6, 68.1, 42.4, 39.0, 33.9, 25.0, 22.1. **ESI MS:** [M+H]<sup>+</sup> calculated: 257.14, found: 257.40.

**Synthesis of Fmoc-His (1-*Trt*)-*N*-(2-tritylthioethyl) amide (35):** **30** (4.00 g, 5.58 mmol, 1.0 eq.) was dissolved in dichloromethane (50 ml). 2-(tritylthio)ethanamine hydrochloride (2.18 g, 6.14 mmol, 1.1 eq.) was added followed by DIPEA (1.87 ml, 11.0 mmol, 2.0 eq.). The reaction mixture was diluted with dichloromethane (50 ml) after 1 hour, washed with sat. ammonium chloride (aq.) and sat. sodium chloride (aq.). The organic layer was dried over sodium sulfate and the concentrated under reduced pressure. The crude product was purified by silica gel column chromatography (dichloromethane/methanol 97:3) to yield the product as white solid (4.28 g, 4.65 mmol, 83%). **<sup>1</sup>H NMR (400 MHz, DMSO-d<sub>6</sub>, δ/ppm)** 8.06 – 7.96 (m, 1H), 7.89 (d, J = 7.6 Hz, 2H), 7.65 (d, J = 7.6 Hz, 2H), 7.52 – 7.14 (m, 30H), 7.10 – 6.97 (m, 6H), 6.68 (s, 1H), 4.23 – 4.03 (m, 4H), 3.01 – 2.88 (m, 2H), 2.83 (dd, J = 14.0, 4.6 Hz, 1H), 2.69 (dd, J = 14.6, 8.7 Hz, 1H), 2.18 (t, J = 6.7 Hz, 2H). **<sup>13</sup>C NMR (126 MHz, DMSO, δ/ppm)** 171.1, 155.7, 144.4, 143.7, 142.2, 137.5, 136.9, 129.2, 129.0, 128.1, 128.0, 127.9, 127.6, 127.0, 126.7,

---

125.3, 120.1, 118.9, 74.5, 65.9, 65.7, 54.6, 46.6, 39.0, 37.6, 31.2, 31.0. **ESI MS:** [M+H]<sup>+</sup> calculated: 921.38, found: 921.30.

**Synthesis of H-His (1-Trt)-N-(2-tritylthioethyl) amide (36):** **35** (2.00 g, 2.17 mmol, 1.0 eq.) was dissolved in dichloromethane (5.0 ml). Piperidine (2.15 ml, 21.7 mmol, 10 eq.) was added. The mixture was stirred overnight then diluted with dichloromethane (200 ml) and washed with half concentrated sodium bicarbonate (aq.) (3 x 100 ml). The organic layer was dried over sodium sulfate and concentrated *in vacuo*. The crude was purified by silica gel column chromatography (dichloromethane/methanol/triethylamine 970:30:1). The product was obtained as a white solid (600 mg, 0.86 mmol, 40%). **<sup>1</sup>H NMR (400 MHz, DMSO-d<sub>6</sub>, δ/ppm)** 7.92 (t, J = 5.8 Hz, 1H), 7.48 – 7.18 (m, 25H), 7.12 – 6.99 (m, 6H), 6.61 (d, J = 1.4 Hz, 1H), 3.31 (dd, J = 8.0, 4.7 Hz, 1H), 2.93 (q, J = 7.0 Hz, 2H), 2.72 (dd, J = 14.2, 4.7 Hz, 1H), 2.47 (dd, J = 14.9, 7.8 Hz, 1H), 2.19 (t, J = 7.1 Hz, 2H), 2.10 – 1.84 (m, 2H). **<sup>13</sup>C NMR (126 MHz, DMSO, δ/ppm)** 170.7, 144.4, 142.3, 137.7, 137.1, 129.2, 129.0, 128.2, 128.0, 127.9, 126.6, 118.5, 74.3, 66.0, 54.3, 44.2, 33.3, 25.8. **ESI MS:** [M+H]<sup>+</sup> calculated: 699.32, found: 699.40.

**Synthesis of Me<sub>2</sub>-His (1-Trt)-N-(2-tritylthioethyl) amide (37):** To a stirred suspension of **36** (600 mg, 0.86 mmol, 1.0 eq.) in a mixture of acetate buffer (1 M, pH 5) methanol and acetonitrile (2:1:1) was added formaldehyde (35 wt. %, 0.28 ml, 3.75 mmol, 3.0 eq.). The mixture was cooled to 0 °C. Sodium cyanoborohydride (265 mg, 4.29 mmol, 5.0 eq.) was added. The mixture was stirred for 15 min at 0 °C, then for 1 h at room temperature. The reaction was diluted with dichloromethane and washed with sat. solution of sodium bicarbonate (aq.) (3 x 100 ml) and brine (100 ml). The organic layer was dried over sodium sulfate and concentrated under reduced pressure. The crude product was purified by silica gel column chromatography (dichloromethane/methanol/triethylamine 970:30:1) to yield the product as white solid (586 mg, 0.81 mmol, 93%). **<sup>1</sup>H NMR (400 MHz, DMSO-d<sub>6</sub>, δ/ppm)** 7.82 (t, J = 5.7 Hz, 1H), 7.47 – 7.19 (m, 24H), 7.17 (d, J = 1.4 Hz, 1H), 7.08 – 6.95 (m, 6H), 6.47 (d, J = 1.5 Hz, 1H), 3.13 (dd, J = 9.2, 5.2 Hz, 1H), 3.02 – 2.92 (m, 1H), 2.83 – 2.70 (m, 2H), 2.55 (dd, J = 14.1, 4.9 Hz, 1H), 2.14 (s, 8H). **<sup>13</sup>C NMR (126 MHz, MeOD, δ/ppm)** 171.5, 144.8, 142.2, 137.7, 137.0, 129.5, 129.4, 128.0, 127.9, 127.6, 126.5, 119.6, 75.4, 68.6, 66.5, 41.3, 38.0, 31.2, 27.6. **ESI MS:** [M+H]<sup>+</sup> calculated: 727.35, found: 727.45.

**Synthesis of Me<sub>2</sub>-His-N-(2-mercaptoethyl) amide 7:** To a stirred solution of **4** (500 mg, 0.69 mmol, 1.0 eq.) in dichloromethane (1.0 ml) was added triethylsilane (0.27 ml, 1.69 mmol, 2.5 eq.). The mixture was cooled to 0 °C. TFA (1.0 ml) was added slowly. The mixture turned yellow and a precipitate formed. The volatiles were removed under reduced pressure and co-



---

evaporated with toluene (3 x 2 ml). The residue was suspended in water and washed with ether. The aqueous phase was lyophilized to yield the product as a colorless oil (323 mg, 0.69 mmol, 100%). **<sup>1</sup>H NMR (400 MHz, DMSO-d<sub>6</sub>, δ/ppm)** 8.69 (s, 1H), 7.41 (s, 1H), 4.08 (dd, J = 11.1, 4.6 Hz, 1H), 3.58 (dd, J = 14.5, 4.7 Hz, 1H), 3.45 – 3.29 (m, 2H), 3.24 (ddd, J = 13.6, 7.3, 5.4 Hz, 1H), 3.00 (s, 6H), 2.66 – 2.35 (m, 2H). **<sup>13</sup>C NMR (126 MHz, D<sub>2</sub>O, δ/ppm)** 166.8, 135.1, 126.2, 119.1, 67.9, 49.5, 43.0, 24.4, 23.5. **ESI MS:** [M+H]<sup>+</sup> calculated: 243.13, found: 243.05.

---

## Recombinant protein production

Proteins for the enzymatic assays were produced and purified according to the protocols published by Goncharenko *et al.*<sup>84</sup> and Stampfli *et al.*<sup>87</sup>

## Enzymatic Assay

The same enzymatic assay as reported by Stampfli *et al.*<sup>87</sup> was used to determine Michaelis-Menten parameters. Sulfoxide synthase activities of *CthEgtB*/*MthEgtB* were measured in reactions containing 100 mM phosphate buffer, pH 8, 100 mM NaCl, 2 mM TCEP, 2 mM ascorbate, FeSO<sub>4</sub> (4 equiv.to protein concentration), histidyl substrate and cysteinyl substrate or bisubstrate. Reactions were initiated by addition of enzyme and were incubated at 26°C. Aliquots of the reactions were quenched by addition of phosphoric acid. Reaction products were quantified by cation exchange HPLC using a Luna® 5 µm SCX 100 Å, LC Column (150 x 4.6 mm, Phenomenex) and 20 mM phosphoric acid at pH 2 with a NaCl gradient as a mobile phase.<sup>116</sup> Chromatograms were recorded at 265nm. Averages of at least two independently determined initial rates of sulfoxide production were fitted to the function  $v = V_{\max}[s]/(K_M + [s])$  (Figures 1a –1l). The Michaelis-Menten parameters  $k_{\text{cat}}$  and  $k_{\text{cat}}/K_M$  were determined in the presence of co-substrate at a concentration at least 3-fold higher than the corresponding  $K_M$  and in air saturated buffers.

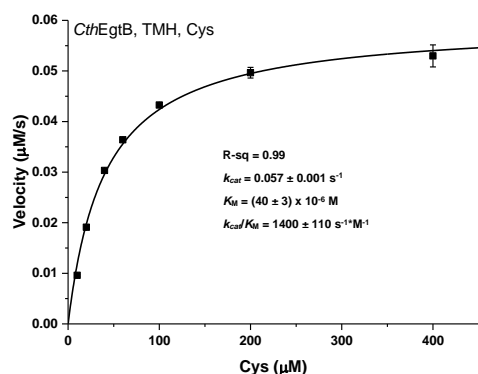


Figure 30. Sulfoxide formation-CthEgtB, [TMH] = 1 mM

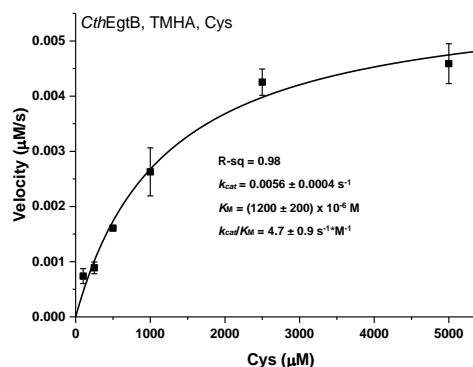


Figure 31. Sulfoxide formation-CthEgtB, [TMHA] = 1 mM

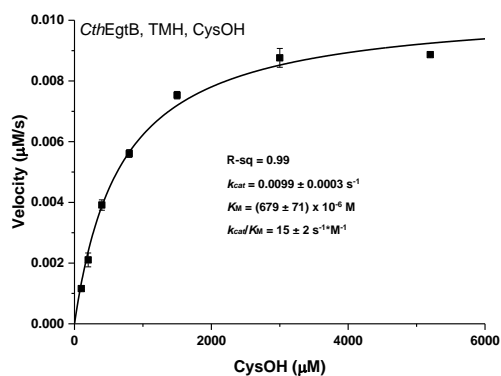


Figure 32. Sulfoxide formation-CthEgtB, [TMH] = 1 mM

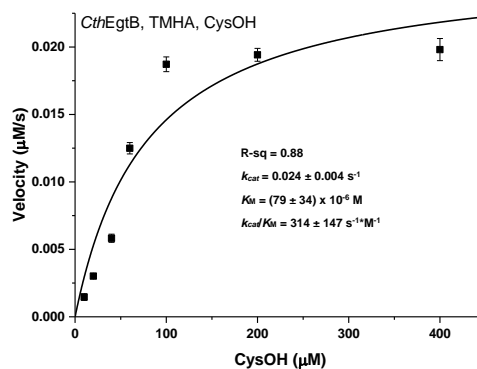


Figure 33. Sulfoxide formation-CthEgtB, [TMHA] = 1 mM

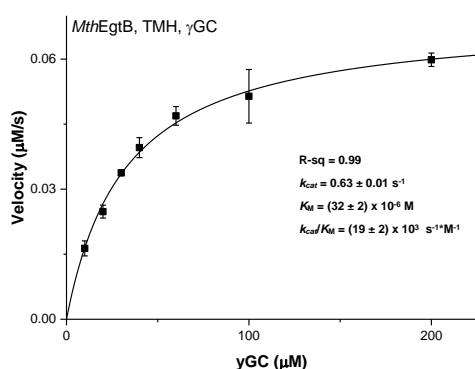


Figure 34. Sulfoxide formation-MthEgtB, [TMH] = 1 mM

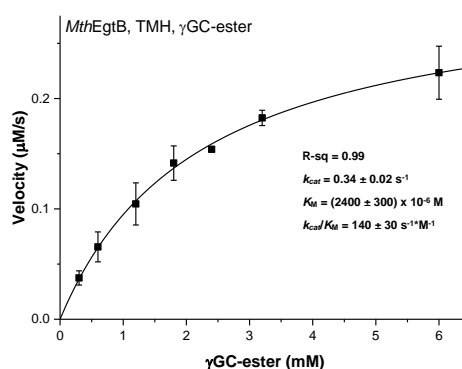


Figure 35. Sulfoxide formation-MthEgtB, [TMH] = 1 mM

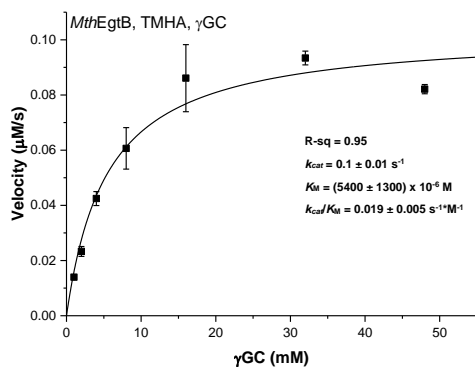


Figure 36. Sulfoxide formation-MthEgtB, [TMHA] = 1 mM

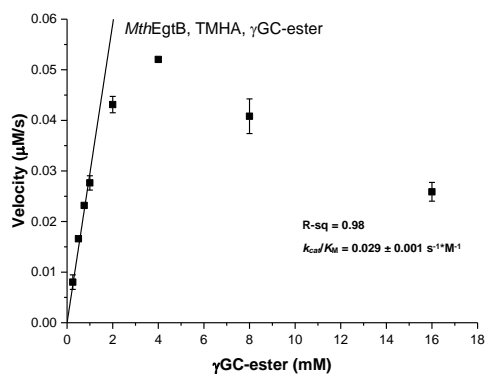
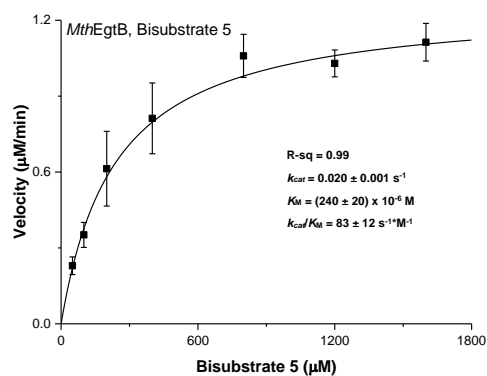
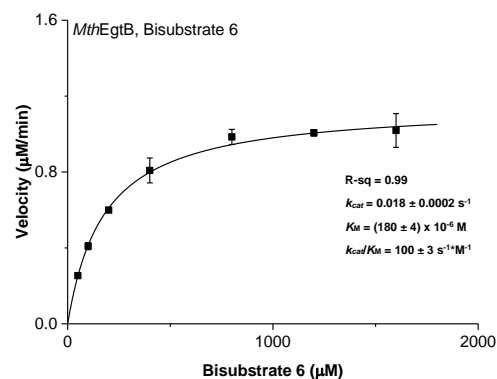


Figure 37. Sulfoxide formation-MthEgtB, [TMHA] = 1 mM



**Figure 38.** Sulfenic acid formation-*MthEgtB*, Bisubstrate 5



**Figure 39.** Sulfoxide formation-*MthEgtB*, Bisubstrate 6

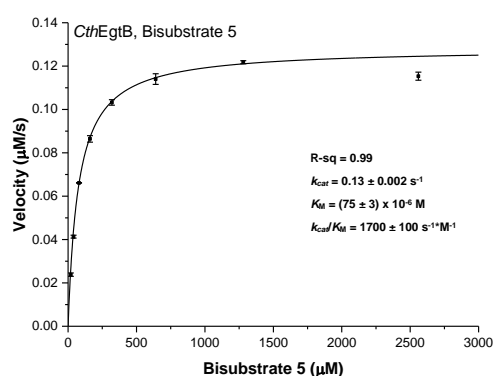


**Figure 40.** Sulfoxide formation-*CthEgtB*, Bisubstrate 5

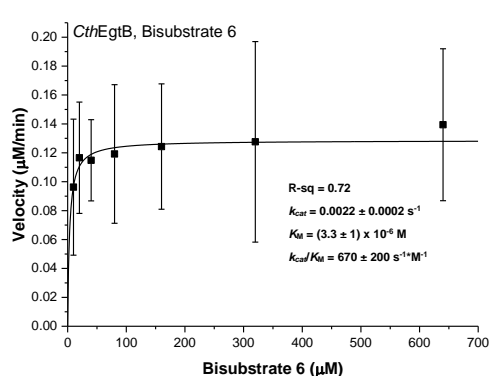


**Figure 41.** Sulfoxide formation-*CthEgtB*, Bisubstrate 6

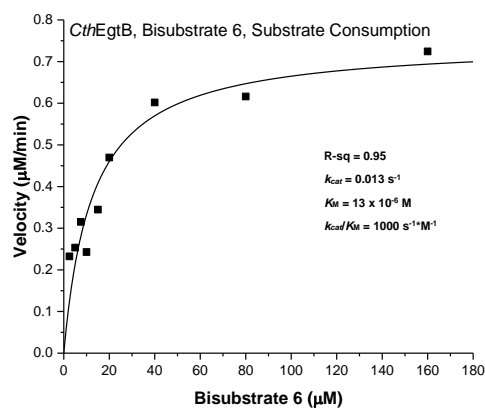


**Figure 42.** Substrate consumption-*CthEgtB*, Bisubstrate 6

---

### Burst kinetics for *CthEgtB*

The same enzymatic assay as described above was used. Sulfoxide synthase activities of *CthEgtB*/*MthEgtB* were measured in reactions containing 100 mM phosphate buffer, pH 8, 100 mM NaCl, 2 mM TCEP, 2 mM ascorbate, FeSO<sub>4</sub> (4 equiv.to protein concentration), 1 mM bisubstrate **5**. The data was fitted to the function [sulfoxide] = A<sub>0</sub>(1-exp(-k<sub>obs</sub>t)) + vt where k<sub>obs</sub> is the first-order rate constant, A<sub>0</sub> is the amplitude of the burst and v is the steady state velocity.<sup>117</sup>

### Characterization of reaction products by <sup>1</sup>H NMR

The same experimental set up as described by Stampfli *et al.* was used for the characterization of the reaction products by <sup>1</sup>H NMR. *CthEgtB* or *MthEgtB* containing reaction mixtures were analyzed by <sup>1</sup>H NMR to identify the formed products. The reactions contained 100 mM phosphate buffer-pH 8.0, 100 mM NaCl, 2 mM ascorbate, 2 mM TCEP, 4 μM FeSO<sub>4</sub>, 1.2 mM TMH/TMHA, 1 mM L-cysteine/CysOH/γGC/γGC-ester, or bisubstrate **5/6** and 5 μM of *CthEgtB*/*MthEgtB* to a final volume of 2ml. These solutions were incubated overnight at room temperature. After lyophilization the residue was dissolved in D<sub>2</sub>O. <sup>1</sup>H NMR (500 MHz, D<sub>2</sub>O) was measured with 128 scans and analyzed by MestReNova software. Substrates and products of the mono substrate were identified based on β-protons of the cysteine moiety and the aromatic protons of TMH. The bisubstrate reactions were run to completion and products were identified based on the aromatic protons.

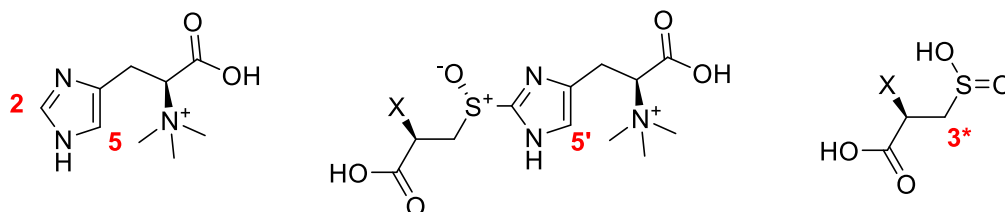


**Figure 43.** Sulfoxide synthase mono substrates and products. C-H functions used for identification by <sup>1</sup>H NMR are labeled in red.

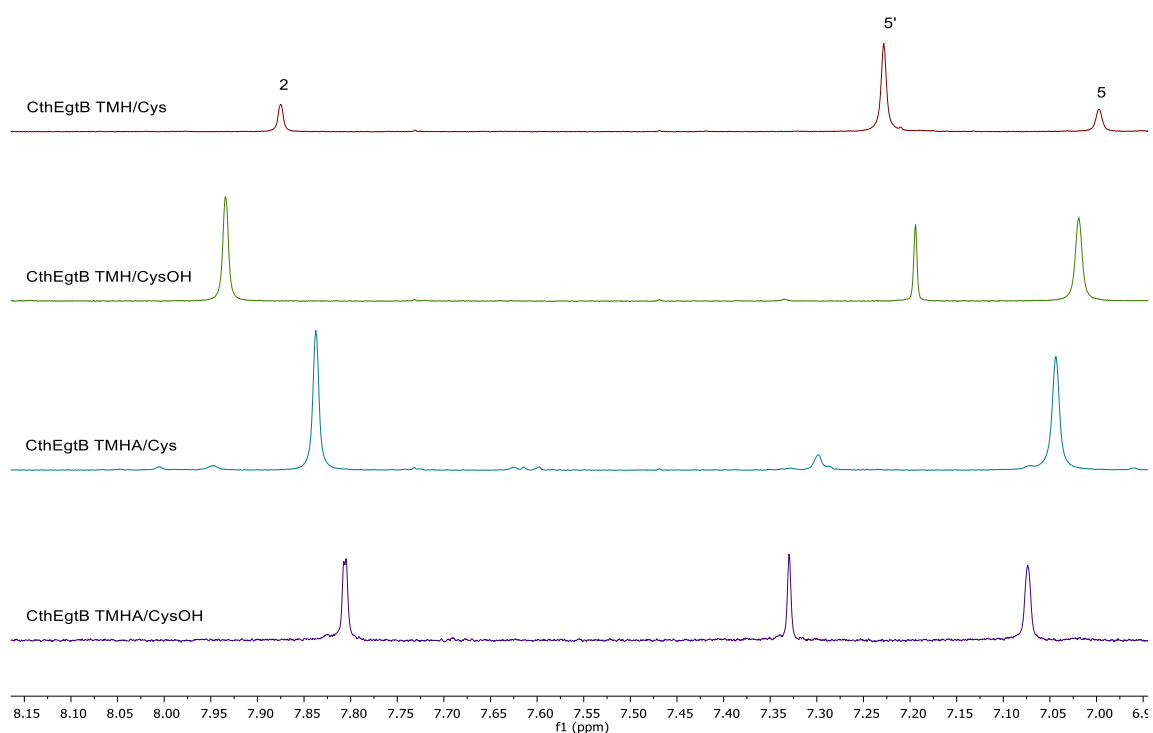


**Figure 44.** Aromatic region of the CthEgtB catalyzed reactions in excess of TMH/TMHA

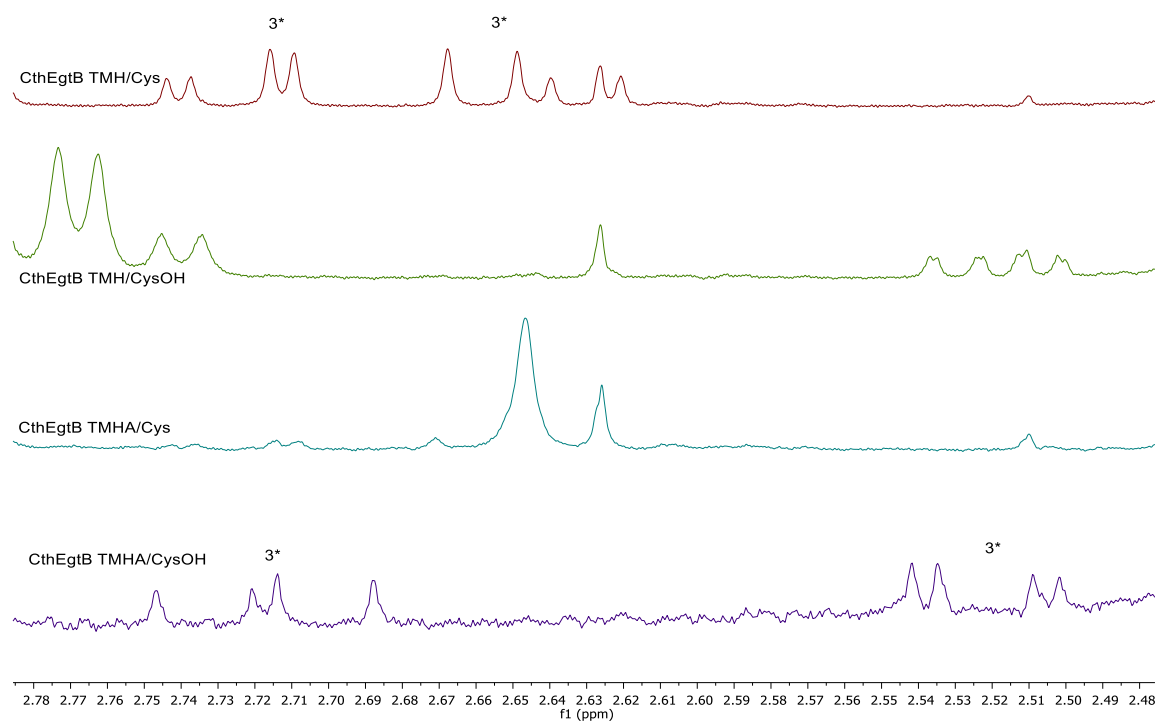


**Figure 45.** 6-protons of sulfinic acid in CthEgtB catalyzed reactions in excess of TMH/TMHA

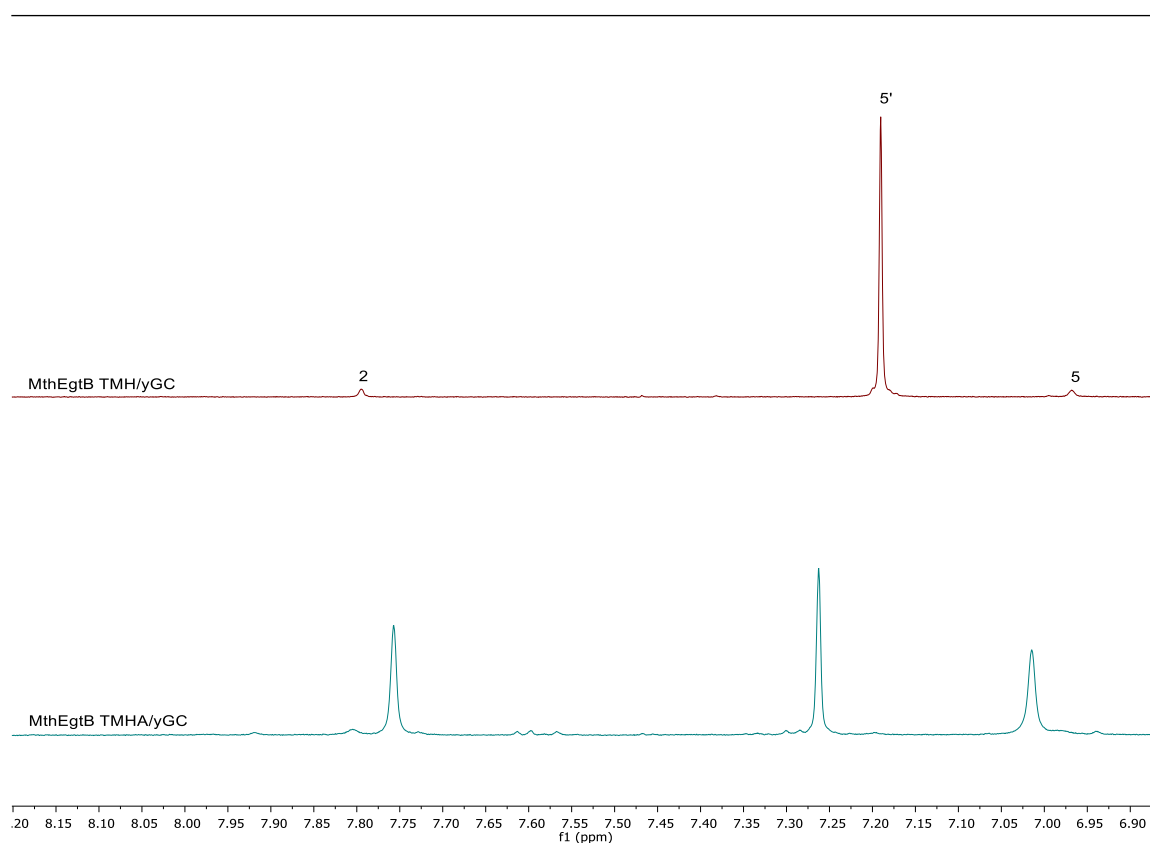


**Figure 46.** Aromatic region of the MthEgtB catalyzed reactions in excess of TMH/TMHA

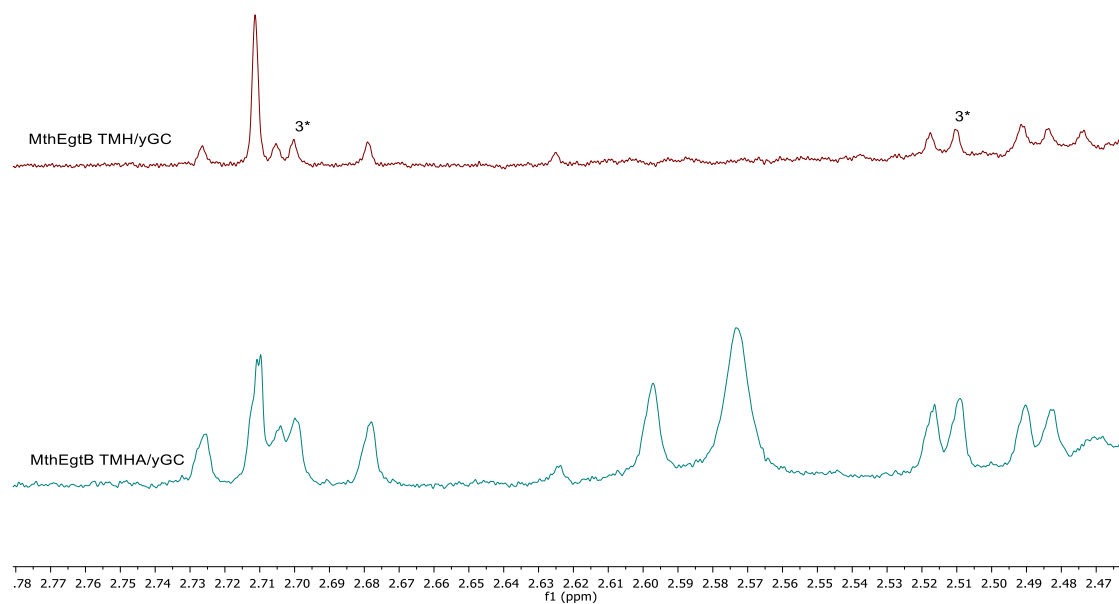


**Figure 47.**  $\beta$ -protons of sulfinic acid in MthEgtB catalyzed reactions in excess of TMH/TMHA

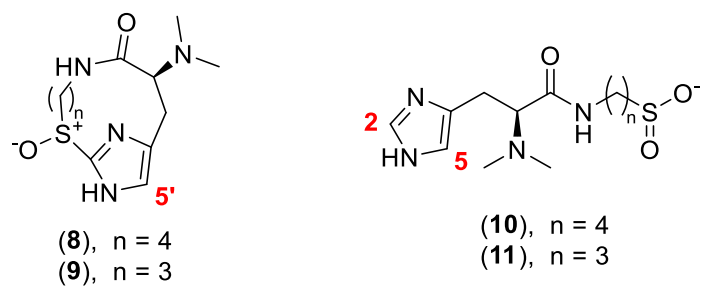


**Figure 48.** Sulfoxide synthase bisubstrate products. C-H functions used for identification by  $^1\text{H}$  NMR are labeled in red.

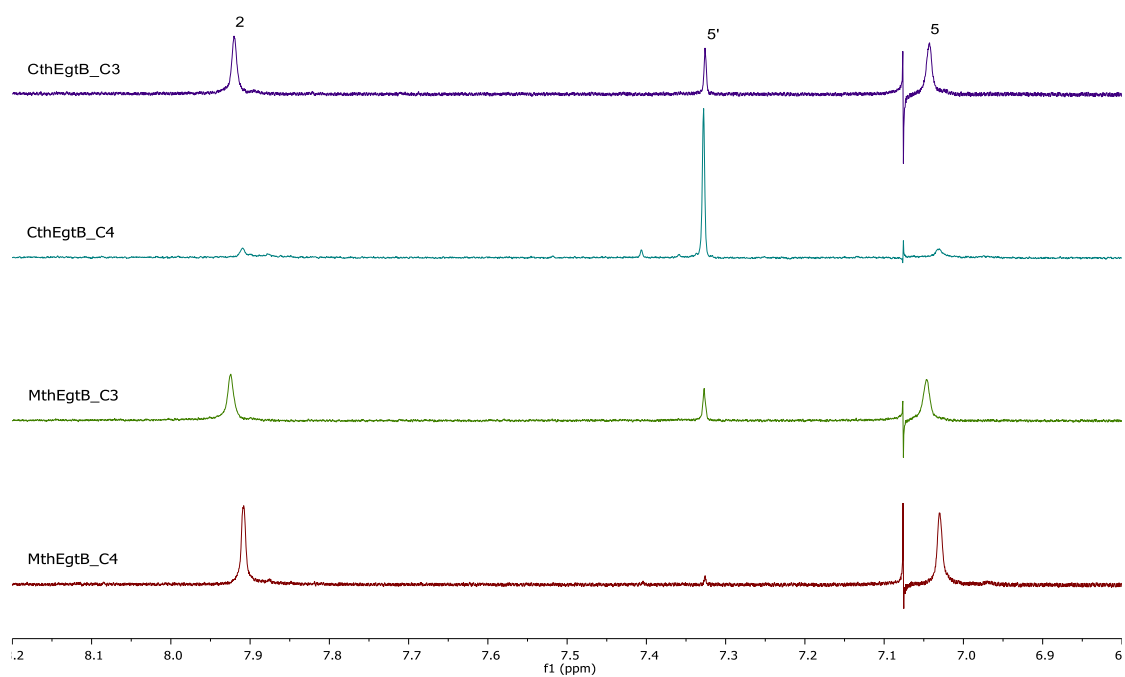


**Figure 49.** Aromatic region of the CthEgtB/MthEgtB catalyzed reactions with bisubstrate 5/6.



---

## 6 Inhibition and Regulation of the Ergothioneine Biosynthetic Methyltransferase EgtD

As discussed in **Chapter 3**, ergothioneine is an important factor for redox homeostasis and other cytoprotective functions. Additionally, it may be important for the pathogenicity of some microorganisms. Hence, understanding the regulation of the ergothioneine biosynthetic pathway and investigating how the enzymes can be inhibited contributes to progress towards the development of novel antibiotics against ergothioneine-producing microorganisms. EgtD is the first enzyme in ergothioneine biosynthetic pathway and is assumed to be essential for both aerobic and anaerobic ergothioneine biosynthesis. Therefore, it is an ideal target for inhibition of ergothioneine biosynthesis. In a study performed during this thesis, the kinetic, thermodynamic and structural basis for substrate, product, and inhibitor binding to EgtD from *Mycobacterium smegmatis* was analyzed. The study is described in the following publication:

- Misson, L.; Burn, R.; Vit, A.; Hildesheim, J.; Beliaeva, M. A.; Blankenfeldt, W.; Seebeck, F. *P. ACS Chem. Biol.* **2018**, *13* (5), 1333.

Based on structural and kinetic data, the binding order of the substrates to EgtD was elucidated. An ordered sequential substrate binding mechanism with histidine as the mandatory first substrate was observed. Furthermore, affinities for different methylation states of histidine to EgtD were determined. It was found that EgtD had the lowest affinity for unmethylated histidine and that the affinity for the substrate increases with the first two methylations whilst slightly decreasing with the final methylation. However, the relatively high affinity of the enzyme for the trimethylated product leads to product inhibition of EgtD and thereby to a feedback regulation of the pathway.

Based on the crystal structure and the mechanistic understanding of EgtD catalysis, the first series of inhibitors were designed in a way that they form the same bonding interactions as dimethyl histidine in the active site but without the possibility of methylation.

The second series of inhibitors were designed to compete with histidine for the active site. These compounds generally had low  $\mu\text{M}$  affinities to EgtD.

In the final strategy for inhibitor design, bisubstrate analogs were examined. These bisubstrates analogues mimicked histidine and the methionyl moiety of SAM together to make interactions to each of the binding sites. These inhibitors had very low affinities to EgtD, either because the linker between the histidyl and the methionyl moiety of SAM was too short to span the full binding site or because the additional competition with SAM is unfavorable.

---

Overall, this study revealed the binding mechanism of the substrates to EgtD and regulation of the ergothioneine biosynthetic pathway whilst providing leads for the design of further EgtD inhibitors.

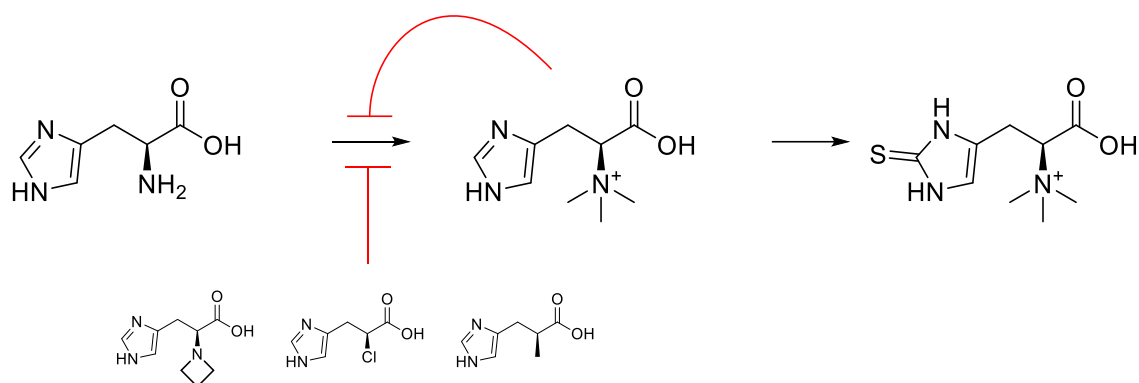


**Figure 50.** Regulation and inhibition of ergothioneine biosynthesis.<sup>118</sup>

#### Author Contributions:

- R. B. helped with the inhibitor design, designed the synthetic route for and performed the synthesis of inhibitors 1-9 and supervised the synthesis of inhibitors 10-13

# Inhibition and Regulation of the Ergothioneine Biosynthetic Methyltransferase EgtD

Laëtitia Misson,<sup>†,||</sup> Reto Burn,<sup>†,||</sup> Allegra Vit,<sup>‡,||</sup> Julia Hildesheim,<sup>†</sup> Mariia A. Beliaeva,<sup>†</sup> Wulf Blankenfeldt,<sup>‡,§</sup> and Florian P. Seebeck<sup>\*,†,§</sup>

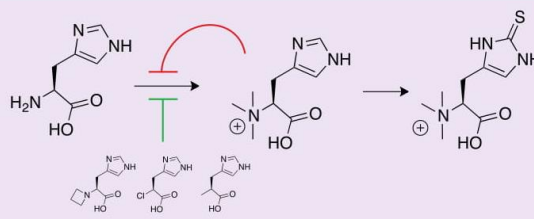
<sup>†</sup>Department for Chemistry, University of Basel, BPR 1096, Mattenstrasse 24a, Basel, Switzerland

<sup>‡</sup>Structure and Function of Proteins, Helmholtz Centre for Infection Research, Inhoffenstr. 7, 38124, Braunschweig, Germany

<sup>§</sup>Institute for Biochemistry, Biotechnology and Bioinformatics, Technische Universität Braunschweig, 38106 Braunschweig, Germany

## Supporting Information

**ABSTRACT:** Ergothioneine is an emerging factor in cellular redox homeostasis in bacteria, fungi, plants, and animals. Reports that ergothioneine biosynthesis may be important for the pathogenicity of bacteria and fungi raise the question as to how this pathway is regulated and whether the corresponding enzymes may be therapeutic targets. The first step in ergothioneine biosynthesis is catalyzed by the methyltransferase EgtD that converts histidine into N- $\alpha$ -trimethylhistidine. This report examines the kinetic, thermodynamic and structural basis for substrate, product, and inhibitor binding by EgtD from *Mycobacterium smegmatis*. This study reveals an unprecedented substrate binding mechanism and a fine-tuned affinity landscape as determinants for product specificity and product inhibition. Both properties are evolved features that optimize the function of EgtD in the context of cellular ergothioneine production. On the basis of these findings, we developed a series of simple histidine derivatives that inhibit methyltransferase activity at low micromolar concentrations. Crystal structures of inhibited complexes validate this structure- and mechanism-based design strategy.



Ergothioneine (EGT, Figure 1), the betaine of 2-mercaptohistidine, is a ubiquitous metabolite. Many

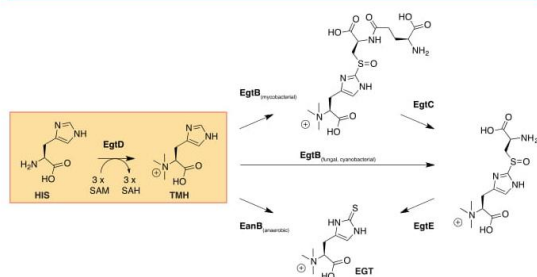


**Figure 1.** Four biosynthetic pathways for ergothioneine (EGT) production in mycobacteria,<sup>2</sup> fungi,<sup>27,38–40</sup> cyanobacteria,<sup>41</sup> and anaerobic green sulfur bacteria.<sup>5</sup>

bacteria<sup>1–5</sup> and most fungi biosynthesize EGT.<sup>1,6</sup> Plants and animals absorb EGT from their environment through a dedicated EGT transporter protein.<sup>7,8</sup> Active procurement of EGT by such a diverse array of organisms indicates the EGT may play a fundamental role in cellular life. This hypothesis is more than half a century old but is now being tested and debated with increasing effort.<sup>9–14</sup> Despite this recent attention, precise mechanisms by which EGT protects

prokaryotic and eukaryotic cells are still elusive.<sup>11,13,14</sup> The unusual redox activity and metal binding properties of the mercaptoimidazole side chain<sup>15–18</sup> could enable EGT to participate in a broad range of processes<sup>19</sup> including protection against reactive oxygen species,<sup>20</sup> reduction of oxidized heme-proteins,<sup>21</sup> or passivating redox-active transition metals.<sup>22,23</sup>

Cellular dependence on EGT has been demonstrated for several microbial organisms.<sup>24</sup> Deletion of EGT biosynthetic genes in *Mycobacterium smegmatis*, *Mycobacterium tuberculosis*, *Streptomyces coelicolor*, *Neurospora crassa*, and *Aspergillus fumigatus* produced strains with reduced resistance against oxidative stress.<sup>25–31</sup> In *M. tuberculosis*, these deletions increased susceptibility to antimycobacterial drugs and decreased viability in macrophages and in mice.<sup>30</sup> These recent findings raise the possibility that EGT biosynthesis—a process that does not occur in human cells—may be a target for novel anti-infective therapeutics. The genetic studies also agree that mutating the gene for the S-adenosylmethionine (SAM) dependent methyltransferase EgtD induces complete EGT deficiency in bacteria and fungi. This dependence validates EgtD as a potential target for EGT biosynthesis inhibitors.

Received: February 6, 2018

Accepted: April 9, 2018

Published: April 16, 2018

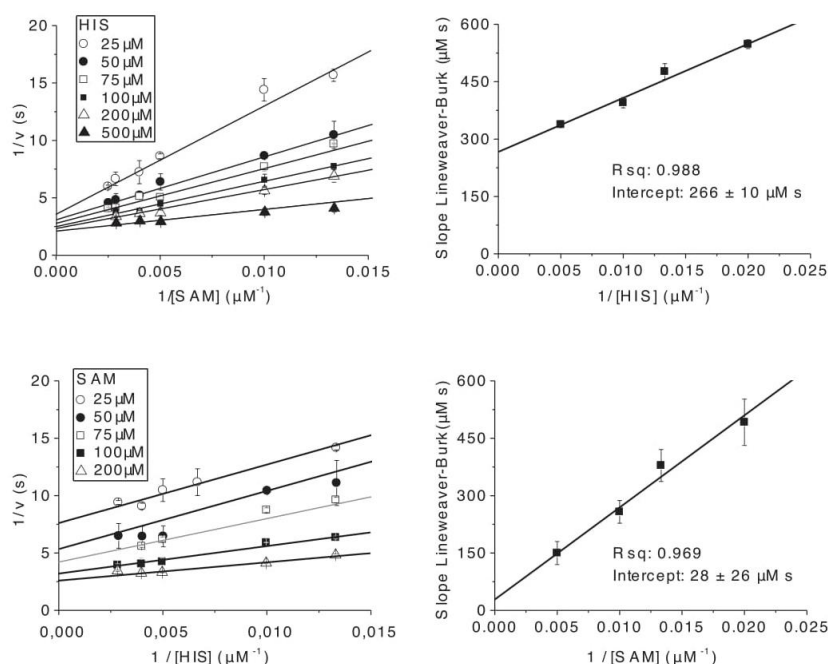


**Figure 2.** Lineweaver–Burk plots of kinetic data used to examine the substrate binding mechanism of EgtD. Top: Primary and secondary plots with SAM as the variable substrate in the presence of different concentrations of HIS. Bottom: Primary and secondary plots with HIS as the variable substrate in the presence of different concentrations of SAM.

EgtD initiates EGT biosynthesis by methylating histidine (HIS) to produce *N*- $\alpha$ -trimethylhistidine (TMH) via the intermediates *N*- $\alpha$ -monomethyl- (MMH) and *N*- $\alpha$ -dimethylhistidine (DMH).<sup>2,32,33</sup> TMH is consumed by the oxygen- and iron-dependent sulfoxide synthase EgtB. This enzyme attaches the sulfur atom of  $\gamma$ -glutamylcysteine ( $\gamma$ GC) to carbon 2 on the imidazole ring of TMH.<sup>34,35</sup> Subsequent steps catalyzed by the amidohydrolase EgtC and the  $\beta$ -lyase EgtE result in EGT (Figure 1).<sup>36,37</sup> Fungal homologues of EgtB utilize cysteine instead of  $\gamma$ GC as a sulfur donor, but the chemistry of this reaction is likely similar to that of mycobacterial enzymes.<sup>27,38–40</sup> Some cyanobacterial species recruited a homologous iron-dependent enzyme from a different pathway to act as an EgtB surrogate in EGT production.<sup>41</sup> An even more surprising variation of this pathway occurs in anaerobic green sulfur bacteria. These organisms utilize a rhodanese-like enzyme (EanB) to attach sulfur to TMH in an oxygen-independent reaction.<sup>5</sup> All these pathway variations include an EgtD-type methyltransferase, making this enzyme the sole indispensable component of EGT production (Figure 1).

The growing recognition of EGT as a relevant factor in microbial metabolism and the key role of EgtD in EGT biosynthesis motivated us to examine the kinetic, thermodynamic, and structural basis for ligand recognition by EgtD from *M. smegmatis*. This analysis revealed (i) that EgtD binds its substrate by a mechanism which is unprecedented among SAM-dependent methyltransferases, (ii) that EgtD activity is subject to stringent feedback regulation, and (iii) that the EgtD active site can adapt to methylate a primary, a secondary, and a tertiary amine with increasing efficiency. These findings were used to develop and validate the first designs of specific EgtD inhibitors.

## RESULTS AND DISCUSSION

**Substrate-Binding Order.** EgtD consumes three SAM equivalents to methylate HIS to TMH in three consecutive two-substrate–two-product reactions with MMH and DMH as reaction intermediates.<sup>42</sup> In principle, it is possible that trimethylation is processive, meaning that HIS only leaves the enzyme after all three methyl groups are installed. This model is unlikely. Assuming diffusion-limited substrate binding, and a dissociation constant of 4  $\mu$ M for the EgtD:DMH complex, we find that unproductive dissociation of this complex is at least  $10^3$ -fold faster than turnover to TMH.<sup>33</sup> Hence, EgtD-catalyzed trimethylation is a distributive process. The efficiency of EgtD-catalyzed consumption of SAM is 2-fold and 3-fold less efficient when the methyl acceptor is HIS instead of DMH or MMH,<sup>33</sup> showing that the first methyl transfer is the rate limiting step of TMH production. Therefore, we concluded that the steady-state behavior of EgtD is dominated by the first methylation step.

The order of substrate binding was elucidated by measuring the apparent Michaelis–Menten parameters  $k_{\text{cat}}$  and  $K_M$  for HIS and SAM as a function of both substrate concentrations (Figure S1).<sup>33</sup> EgtD-catalyzed consumption of SAM was monitored by an enzyme-coupled UV assay.<sup>43</sup> The recorded data revealed that the apparent  $K_{M,\text{SAM}}$  depends on [HIS], but that the apparent  $K_{M,\text{HIS}}$  is largely independent of [SAM] (Figure 2). This behavior is diagnostic for an ordered sequential substrate binding mechanism, with HIS as the leading substrate.<sup>42</sup>

An obligatory binding order is consistent with the structure of EgtD (Figure 3). The active site of this enzyme is located in a cleft between the SAM-binding Rossmann-fold domain and



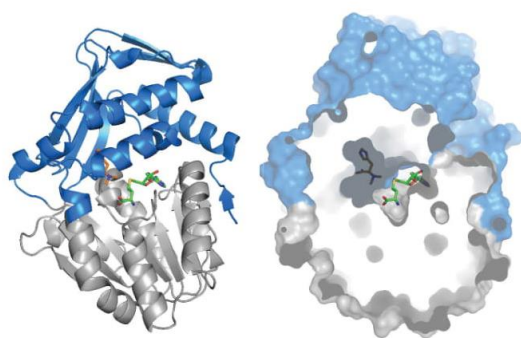


**Figure 3.** Structure of EgtD in complex with S-adenosyl homocysteine (SAH, green) and N- $\alpha$ -dimethylhistidine (DMH, orange; PDB: 4PIO).<sup>5</sup> The substrate-binding domain (blue) is formed by residues 1–60 and 196–286. The SAM-binding domain is conserved in most SAM-dependent methyltransferases.

the HIS-binding domain. The first domain is conserved among class I methyltransferases,<sup>44,45</sup> but the second domain is exclusive to *Methyltransf*\_33 enzyme family members, such as the Trp-, Tyr-, and dimethylallyl-tryptophan methyltransferases.<sup>33,46</sup>

The crystal structure of EgtD in complex with DMH and SAH shows that the enzyme completely sequesters the methyl acceptor from bulk solvent (Figure 3). The only direct nonprotein contact to DMH is provided by the sulfur atom of SAH. The only path for HIS in and out of this pocket leads through the SAM/SAH-binding site. Unless substrate binding is

accompanied by large scale unfolding and refolding of the HIS-binding domain, the methyl-acceptor can reach its binding pocket only in the absence of SAM/SAH. Therefore, substrate binding and product release must follow an ordered sequence.

This methyl-acceptor first binding order distinguishes EgtD from all characterized natural product methyltransferases.<sup>47</sup> Methyltransferases which methylate small substrates<sup>47</sup> usually follow a SAM-first or a random binding mechanism. Some DNA-, RNA-, or protein-methyltransferases may follow an apparent substrate-first binding mechanism.<sup>48</sup> However, these enzymes often bind their macromolecular substrates through interactions outside the active site, which makes the comparison to enzymes with small substrates difficult.

**Product Inhibition by TMH.** EgtD is characterized by significant HIS-competitive inhibition by the product TMH. This behavior is also unusual for a SAM-dependent methyltransferase. To examine this trait of EgtD, we recorded methyl-transfer activities in the presence of several TMH concentrations with either HIS or SAM as the substrate with variable concentration, while keeping the second substrate concentration constant. Plotting these data in the form of Lineweaver–Burk plots showed that TMH behaves as a competitive inhibitor with respect to both substrates (Figure 4). The  $K_i$  for HIS-competitive inhibition of EgtD by TMH was determined by measuring the apparent  $K_{M,HIS}$  in the presence of 500  $\mu$ M SAM and three different concentrations of TMH. From these data,  $K_i$  was calculated using the equation  $K_i = K_M[TMH]/(K_{M,app} - K_M)$  (Table 1, Figure S2).

The value of  $K_i$  for TMH corresponds well with the dissociation constant ( $K_d$ ) of the EgtD:TMH complex as determined by isothermal titration calorimetry (Table 2, Figure S3). The affinity of EgtD for TMH increased by 240-fold in the

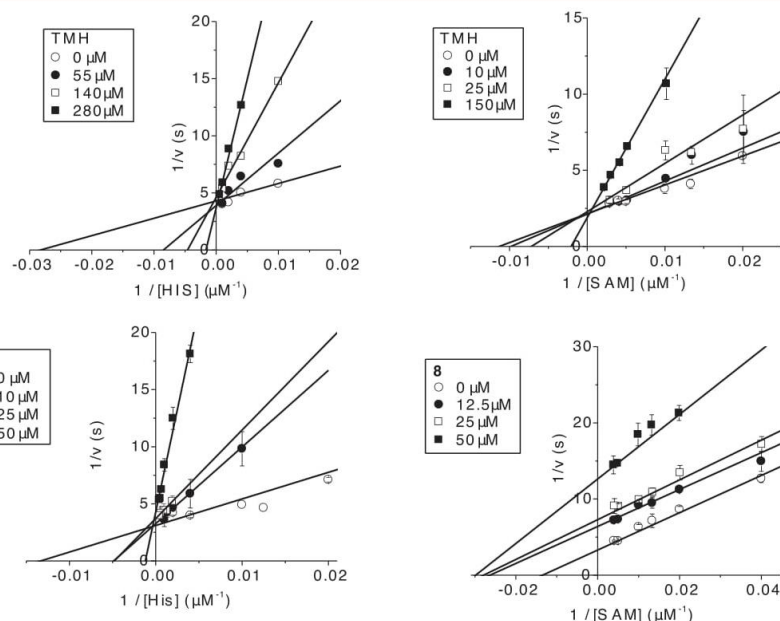


**Figure 4.** Lineweaver–Burk plots of the data used to examine EgtD inhibition by TMH and 8. Top: Primary plots with HIS or SAM as the variable substrate in the presence of different concentrations of TMH. Bottom: Primary plots with HIS or SAM as the variable substrate in the presence of different concentrations of 8.

**Table 1. Inhibition Constants ( $K_i$ ) for EgtD Inhibitors<sup>a</sup>**

EgtD ligands	$K_i$ ( $\mu$ M) L-derivative	$K_i$ ( $\mu$ M) racemic
TMH	39 $\pm$ 6	
1		8.5 $\pm$ 2.1
2	21 $\pm$ 3	41 $\pm$ 6
3		93 $\pm$ 11
4		49 $\pm$ 14
5		5.4 $\pm$ 1.6
6		72 $\pm$ 17
7		25 $\pm$ 1
8	2.6 $\pm$ 0.4	6.2 $\pm$ 1.5
9		8.2 $\pm$ 2.4
10	800 $\pm$ 200	
11	100 $\pm$ 40	
12	800 $\pm$ 200	
13	200 $\pm$ 80	

<sup>a</sup>HIS-competitive inhibition of EgtD was quantified by measuring the apparent  $K_{M,HIS}$  at three different inhibitor concentrations in the presence of 500  $\mu$ M SAM. Inhibition constants were determined using the equation  $K_i = K_M[TMH]/(K_{M,app} - K_M)$ .

**Table 2. Binding Constants ( $K_D$ ) Binary and Ternary EgtD Complexes<sup>a</sup>**

EgtD ligands	$K_D$ ( $\mu$ M)	$\Delta G$ (kcal/mol)	$\Delta H$ (kcal/mol)	$T\Delta S$ (kcal/mol)
HIS <sup>b</sup>	290 $\pm$ 14	-4.8	-8.0	-3.3
HIS:SAH <sup>b</sup>	37 $\pm$ 1	-6.1	-10	-3.9
MMH <sup>b</sup>	70 $\pm$ 30	-5.7	-13	-7.5
MMH:SAH <sup>b</sup>	14 $\pm$ 7	-6.6	-11	-4.5
DMH <sup>b</sup>	4 $\pm$ 2	-7.4	-5.0	2.4
DMH:SAH <sup>b</sup>	2 $\pm$ 1	-7.8	-27	-19
TMH	26 $\pm$ 4	-6.3	-8.0	-1.6
TMH:SAH	0.11 $\pm$ 0.01	-9.7	-9.2	0.2

<sup>a</sup>Dissociation constants [ $K_D$ ] were determined by isothermal calorimetry titration at 25  $^{\circ}$ C. <sup>b</sup>Data from ref 33.

presence of 7 mM SAH (Figure S3). However, because the reaction mixtures used for the kinetic measurements contained SAH nucleosidase and adenine deaminase, SAH cannot accumulate<sup>43</sup> and does not contribute to inhibition. Similarly, the SAH concentrations in living cells are also kept in the low micromolar range, suggesting that EgtD inhibition by SAH may not be significant *in vivo*.<sup>49</sup> On the other hand, stress factors that lead to accumulation of SAH might indeed interfere with EGT production.

**Comparison to Related Methyltransferases.** Methyltransferases are commonly inhibited by the consumed methyl donor, S-adenosyl homocysteine (SAH), which acts as a SAM-competitive inhibitor.<sup>49</sup> Inhibition by the methylated product is

far less common among methyltransferases. Therefore, we wondered whether product inhibition by TMH is a specifically evolved feature of EgtD or whether this behavior is a mere consequence of the unusual substrate binding order or of the per-methylation reaction. To address this question, two close EgtD homologues were examined. The first enzyme is the tyrosine betaine synthase (Ybs) from *Aspergillus nidulans*. Although Ybs shares only 28% sequence identity with EgtD,<sup>33</sup> this fungal enzyme contains an almost identical set of active site residues. The only apparent differences between EgtD and Ybs map to the side chain binding pocket for the substrate. Hence, Ybs and EgtD should share all catalytic properties that are inescapable consequences of the protein architecture or the catalyzed reaction.

Using the same kinetic assay as described above, we determined that Ybs catalyzes tyrosine methylation with similar efficiency as EgtD catalyzed methylation of HIS (Table 3, Figure S4). In contrast to EgtD, Ybs is not inhibited by its final product N- $\alpha$ -trimethyltyrosine (TMY,  $K_i > 1$  mM, Figure S5). The efficiencies at which the two enzymes catalyze the conversion of DMH or DMY to TMH or TMY, respectively, were also determined. EgtD-catalyzed methyl transfer is 3-fold more efficient when the methyl acceptor is DMH instead of HIS.<sup>33</sup> In contrast, Ybs-catalyzed methyl transfer is 4-fold less efficient when the methyl acceptor is DMY instead of Tyr. As a consequence, EgtD and Ybs give rise to different product distributions when SAM is the limiting substrate. EgtD produces predominantly TMH, while Ybs produces predominantly DMY (Table 3).

Similar observations were made with an engineered EgtD variant (EgtD<sub>E282A,M252V</sub>) that methylates tryptophan instead of HIS.<sup>33</sup> The variant contains two mutations in the substrate-binding domain that accommodate an indole instead of an imidazole ring. The crystal structure of this enzyme in complex with tryptophan (Trp) revealed an otherwise unchanged active site geometry.<sup>33</sup> EgtD<sub>E282A,M252V</sub> catalyzed methylation of Trp with an efficiency only 6-fold lower than that of the wild type enzyme with HIS as a substrate (Table 3, Figure S6). However, methylation of N- $\alpha$ -dimethyltryptophan (DMW) to N- $\alpha$ -trimethyltryptophan (TMW) is 20-fold less efficient than the corresponding transformation of DMH by EgtD. The reduced efficiency is due to a reduced  $k_{cat}$ , suggesting that suboptimal positioning of the non-native substrate in the mutated active site specifically affects methyl transfer to DMW.

On the basis of the comparison of these three methyltransferases, we conclude that efficient trimethylation and product inhibition as observed by EgtD are not inescapable consequences of the active site architecture, the catalyzed reaction type, or the substrate binding mechanism. More likely, the two behaviors rely on structural optimization of the EgtD

**Table 3. Kinetic Parameters of the Aromatic Amino Acid Betaine Synthases<sup>a</sup>**

substrates	enzyme	$k_{cat}$ ( $s^{-1}$ )	$K_M$ ( $\mu$ M)	$k_{cat}/K_M$ ( $M^{-1} s^{-1}$ )	MMH/DMH/TMH ratio (%)
HIS <sup>b</sup>	EgtD	$5.8 \times 10^{-1}$	110	$5.3 \times 10^3$	
DMH <sup>b</sup>	EgtD	$4.3 \times 10^{-1}$	32	$1.7 \times 10^4$	<1/17/83
Tyr <sup>b</sup>	Ybs	$1.1 \times 10^{-1}$	21	$5.2 \times 10^3$	
DMY	Ybs	$5.0 \times 10^{-2}$	43	$1.2 \times 10^3$	<1/60/40
Trp <sup>b</sup>	EgtD <sub>E282A,M252V</sub>	$1.1 \times 10^{-1}$	20	$5.5 \times 10^3$	
DMW	EgtD <sub>E282A,M252V</sub>	$0.9 \times 10^{-2}$	11	$8.2 \times 10^2$	<1/95/5

<sup>a</sup>Reaction conditions: 25  $^{\circ}$ C, Tris HCl 50 mM, pH 8, NaCl 50 mM, MnCl 200  $\mu$ M, 500  $\mu$ M SAM, SAH nucleosidase 5  $\mu$ M, adenine deaminase 10  $\mu$ M. <sup>b</sup>Data from ref 33.



active site and must have emerged by positive selection to serve a function. As will be discussed below, cooperative trimethylation and product inhibition may play important roles in quality control and regulation of EGT biosynthesis in *Mycobacteria*.

**Structure of EgtD in Complex with TMH.** In order to mediate efficient trimethylation and to allow for product inhibition, EgtD must be able to bind to a primary, a secondary, a tertiary, and a quaternary amine. How can this enzyme accommodate the changing hydrogen-bonding requirements of its ligand? To examine this question, we solved the crystal structure of EgtD in complex with TMH (Tables S1 and S2). This structure superimposes with the EgtD:HIS<sup>50</sup> and the EgtD:DMH<sup>33</sup> complexes a mutual RMSD of 0.4 Å (entire chain). The three ligands HIS, DMH, and TMH occupy essentially the same position, and almost all atoms of the active site residues superimpose (Figure 5). The important exceptions are residues in direct contact with the  $\alpha$ -amino moiety. These residues are Asn166 and Gly161.

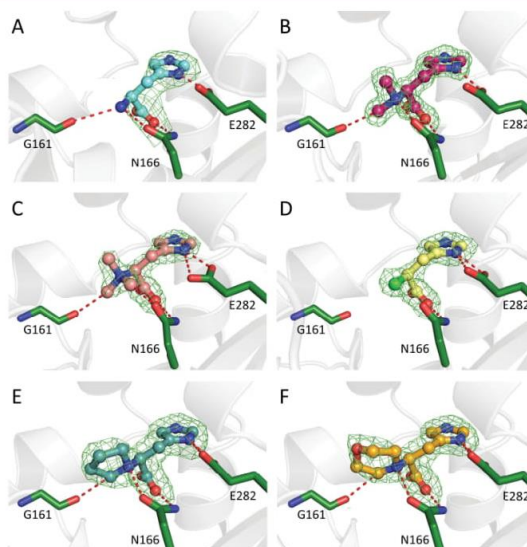


**Figure 5.** Crystal structures of EgtD in complex. (A) HIS (PDB entry 4UY7<sup>50</sup>), (B) DMH (PDB entry 4PIN<sup>33</sup>), (C) TMH, (D) **8**, (E) **2**, (F) **3**. Unbiased  $mF_{\text{obs}} - DF_{\text{calc}}$  electron density ( $\sigma$  level = 2) of the compounds is shown in green.

In the TMH complex, two  $N$ - $\alpha$ -methyl groups make close contact with the backbone carbonyl of Gly161 (3.1 Å) and with the side chain carbonyl of Asn166 (3.2 Å). The carbonyls

approach the  $N$ - $\alpha$ -methyl groups in a ( $O-C-N\alpha$ ) angle of 167° (Gly161) and 177° (Asn166). This geometry is suggestive of attractive interaction between the positively polarized methyl groups and the carbonyl functions. The third  $N$ - $\alpha$ -methyl group points toward the SAM-binding site.

In the DMH complex, one  $N$ - $\alpha$ -methyl group makes the same interaction with the Gly161 carbonyl function (3.0 Å), and the other  $N$ - $\alpha$ -methyl group points toward the SAM-binding site. Asn166 moved 1.3 Å closer to the substrate to form a 2.7 Å hydrogen bond to the  $\alpha$ -amino group of the ligand. In the HIS complex, the ligand forms two rather loose hydrogen bonds to Asn166 (3.1 Å) and Gly161 (3.4 Å). In order to establish a hydrogen bond, the Gly161 carbonyl oxygen moved by 1.8 Å toward the  $\alpha$ -amino group of HIS. This rearrangement is made possible by conformational changes of the backbone including residues 159–162.

The three structures show that EgtD solvates the  $N$ - $\alpha$ -amino moiety of its substrates and product by a highly polar pocket with adaptable size (see Figure 5). Remarkably, HIS is by far the weakest binder, despite forming two classical hydrogen bonds (Table 2).<sup>33</sup> In the DMH complex, the hydrogen bond to Gly161 is lost, but the hydrogen bond to Asn166 becomes shorter and, hence, stronger. As a consequence, DMH is a 100-fold stronger EgtD ligand ( $K_D = 4 \mu\text{M}$ ) than HIS. Surprisingly, TMH is still a comparatively strong ligand ( $K_i = 40 \mu\text{M}$ ), even though both hydrogen bonds are lost. It is possible that the close interaction between two  $N$ - $\alpha$ -methyl groups and the carbonyls from Gly161 and Asn166 are attractive and partially compensate for the lack of hydrogen bonding.

**Catalytic Cycle.** The structure of the EgtD:TMH complex also illustrates why TMH is necessarily a competitive inhibitor with respect to both HIS and SAM. A model of EgtD in complex with SAM and TMH indicates that the third  $N$ - $\alpha$ -methyl groups of TMH and the sulfonium methyl group of SAM would clash (Figure S7). Hence, binding to the two ligands is mutually exclusive. In the conformation of DMH observed in the EgtD:DMH complex, the same steric clash would prevent binding of SAM. In order to form the ternary complex DMH (a, Figure 6) must first adopt an alternative conformation in which the two  $N$ - $\alpha$ -methyl groups point toward Asn166 and Gly161 (b). This conformer can accept SAM (c) to form the reactive complex that decays via S- to N-methyl transfer to form the product complex (d). On the basis of this mechanistic model, we hypothesized that DMH analogs that make the same interactions in the active site but cannot undergo the same conformational change could be potent EgtD inhibitors.

**Strategies for Inhibitor Design.** To test this idea, we synthesized histidine derivatives with cyclic tertiary amines in place of the  $N$ - $\alpha$ -dimethyl amino moiety of DMH (Figure 5, see Supporting Information). The syntheses and character-

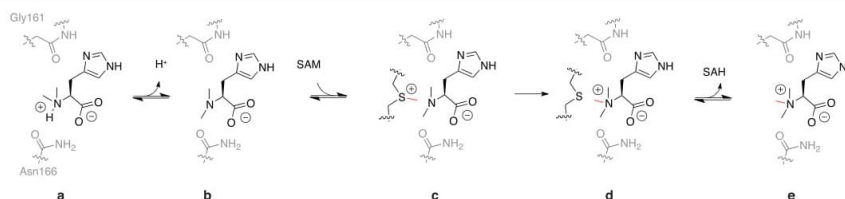


**Figure 6.** Mechanism of EgtD-catalyzed methylation of DMH. Residues Asn166 and Gly161 are shown in gray.

ization of compounds depicted in Figure 7 are described in the Supporting Information. The inhibitory activities were

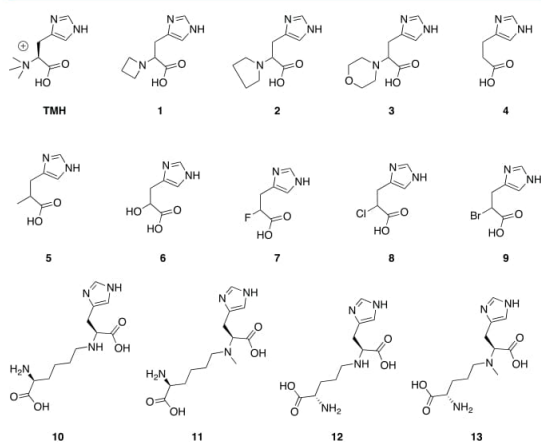


Figure 7. Structure of tested EgtD inhibitors.

measured using the same assay as described above. Consistent with the design strategy, compounds 1, 2, and 3 were not methylated by EgtD but instead inhibit EgtD-catalyzed methylation of HIS (Figures S8 and S9, Table 1). In the presence of 0.5 mM SAM, inhibition by 1, 2, and 3 is characterized by inhibition constants ( $K_i$ ) of 9, 40, and 90  $\mu$ M, respectively (Table 1). Compounds 1, 2, and 3 were synthesized in racemic form. Given that EgtD only interacts with L-amino acids, it is fair to assume that only the L-isomers of the inhibitors would bind (Figure S10). This assumption is corroborated by the finding that the pure L-form of 2 inhibits EgtD with a 2-fold lower  $K_i$  than measured for the racemic mixture (Table 1).

To examine the binding mode of these inhibitors, we determined the crystal structures of EgtD in complex with 2 and with 3 (Figure 5). Both structures show that the tertiary amines of 2 and 3 form the same hydrogen bond to Asn166 (2.9 and 3.0 Å) as seen in the EgtD:DMH complex (Figure 5). The electron density around ligands clearly shows that EgtD binds only the L-isomer of 2 and 3. One of the N- $\alpha$ -methylene carbons of 2 and 3 stacks against the carbonyl group of Gly161 (3.2 and 3.1 Å), and the rest of the pyrrolidino- and morpholino- rings block the space where the methyl group of SAM would approach the methyl acceptor. Both rings push the side chain of Thr163 which is pushed by 0.5 Å away from its position in the EgtD:TMH and EgtD:DMH structures. This steric stress also provides an explanation for why the size of the cyclic substituents in 1, 2, and 3 correlates inversely with their inhibitory activity (Table 1).

**Avoiding Competition with SAM.** As an alternative design strategy, we examined inhibitors that only compete with HIS but do not compete with SAM. Such compounds could form inhibited complexes with EgtD that are not destabilized by the generally high cellular concentration of SAM. To test this idea we synthesized racemic histidine derivatives with a proton (4), methyl group (5), hydroxyl group (6), fluoride (7), chloride (8), or bromide (9) in place of the  $\alpha$ -amine group. In kinetic assays, these compounds, except for 5, proved stronger HIS-competitive inhibitors than TMH (Table 1). The

inhibition constant of the L-form of 8 was again 2-fold lower than that of the racemic form, indicating that the active site selectively binds one isomer. Determination of the inhibition mechanism of chlorohistidine (8, Figure 4) revealed HIS-competitive and SAM-uncompetitive inhibition, suggesting that the EgtD:8 complex can still bind SAM.

The crystal structure of EgtD in complex with 8 confirms that this ligand occupies the same active site position as all other cocrystallized histidine derivatives (Figure 5). Unlike the  $\alpha$ -amine substituents in HIS, DMH, TMH, 2, and 3, the chloride substituent makes no direct contact with any protein residue. Solvation of the carboxylate and the imidazole ring by the active site apparently provides enough attractive interaction to induce strong inhibitory activity of the methyl- (5), chloro- (8), and bromo-substituted derivatives (9). The lower affinities of compounds 4, 6, and 7 are most likely due to stronger solvation of the free ligand by water. The relatively poor affinity of EgtD for 6 mirrors the low affinity for HIS and corroborates the notion that the residues Gly161 and Asn166 are not particularly well positioned to engage in hydrogen bonding.

**Bisubstrate Inhibitors.** A more common strategy to design inhibitors for methyltransferases targets the SAM-binding pocket. One successful way to increase the specificity toward one particular type of methyltransferase is to integrate structural motifs from SAM with those of the specific methyl acceptor into a single bisubstrate inhibitor.<sup>51–56</sup> To explore this approach for the design of EgtD inhibitors, we synthesized four histidine derivatives (10–13) that are N-substituted to mimic the methionyl moiety of SAM. All four compounds displayed weak inhibitory activity (Table 1, Figure S11). One explanation could be that the amino acid substituents are not recognized by the methionyl-binding site in EgtD. Indeed, reinspection of EgtD in complex with DMH and SAH showed the possibility that the chosen methionyl mimics may be too short to bridge the histidine binding site and the methionyl-binding site. It is also possible that the compounds do bind as intended, but that recognition of the methionyl-moiety does not produce enough attractive interaction to outweigh competition with SAM and HIS. The observation that the additional N- $\alpha$ -methyl group on compounds 11 and 13 increases the affinity by 4 to 8-fold provides further evidence that tertiary amines bind more strongly to EgtD than secondary amines.

**Feedback Inhibition.** EgtD catalyzes the first step in EGT biosynthesis (Figure 1). This reaction converts the primary metabolites HIS and SAM to TMH as a substrate for the subsequent enzyme EgtB. Methyltransferases are very common contributors to biosynthetic pathways in natural product biosynthesis.<sup>57</sup> However, a cursory inspection of all methyltransferase entries in the Braunschweig Enzyme Database (BRENDA) shows that SAM-dependent methyl transfers rarely occur as first biosynthetic steps.<sup>58</sup> For example, alkaloids or phenylpropanoids usually receive methyl groups at later biosynthetic stages.<sup>59–62</sup>

The unique role of EgtD as the gateway to EGT production raises the specific problem of regulation. Two studies on a gliotoxin deficient strain of *A. fumigatus* and a mycothiol-deficient strain of *M. smegmatis* revealed that these deficiencies are compensated by EGT overproduction.<sup>63,64</sup> The mechanism by which EGT productivity is coupled to seemingly unrelated biosynthetic activity is not known. However, the two studies provide first indications that EGT production may be regulated.



Because methyl transfer from SAM to His is essentially irreversible, and because both substrates are abundant metabolites, regulation of EgtD activity is essential, either by transcriptional control, by reversible inhibition, or by destruction of the enzyme. One regulatory mechanism has been proposed based on the finding that EgtD from *Mycobacterium tuberculosis* may be a substrate of the protein kinase PknD.<sup>31</sup> According to this model, the kinase phosphorylates a key active site residue of EgtD (Thr213) to block activity.

The observation that EgtD is subject to significant product inhibition highlights an alternative mode of regulation. Most SAM-dependent methyltransferases are inhibited by the side product S-adenosyl homocysteine (SAH). Therefore, methyltransferase activities are often modulated by the cellular concentration of SAH or the ratio of SAH/SAM.<sup>49</sup> Inhibition by the methylated product is far less common.<sup>65–70</sup> The caffeoyl-coenzyme A 3-O-methyltransferase from *Petroselinum crispum* (parsley) provides a rare exception. This enzyme is inhibited by its product feruloyl-CoA ( $K_{i, \text{feruloyl-CoA}} = 11 \mu\text{M}$ ), which allows strict regulation of the steady-state product concentration.<sup>70</sup>

By analogy, we hypothesize that product inhibition of EgtD may also have physiological relevance. Incidentally, the value of the associated inhibition constant ( $K_{i, \text{TMH}} = 40 \mu\text{M}$ , Table 1) lies in the same range as the  $K_M$  for TMH ( $K_{M, \text{TMH}} = 43 \mu\text{M}$ ) of the next enzyme in the pathway, EgtB (Figure 1).<sup>34</sup> These parameters ensure that TMH cannot accumulate to high concentrations even if EgtB activity decreases, for example, due to a limiting supply of the cosubstrates  $\gamma\text{GC}$  and  $\text{O}_2$ . Consequently, the cellular supply of TMH is adjusted to the rate of EGT production. In addition, the stabilizing effect of SAH on the EgtD:TMH complex raises the possibility that EGT biosynthesis is also regulated by the cellular concentration of SAH. The underlying prediction that product inhibition of EgtD is a specifically evolved trait is corroborated by the finding that the homologous tyrosine betaine synthase Ybs is not inhibited by the product despite significant active site similarity to EgtD.

**Proofreading.** In addition to making the first intermediate in EGT biosynthesis, EgtD also serves as a quality control element of this pathway. Although EGT has been identified from a large range of sources,<sup>1,4,5,23</sup> there are no isolation reports of EGT derivatives that lack one, two, or all N- $\alpha$ -methyl groups. For reasons that are not exactly clear, the betaine moiety of EGT is important for physiological function. Subsequent enzymes in the EGT pathway are unable to proofread the methylation state of their substrates.<sup>2,36,37</sup> For example, EgtB from *M. smegmatis* turns over DMH and TMH with almost the same efficiency.<sup>2</sup> EgtC and EgtE are unlikely to prevent alternative products because the reaction catalyzed by EgtB is irreversible. Hence, the only mechanism to prevent the formation of unwanted EGT derivatives is to limit the cellular concentration of DMH. Limiting this concentration is an important role of EgtD. As shown in Table 2, EgtD binds HIS, MMH, and DMH with increasing affinity. As a result, each added methyl group on the methyl acceptor increases the probability of further methylation. The three methyl groups are transferred in a cooperative process that avoids the accumulation of MMH or DMH.<sup>33</sup> By contrast, the catalytic efficiency of the homologous enzymes Ybs and EgtD<sub>E282A,M252V</sub> drops significantly after the first two methyl transfers to Tyr and Trp, respectively (Table 3). Comparisons of the EgtD structure

with the homology model of Ybs and the crystal structure of EgtD<sub>E282A,M252V</sub> do not reveal clear structural explanations for these different activities. One possibility is that transfer of the last methyl group is particularly sensitive to precise positioning of the N- $\alpha$ -dimethylated amino acid in the active site. Therefore, it is possible to conclude that the ability of EgtD to catalyze cooperative trimethylation is also an essential and specifically evolved feature.

**Mechanistic Implications.** Finally, we would like to summarize what can be learned about the catalytic mechanism and about inhibitor design from the ligand binding preferences of EgtD. EgtD can form up to 13 binary and ternary complexes with its six native ligands HIS, MMH, DMH, TMH, SAM, and SAH (Figure 8). Among these, EgtD:DMH and EgtD:TMH:-

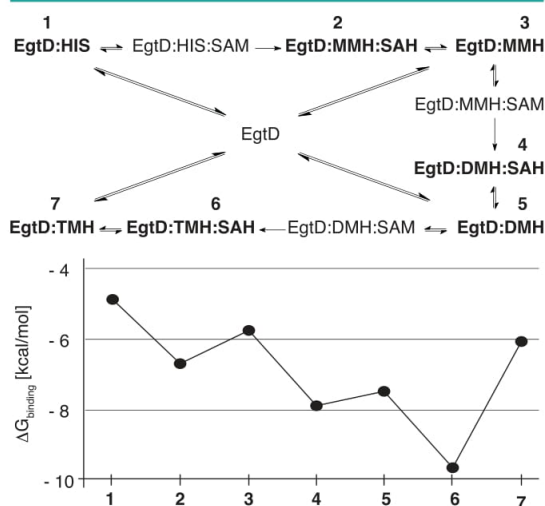


**Figure 8.** Top: Complete reaction scheme of EgtD catalyzed trimethylation of HIS. EgtD can combine with its six native ligands to 13 binary and ternary complexes. Bottom: The stability of EgtD complexes as determined by ITC (Table 2).

SAH are the strongest binary and ternary complexes (Table 2). The interaction between the amide side chain of Asn166 and the  $\alpha$ -amino function of DMH shows that the  $\alpha$ -amino function of the methyl acceptor is protonated in the binary complex (Figure 5). Apparently, the active site stabilizes a cationic moiety in this position. Unreactive histidine derivatives with neutral substituents (5, 8, and 9) form strong complexes with EgtD and SAM, suggesting that in the ternary complex the sulfonium moiety of SAM fully satisfies the requirement for a cationic charge in the active site. Consequently, the methyl acceptors HIS, MMH, and DMH must lose a proton before or concomitant to SAM binding. Also, in order to make room for the second substrate, deprotonation must be accompanied by inversion of the  $\alpha$ -amine. For example, DMH must turn the two N- $\alpha$ -methyl groups toward Gly161 and Asn166 in order to juxtapose the nucleophilic lone pair with the sulfonium methyl group of SAM (Figure 6). Each methyl transfer from HIS to TMH makes the ligand larger. The structures of EgtD in complex with HIS, DMH, and TMH show how the active site undergoes stepwise expansion by repositioning of Gly161 and Asn166 to accommodate the growing size of the ligand.

To support efficient trimethylation, the energy landscape of this expansion must be adjusted to increase the affinity for the methyl acceptor with each additional N- $\alpha$ -methyl group. As the thermodynamic binding data show, EgtD follows exactly this expected behavior. A plot of the complex stabilities ( $\Delta G_{\text{binding}}$ ) of EgtD with SAH and HIS, DMH, or TMH shows that each additional methyl group on the methyl acceptor increases the complex stability by 1.2 kcal/mol (Figure 8, Table 2). A similar trend is apparent in the absence of SAH. Notably, the EgtD:TMH complex deviates from this trend. It seems possible that the stability of the EgtD:TMH complex is purposefully decreased to avoid inhibition by submicromolar concentrations of TMH.

A glance at the enthalpic and entropic contributions to the stability of the six complexes cautions that a purely structural interpretation of the binding data may be misleading (Table 2). For example, formation of the EgtD:DMH:SAH complex liberates more heat than formation of the EgtD:TMH:SAH complex. However, because the latter suffers almost no entropic penalty, the TMH complex is 20-fold more stable. The enthalpic term indicates that formation of a hydrogen bond to Asn166 and stacking one N- $\alpha$ -methyl group toward Gly161 in the EgtD:DMH:SAH complex amounts to more attraction than the two N- $\alpha$ -methyl interactions with Gly161 and Asn166 in the EgtD:TMH:SAH complex. The basis for the large entropic difference is more difficult to localize. It is also interesting to note that conversion of the EgtD:HIS:SAH complex to the EgtD:TMH:SAH complex is accompanied by 300-fold stabilization, which is entirely due to entropic contributions. The same trend applies to the binary complexes in the absence of SAH. This result indicates that the two N- $\alpha$ -methyl interactions with Gly161 and Asn166 can at least partially compensate for the loss of the two hydrogen bonds in the EgtD:HIS:SAH complex. One interpretation of this result is that the two N- $\alpha$ -methyl interactions with protein carbonyl groups are at least weakly attractive.

**Conclusion.** This report describes the unusual substrate binding mechanism of the SAM-dependent methyltransferase EgtD. Unlike most methyltransferases, this enzyme follows an obligatory sequential binding mechanism with the methyl acceptor as the leading substrate. Second, this enzyme can regulate EGT production by way of product inhibition. Third, the enzyme ensures efficient permethylation of its substrate and suppresses the accumulation of mono- and dimethylated intermediates. Product inhibition and efficient permethylation are the result of specific evolutionary optimization. These findings were exploited to design three types of substrate competitive EgtD inhibitors. The most efficient inhibitors (5 and 8) are very simple histidine derivatives that provide promising leads for further development of EGT biosynthesis inhibitors.

## ■ ASSOCIATED CONTENT

### ● Supporting Information

The Supporting Information is available free of charge on the ACS Publications website at DOI: 10.1021/acschembio.8b00127.

Detailed descriptions of all experiments, supporting figures (S1–S11), schemes (S1–S8), and tables (S1 and S2) (PDF)

## ■ AUTHOR INFORMATION

### Corresponding Author

\*E-mail: [florian.seebeck@unibas.ch](mailto:florian.seebeck@unibas.ch).

### ORCID

Wulf Blankenfeldt: 0000-0001-9886-9668

Florian P. Seebeck: 0000-0003-4625-1369

### Author Contributions

<sup>†</sup>These authors contributed equally to this work.

### Notes

The authors declare no competing financial interest.

## ■ ACKNOWLEDGMENTS

The authors would like to thank the BESSY II Synchrotron (Helmholtz Centre Berlin, Berlin, Germany) for providing beamline access. This project was supported by the Swiss National Science Foundation, the University of Basel, the “Professur für Molekulare Bionik,” and a starting grant from the European Research Council (ERC-2013- StG 336559). A.V. was supported by the HZI Graduate School for Infection Research.

## ■ REFERENCES

- (1) Genghof, D. S.; Inamine, E.; Kovalenko, V.; and Melville, D. B. (1956) Ergothioneine in microorganisms. *J. Biol. Chem.* 223, 9–17.
- (2) Seebeck, F. P. (2010) In vitro reconstitution of Mycobacterial ergothioneine biosynthesis. *J. Am. Chem. Soc.* 132, 6632–6633.
- (3) Pfeiffer, C.; Surek, B.; Schömig, E.; Gründemann, D.; and Bauer, T. (2011) Cyanobacteria produce high levels of ergothioneine. *Food Chem.* 129, 1766–1769.
- (4) Alamgir, K. M.; Masuda, S.; Fujitani, Y.; Fukuda, F.; and Tani, A. (2015) Production of ergothioneine by *Methylobacterium* species. *Front. Microbiol.* 6, DOI: 10.3389/fmicb.2015.01185.
- (5) Burn, R.; Misson, L. E.; Meury, M.; and Seebeck, F. P. (2017) Anaerobic Origin of Ergothioneine. *Angew. Chem., Int. Ed.* 56, 12508–12511.
- (6) Jones, G. W.; Doyle, S.; and Fitzpatrick, D. A. (2014) The evolutionary history of the genes involved in the biosynthesis of the antioxidant ergothioneine. *Gene* 549, 161–170.
- (7) Gründemann, D.; Harlfinger, S.; Goltz, S.; Geerts, A.; Lazar, A.; Berkels, R.; Jung, N.; Rubbert, A.; and Schoemig, E. (2005) Discovery of the ergothioneine transporter. *Proc. Natl. Acad. Sci. U. S. A.* 102, 5256–5261.
- (8) Melville, D. B., and Eich, S. (1956) The occurrence of ergothioneine in plant material. *J. Biol. Chem.* 218, 647–651.
- (9) Servillo, L.; D’Onofrio, N.; and Balestrieri, M. L. (2017) Ergothioneine products derived by superoxide oxidation in endothelial cells exposed to high-glucose. *J. Cardiovasc. Pharmacol.* 69, 183–191.
- (10) Melville, D. B. (1959) Ergothioneine. *Vitam. Horm.* 17, 155–204.
- (11) Halliwell, B.; Cheah, I. K.; and Drum, C. L. (2016) Ergothioneine, an adaptive antioxidant for the protection of injured tissues? A hypothesis. *Biochem. Biophys. Res. Commun.* 470, 245–250.
- (12) Kerley, R. N.; McCarthy, C.; Kell, D. B.; and Kenny, L. C. (2018) The Potential Therapeutic Effects of Ergothioneine in Pre-eclampsia. *Free Radical Biol. Med.* 117, 145.
- (13) Cumming, B. M.; Lamprecht, D. A.; Wells, R. M.; Saini, V.; Mazorodze, J. H.; and Steyn, A. J. C. (2014) The Physiology and Genetics of Oxidative Stress in Mycobacteria. *Microbiol. Spectrum* 2, DOI: 10.1128/microbiolspec.MGM2-0019-2013.
- (14) Cheah, I. K., and Halliwell, B. (2012) Ergothioneine; antioxidant potential, physiological function and role in disease. *Biochim. Biophys. Acta, Mol. Basis Dis.* 1822, 784–793.
- (15) Asmus, K. D.; Bensasson, R. V.; Bernier, J. L.; Houssin, R.; and Land, E. J. (1996) One-electron oxidation of ergothioneine and



- analogues investigated by pulse radiolysis: redox reaction involving ergothioneine and vitamin C. *Biochem. J.* 315, 625–629.
- (16) De Luna, P., Bushnell, E. A., and Gault, J. W. (2013) A Density Functional Theory Investigation into the Binding of the Antioxidants Ergothioneine and Ovothiol to Copper. *J. Phys. Chem. A* 117, 4057–4065.
- (17) Melnick, J. G., and Parkin, G. (2007) Cleaving Mercury-Alkyl Bonds: A Functional Model for Mercury Detoxification by MerB. *Science* 317, 225–227.
- (18) Servillo, L., Castaldo, D., Casale, R., D'Onofrio, N., Giovane, A., Cautela, D., and Balestrieri, M. L. (2015) An uncommon redox behavior sheds light on the cellular antioxidant properties of ergothioneine. *Free Radical Biol. Med.* 79, 228–236.
- (19) Brummel, M. C. (1985) In search of a physiological function for L-ergothioneine. *Med. Med. Hypotheses* 18, 351–370.
- (20) Stoffels, C., Oumari, M., Perrou, A., Termath, A., Schlundt, W., Schmalz, H. G., Schäfer, M., Wewer, V., Metzger, S., Schömig, E., and Gründemann, D. (2017) Ergothioneine stands out from hercynine in the reaction with singlet oxygen: Resistance to glutathione and TRIS in the generation of specific products indicates high reactivity. *Free Radical Biol. Med.* 113, 385–394.
- (21) Arduini, A., Eddy, L., and Hochstein, P. (1990) The reduction of ferryl myoglobin by ergothioneine: a novel function for ergothioneine. *Arch. Biochem. Biophys.* 281, 41–43.
- (22) Zhu, B.-Z., Mao, L., Fan, R.-M., Zhu, J.-G., Zhang, Y.-N., Wang, J., Kalyanaraman, B., and Frei, B. (2011) Ergothioneine Prevents Copper-Induced Oxidative Damage to DNA and Protein by Forming a Redox-Inactive Ergothioneine-Copper Complex. *Chem. Res. Toxicol.* 24, 30–34.
- (23) Ey, J., Schomig, E., and Taubert, D. (2007) Dietary Sources and Antioxidant Effects of Ergothioneine. *J. Agric. Food Chem.* 55, 6466–6474.
- (24) Cumming, B. M., Chinta, K. C., Reddy, V. P., and Steyn, A. J. C. (2018) Role of Ergothioneine in Microbial Physiology and Pathogenesis. *Antioxid. Redox Signaling* 28, 431–444.
- (25) Bello, M. H., Barrera-Perez, V., Morin, D., and Epstein, L. (2012) The *Neurospora crassa* mutant NcDEgt-1 identifies an ergothioneine biosynthetic gene and demonstrates that ergothioneine enhances conidial survival and protects against peroxide toxicity during conidial germination. *Fungal Genet. Biol.* 49, 160–172.
- (26) Nakajima, S., Satoh, Y., Yanashima, K., Matsui, T., and Dai, T. (2015) Ergothioneine protects *Streptomyces coelicolor* A3(2) from oxidative stresses. *J. Biosci. Bioeng.* 120, 294–298.
- (27) Sheridan, K. J., Lechner, B. E., Keeffe, G. O., Keller, M. A., Werner, E. R., Lindner, H., Jones, G. W., Haas, H., and Doyle, S. (2016) Ergothioneine Biosynthesis and Functionality in the Opportunistic Fungal Pathogen, *Aspergillus fumigatus*. *Sci. Rep.* 6, 35306.
- (28) Singh, A. R., Strankman, A., Orkusyan, R., Purwantini, E., and Rawat, M. (2016) Lack of mycothiol and ergothioneine induces different protective mechanisms in *Mycobacterium smegmatis*. *Biochem. Biophys. Res. Commun.* 495, 174–178.
- (29) Saini, H. S., Cumming, B. M., Guidry, L., Lamprecht, D. A., Adamson, J. H., Reddy, V. P., Chinta, K. C., Mazorodze, J. H., Glasgow, J. N., Richard-Greenblatt, M., Gomez-Velasco, A., Bach, H., Av-Gay, Y., Eoh, H., Rhee, K., and Steyn, A. J. C. (2016) Ergothioneine Maintains Redox and Bioenergetic Homeostasis Essential for Drug Susceptibility and Virulence of *Mycobacterium tuberculosis*. *Cell Rep.* 14, 572–585.
- (30) Richard-Greenblatt, M., Bach, H., Adamson, J. H., Pena-Diaz, S., Li, W., Steyn, A. J. C., and Av-Gay, Y. (2015) Regulation of Ergothioneine Biosynthesis and Its Effect on *Mycobacterium tuberculosis* Growth and Infectivity. *J. Biol. Chem.* 290, 23064–23076.
- (31) Ishikawa, Y., and Melville, D. B. (1970) The Enzymatic a-N-Methylation of Histidine. *J. Biol. Chem.* 245, S967–S973.
- (32) Vit, A., Misson, L. E., Blankenfeldt, W., and Seebeck, F. P. (2015) Ergothioneine Biosynthetic Methyltransferase EgtD Reveals the Structural Basis of Aromatic Amino Acid Betaine Biosynthesis. *ChemBioChem* 16, 119–125.
- (33) Goncharenko, K. V., Vit, A., Blankenfeldt, W., and Seebeck, F. P. (2015) Structure of the Sulfoxide Synthase EgtB from the Ergothioneine Biosynthetic Pathway. *Angew. Chem., Int. Ed.* 54, 2821–2824.
- (34) Faponle, A. S., Seebeck, F. P., and de Visser, S. P. (2017) Sulfoxide Synthase versus Cysteine Dioxygenase Reactivity in a Nonheme Iron Enzyme. *J. Am. Chem. Soc.* 139, 9259–9270.
- (35) Vit, A., Mashabela, G. T., Blankenfeldt, W., and Seebeck, F. P. (2015) Structure of the Ergothioneine-Biosynthesis Amidohydrolase EgtC. *ChemBioChem* 16, 1490–1496.
- (36) Song, H., Hu, W., Naowarojna, N., Her, A. S., Wang, S. G., Desai, R., Qin, L., Chen, X., and Liu, P. (2015) Mechanistic studies of a novel C-S lyase in ergothioneine biosynthesis: the involvement of a sulfenic acid intermediate. *Sci. Rep.* 5, DOI: 10.1038/srep11870.
- (37) Pluskal, T., Ueno, M., and Yanagida, M. (2014) Genetic and Metabolomic Dissection of the Ergothioneine and Selenoneine Biosynthetic Pathway in the Fission Yeast, *S. pombe*, and Construction of an Overproduction System. *PLoS One* 9, e97774.
- (38) Hu, W., Song, H., Sae Her, A., Bak, D. W., Naowarojna, N., Elliott, S. J., Qin, L., Chen, X., and Liu, P. (2014) Bioinformatic and Biochemical Characterizations of C–S Bond Formation and Cleavage Enzymes in the Fungus *Neurospora crassa* Ergothioneine Biosynthetic Pathway. *Org. Lett.* 16, 5382–5385.
- (39) Askari, A., and Melville, D. B. (1962) The reaction sequence in ergothioneine biosynthesis: hercynine as an intermediate. *J. Biol. Chem.* 237, 1615.
- (40) Liao, C., and Seebeck, F. P. (2017) Convergent Evolution of Ergothioneine Biosynthesis in Cyanobacteria. *ChemBioChem* 18, 2115–2118.
- (41) Cook, P. F., and Cleland, W. W. (2007) *Enzyme Kinetics and Mechanism*, Garland Science Publishing, New York.
- (42) Dorgan, K. M., Woodechak, W. L., Wynn, D. P., Karschner, E. L., Alfaro, J. F., Cui, Y. Q., Zhou, Z. S., and Hevel, J. M. (2006) An enzyme-coupled continuous spectrophotometric assay for S-adenosylmethionine-dependent methyltransferases. *Anal. Biochem.* 350, 249–255.
- (43) Martin, J. L., and McMillan, F. M. (2002) SAM (dependent) I AM: the S-adenosylmethionine-dependent methyltransferase fold. *Curr. Opin. Struct. Biol.* 12, 783–793.
- (44) Schubert, H. L., Blumenthal, R. M., and Cheng, X. (2003) Many paths to methyltransfer: a chronicle of convergence. *Trends Biochem. Sci.* 28, 329–335.
- (45) Lorenz, N., Wilson, E. V., Machado, C., Schardl, C. L., and Tudzynski, P. (2007) Comparison of Ergot Alkaloid Biosynthesis Gene Clusters in *Claviceps* Species Indicates Loss of Late Pathway Steps in Evolution of *C. fusiformis*. *Appl. Environ. Microbiol.* 73, 7185–7191.
- (46) Liscombe, D. K., Louie, G. V., and Noel, J. P. (2012) Architectures, mechanisms and molecular evolution of natural product methyltransferases. *Nat. Prod. Rep.* 29, 1238–1250.
- (47) Dirk, L. M. A., Flynn, E. M., Dietzel, K., Couture, J.-F., Triebel, R. C., and Houtz, R. L. (2007) Kinetic Manifestation of Processivity during Multiple Methylations Catalyzed by SET Domain Protein Methyltransferases. *Biochemistry* 46, 3905–3915.
- (48) Kloor, D., and Osswald, H. (2004) S-Adenosylhomocysteine hydrolase as a target for intracellular adenosine action. *Trends Pharmacol. Sci.* 25, 294–297.
- (49) Jeong, J. H., Cha, H. J., Ha, S. C., Rojviriyi, C., and Kim, Y. G. (2014) Structural insights into the histidine trimethylation activity of EgtD from *Mycobacterium smegmatis*. *Biochem. Biophys. Res. Commun.* 452, 1098–1103.
- (50) Lerner, C., Ruf, A., Gramlich, V., Masjost, B., Zürcher, G., Jakob-Roetne, R., Borroni, E., and Diederich, F. (2001) X-ray Crystal

Structure of a Bisubstrate Inhibitor Bound to the Enzyme Catechol-methyltransferase: A Dramatic Effect of Inhibitor Preorganization on Binding Affinity. *Angew. Chem., Int. Ed.* 40, 4040–4042.

(52) Ma, Z., Liu, H. W., and Wu, B. T. (2014) Structure-based drug design of catechol-O-methyltransferase inhibitors for CNS disorders. *Br. J. Clin. Pharmacol.* 77, 410–420.

(53) Zhang, G., Richardson, S. L., Huang, R., and Mao, Y. (2015) Design, synthesis, and kinetic analysis of potent protein N-terminal methyltransferase 1 inhibitors. *Org. Biomol. Chem.* 13, 4149–4154.

(54) Hobley, G., McKelvie, J. C., Harmer, J. E., Howe, J., Oyston, P. C., and Roach, P. L. (2012) Development of rationally designed DNA N6 adenine methyltransferase inhibitors. *Bioorg. Med. Chem. Lett.* 22, 3079–3082.

(55) Vaubourgeix, J., Bardou, F., Boissier, F., Julien, S., Constant, P., Ploux, O., Daffé, M., Quémar, A., and Mourey, L. (2009) S-Adenosyl-N-decyl-aminoethyl, a Potent Bisubstrate Inhibitor of Mycobacterium tuberculosis Mycolic Acid Methyltransferases. *J. Biol. Chem.* 284, 19321–19330.

(56) Osborne, T., Weller Roska, R. L., Rajski, S. R., and Thompson, P. R. (2008) Situ Generation of a Bisubstrate Analogue for Protein Arginine Methyltransferase 1. *J. Am. Chem. Soc.* 130, 4574–4575.

(57) Struck, A. W., Thompson, M. L., Wong, S. L., and Micklefield, J. (2012) S-Adenosyl-Methionine-Dependent Methyltransferases: Highly Versatile Enzymes in Biocatalysis, Biosynthesis and Other Biotechnological Applications. *ChemBioChem* 13, 2642–2655.

(58) Placzek, S., Schomburg, I., Chang, A., Jeske, L., Ulbrich, M., Tillack, J., and Schomburg, D. (2017) BRENDA in 2017: new perspectives and new tools in BRENDA. *Nucleic Acids Res.* 45, D380–D388.

(59) Vogt, T. (2010) Phenylpropanoid biosynthesis. *Mol. Plant* 3, 2–20.

(60) Jakubczyk, D., Cheng, J. Z., and O'Connor, S. E. (2014) Biosynthesis of the ergot alkaloids. *Nat. Prod. Rep.* 31, 1328–1338.

(61) Xu, W., Gavia, D. J., and Tang, Y. (2014) Biosynthesis of fungal indole alkaloids. *Nat. Prod. Rep.* 31, 1474–1487.

(62) Ziegler, J., and Facchini, P. J. (2008) Alkaloid biosynthesis: metabolism and trafficking. *Annu. Rev. Plant Biol.* 59, 735–769.

(63) Gallagher, L., Owens, R. A., Dolan, S. K., O'Keeffe, G., Schrettel, M., Kavanagh, K., Jones, G. W., and Doyle, S. (2012) The *Aspergillus fumigatus* protein GliK protects against oxidative stress and is essential for gliotoxin biosynthesis. *Eukaryotic Cell* 11, 1226–1238.

(64) Ta, P., Buchmeier, N., Newton, G. L., Rawat, M., and Fahey, R. C. (2011) *J. Bacteriol.* 193, 1981–1990.

(65) Orr, E. L., and Quay, W. B. (1978) Product inhibition of rat brain histamine-N-methyltransferase. *J. Neurochem.* 30, 1539–1542.

(66) Wu, Q., and McLeish, M. J. (2013) Kinetic and pH studies on human phenylethanolamine N-methyltransferase. *Arch. Biochem. Biophys.* 539, 1–8.

(67) Baron, R. A., and Casey, P. J. (2004) Analysis of the kinetic mechanism of recombinant human isoprenylcysteine carboxylmethyltransferase (Icmt). *BMC Biochem.* 5, 19.

(68) De Luca, V., and Ibrahim, R. K. (1985) Enzymatic synthesis of polymethylated flavonols in *Chrysosplenium americanum*. II. Substrate interaction and product inhibition studies of flavonol 3-, 6-, and 4'-O-methyltransferases. *Arch. Biochem. Biophys.* 238, 596–605.

(69) Cleland, W. W. (1963) The kinetics of enzyme-catalyzed reactions with two or more substrates or products. III. Prediction of initial velocity and inhibition patterns by inspection. *Biochim. Biophys. Acta, Spec. Sect. Enzymol. Subj.* 67, 173–187.

(70) Pakusch, A. E., and Matern, U. (1991) Kinetic Characterization of Caffeoyl-Coenzyme A-Specific 3-O-Methyltransferase from Elicited Parsley Cell Suspensions. *Plant Physiol.* 96, 327–330.

Reprinted with permission from Misson, L.; Burn, R.; Vit, A.; Hildesheim, J.; Beliaeva, M. A.; Blankenfeldt, W.; Seebeck, F. P. *ACS Chem. Biol.* 2018, 13 (5), 1333. Copyright 2018 American Chemical Society.

---

## 7 Literature

- (1) Ingenbleek, Y. J. *Nutr.* **2006**, 1641.
- (2) Filipovic, M. R.; Zivanovic, J.; Alvarez, B.; Banerjee, R. *Chem. Rev.* **2018**, 118 (3), 1253.
- (3) Wiberg, E.; Wiberg, N. *Lehrbuch der anorganischen Chemie*, 102nd ed.; Walter de Gruyter & Co.: Berlin, New York, 2007.
- (4) Oae, S. *Organic sulfur chemistry*; Doi, J. T., Ed.; CRC Press: Boca Raton, 1991.
- (5) Zimmerman, M. T.; Bayse, C. A.; Ramoutar, R. R.; Brumaghim, J. L. *J. Inorg. Biochem.* **2015**, 145, 30.
- (6) Fontecave, M.; Atta, M.; Mulliez, E. *Trends Biochem. Sci.* **2004**, 29 (5), 243.
- (7) Komarnisky, L. A.; Christopherson, R. J.; Basu, T. K. *Nutrition* **2003**, 19 (1), 54.
- (8) Hand, C. E.; Honek, J. F. *J. Nat. Prod.* **2005**, 68 (2), 293.
- (9) Zheng, C.; Black, K. A.; Dos Santos, P. C. *Biomolecules* **2017**, 7 (4), 33.
- (10) Dunbar, K. L.; Scharf, D. H.; Litomska, A.; Hertweck, C. *Chem. Rev.* **2017**, 117 (8), 5521.
- (11) Jarrett, J. T. *J. Biol. Chem.* **2015**, 290 (7), 3972.
- (12) Paritala, H.; Carroll, K. *Infect. Disord. - Drug Targets* **2013**, 13 (2), 85.
- (13) Devendar, P.; Yang, G. F. *Top. Curr. Chem.* **2017**, 375 (6), 1.
- (14) Feng, M.; Tang, B.; H. Liang, S.; Jiang, X. *Sulfur Containing Scaffolds in Drugs: Synthesis and Application in Medicinal Chemistry*; 2016; Vol. 16.
- (15) [www.genengnews.com https://www.genengnews.com/a-lists/top-10-best-selling-drugs-of-the-21st-century/77899716/](https://www.genengnews.com/a-lists/top-10-best-selling-drugs-of-the-21st-century/77899716/).
- (16) Chauhan, P.; Mahajan, S.; Enders, D. *Chem. Rev.* **2014**, 114 (18), 8807.
- (17) Lee, C.-F.; Basha, R. S.; Badsara, S. S. *Top. Curr. Chem.* **2018**, 376 (3), 25.
- (18) Wimmer, A.; König, B. *Beilstein J. Org. Chem.* **2018**, 14 (Scheme 1), 54.
- (19) Liu, B.; Lim, C.-H.; Miyake, G. M. *J. Am. Chem. Soc.* **2017**, 139 (39), 13616.
- (20) Dong, D.-Q.; Hao, S.-H.; Yang, D.-S.; Li, L.-X.; Wang, Z.-L. *European J. Org. Chem.* **2017**, 2017 (45), 6576.
- (21) Dénès, F.; Pichowicz, M.; Povie, G.; Renaud, P. *Chem. Rev.* **2014**, 114 (5), 2587.
- (22) Shen, C.; Zhang, P.; Sun, Q.; Bai, S.; Hor, T. S. A.; Liu, X. *Chem. Soc. Rev.* **2015**, 44 (1), 291.
- (23) Kosugi, M.; Shimizu, T.; Migita, T. *Chem. Lett.* **1978**, 7 (1), 13.
- (24) Migita, T.; Shimizu, T.; Asami, Y.; Shiobara, J.-I.; Kato, Y.; Kosugi, M. *Bull. Chem. Soc. Jpn.* **1980**, 53 (5), 1385.
- (25) Magano, J.; Dunetz, J. R. *Chem. Rev.* **2011**, 111 (3), 2177.
- (26) Inamoto, K.; Arai, Y.; Hiroya, K.; Doi, T. *Chem. Commun.* **2008**, No. 43, 5529.
- (27) Inamoto, K.; Nozawa, K.; Kondo, Y. *Synlett* **2012**, 23 (11), 1678.
- (28) Joyce, L. L.; Batey, R. A. *Org. Lett.* **2009**, 11 (13), 2792.

- 
- (29) Shen, C.; Xia, H.; Yan, H.; Chen, X.; Ranjit, S.; Xie, X.; Tan, D.; Lee, R.; Yang, Y.; Xing, B.; Huang, K. W.; Zhang, P.; Liu, X. *Chem. Sci.* **2012**, 3 (7), 2388.
- (30) Zhao, X.; Dimitrijević, E.; Dong, V. M. *J. Am. Chem. Soc.* **2009**, 131 (10), 3466.
- (31) Xu, C.; Shen, Q. *Org. Lett.* **2014**, 16 (7), 2046.
- (32) Iwasaki, M.; Iyanaga, M.; Tsuchiya, Y.; Nishimura, Y.; Li, W.; Li, Z.; Nishihara, Y. *Chem. - A Eur. J.* **2014**, 20 (9), 2459.
- (33) Chen, X.; Hao, X.-S.; Goodhue, C. E.; Yu, J.-Q. *J. Am. Chem. Soc.* **2006**, 128 (21), 6790.
- (34) Hyvl, J.; Srogl, J. *European J. Org. Chem.* **2010**, 2010 (15), 2849.
- (35) Chen, F.-J.; Liao, G.; Li, X.; Wu, J.; Shi, B.-F. *Org. Lett.* **2014**, 16 (21), 5644.
- (36) Lan, X.-W.; Wang, N.-X.; Bai, C.-B.; Zhang, W.; Xing, Y.; Wen, J.-L.; Wang, Y.-J.; Li, Y.-H. *Sci. Rep.* **2016**, 5 (1), 18391.
- (37) Srogl, J.; Hývl, J.; Révész, Á.; Schröder, D. *Chem. Commun.* **2009**, No. 23, 3463.
- (38) Wu, Z.; Song, H.; Cui, X.; Pi, C.; Du, W.; Wu, Y. *Org. Lett.* **2013**, 15 (6), 1270.
- (39) Mendelson, W. L.; Liu, J. H.; Killmer, L. B.; Levinson, S. H. *J. Org. Chem.* **1983**, 48 (3), 298.
- (40) Tang, R.-Y.; Xie, Y.-X.; Xie, Y.-L.; Xiang, J.-N.; Li, J.-H. *Chem. Commun.* **2011**, 47 (48), 12867.
- (41) Yuan, J.; Ma, X.; Yi, H.; Liu, C.; Lei, A. *Chem. Commun.* **2014**, 50 (92), 14386.
- (42) Singh, A. K.; Chawla, R.; Yadav, L. D. S. *Tetrahedron Lett.* **2014**, 55 (34), 4742.
- (43) Lu, Q.; Zhang, J.; Zhao, G.; Qi, Y.; Wang, H.; Lei, A. *J. Am. Chem. Soc.* **2013**, 135 (31), 11481.
- (44) Zou, L.-H.; Reball, J.; Mottweiler, J.; Bolm, C. *Chem. Commun.* **2012**, 48 (92), 11307.
- (45) Yang, S. H.; Seo, H. S.; Woo, J. H.; Oh, H. M.; Jang, H.; Lee, J. H.; Kim, S. J.; Kwon, K. K. *Int. J. Syst. Evol. Microbiol.* **2014**, 64 (PART 4), 1351.
- (46) Hostier, T.; Ferey, V.; Ricci, G.; Gomez Pardo, D.; Cossy, J. *Org. Lett.* **2015**, 17 (15), 3898.
- (47) Miao, T.; Li, P.; Zhang, Y.; Wang, L. *Org. Lett.* **2015**, 17 (4), 832.
- (48) Olah, G. A.; Kobayashi, S.; Nishimura, J. *J. Am. Chem. Soc.* **1973**, 95 (2), 564.
- (49) Marcantoni, E.; Cipolletti, R.; Marsili, L.; Menichetti, S.; Properzi, R.; Viglianisi, C. *European J. Org. Chem.* **2013**, 2013 (1), 132.
- (50) Singh, S.; Yadav, L. D. S. *Tetrahedron Lett.* **2012**, 53 (38), 5136.
- (51) Uno, T.; Inokuma, T.; Takemoto, Y. *Chem. Commun.* **2012**, 48 (13), 1901.
- (52) Kredich, N. M. *EcoSal Plus* **2008**, 3 (1).
- (53) Struck, A. W.; Thompson, M. L.; Wong, L. S.; Micklefield, J. *ChemBioChem* **2012**, 13 (18), 2642.
- (54) Fontecave, M.; Ollagnier-de-Choudens, S.; Mulliez, E. *Chem. Rev.* **2003**, 103 (6), 2149.
- (55) Begley, T. P.; Xi, J.; Kinsland, C.; Taylor, S.; McLafferty, F. *Curr. Opin. Chem. Biol.* **1999**, 3 (5), 623.
-

- 
- (56) Mueller, E. G. *Nat. Chem. Biol.* **2006**, 2 (4), 185.
- (57) Kessler, D. *FEMS Microbiol. Rev.* **2006**, 30 (6), 825.
- (58) Black, K. A.; Dos Santos, P. C. *Biochim. Biophys. Acta - Mol. Cell Res.* **2015**, 1853 (6), 1470.
- (59) Papenbrock, J.; Guretzki, S.; Henne, M. *Amino Acids* **2011**, 41 (1), 43.
- (60) Hidese, R.; Mihara, H.; Esaki, N. *Appl. Microbiol. Biotechnol.* **2011**, 91 (1), 47.
- (61) Dickschat, J. S.; Rinkel, J.; Klapschinski, T.; Petersen, J. *ChemBioChem* **2017**, 18 (22), 2260.
- (62) Dolan, S. K.; O'Keeffe, G.; Jones, G. W.; Doyle, S. *Trends Microbiol.* **2015**, 23 (7), 419.
- (63) Scharf, D. H.; Remme, N.; Habel, A.; Chankhamjon, P.; Scherlach, K.; Heinekamp, T.; Hortschansky, P.; Brakhage, A. A.; Hertweck, C. *J. Am. Chem. Soc.* **2011**, 133 (32), 12322.
- (64) Scharf, D. H.; Chankhamjon, P.; Scherlach, K.; Heinekamp, T.; Willing, K.; Brakhage, A. A.; Hertweck, C. *Angew. Chemie - Int. Ed.* **2013**, 52 (42), 11092.
- (65) Suzuki, H.; Furusho, Y.; Higashi, T.; Ohnishi, Y.; Horinouchi, S. *J. Biol. Chem.* **2006**, 281 (2), 824.
- (66) Brock, N. L.; Nikolay, A.; Dickschat, J. S. *Chem. Commun.* **2014**, 50 (41), 5487.
- (67) Ploegman, J. H.; Drent, G.; Kalk, K. H.; Hol, W. G. J.; Heinrikson, R. L.; Keim, P.; Weng, L.; Russell, J. *Nature* **1978**, 273 (5658), 124.
- (68) Cipollone, R.; Ascenzi, P.; Visca, P. *IUBMB Life* **2007**, 59 (2), 51.
- (69) Cipollone, R.; Ascenzi, P.; Tomao, P.; Imperi, F.; Visca, P. *J. Mol. Microbiol. Biotechnol.* **2008**, 15 (2–3), 199.
- (70) Lewis, J. C.; Coelho, P. S.; Arnold, F. H. *Chem. Soc. Rev.* **2011**, 40 (4), 2003.
- (71) Broderick, J. B.; Du, B. R.; Duschene, K. S.; Shepard, E. M.; Duffus, B. R.; Duschene, K. S.; Shepard, E. M.; Du, B. R.; Duschene, K. S.; Shepard, E. M. *Chem. Rev.* **2014**, 114 (2014 Bioinorganic Enzymology (8)), 4229.
- (72) Xie, Y.; Li, Q.; Song, Y.; Ma, J.; Ju, J. *ChemBioChem* **2014**, 15 (8), 1183.
- (73) Xie, Y.; Wang, B.; Liu, J.; Zhou, J.; Ma, J.; Huang, H.; Ju, J. *ChemBioChem* **2012**, 13 (18), 2745.
- (74) Kuligowski, C.; Bezzenine-Lafollée, S.; Chaume, G.; Mahuteau, J.; Barrière, J.-C.; Bacqué, E.; Pancrazi, A.; Ardisson, J. *J. Org. Chem.* **2002**, 67 (13), 4565.
- (75) Dvorak, C. A.; Schmitz, W. D.; Poon, D. J.; Pryde, D. C.; Lawson, J. P.; Amos, R. A.; Meyers, A. I. *Angew. Chemie Int. Ed.* **2000**, 39 (9), 1664.
- (76) Su, X.; Lin, Z.; Lin, H. *Crit. Rev. Biochem. Mol. Biol.* **2013**, 48 (6), 515.
- (77) Fugate, C. J.; Jarrett, J. T. *Biochim. Biophys. Acta - Proteins Proteomics* **2012**, 1824 (11), 1213.
- (78) Cronan, J. E. *EcoSal Plus* **2013**, 1 (3).
- (79) McCarthy, E. L.; Booker, S. J. *Science (80-. )*. **2017**, 358 (6361), 373.
- (80) Rigby, S. E. J.; Hynson, R. M. G.; Ramsay, R. R.; Munro, A. W.; Scrutton, N. S. *J. Biol. Chem.*
-

- 
- 2005**, 280 (6), 4627.
- (81) Baunach, M.; Ding, L.; Willing, K.; Hertweck, C. *Angew. Chemie Int. Ed.* **2015**, 54 (45), 13279.
- (82) Hamed, R. B.; Gomez-Castellanos, J. R.; Henry, L.; Ducho, C.; McDonough, M. A.; Schofield, C. J. *Nat. Prod. Rep.* **2013**, 30 (1), 21.
- (83) Baldwin, J. E.; Bradley, M. *Chem. Rev.* **1990**, 90 (7), 1079.
- (84) Goncharenko, K. V.; Vit, A.; Blankenfeldt, W.; Seebeck, F. P. *Angew. Chemie Int. Ed.* **2015**, 54 (9), 2821.
- (85) Goncharenko, K. V.; Seebeck, F. P. *Chem. Commun.* **2016**, 52, 1945.
- (86) Faponle, A. S.; Seebeck, F. P.; de Visser, S. P. *J. Am. Chem. Soc.* **2017**, 139 (27), 9259.
- (87) Stampfli, A. R.; Goncharenko, K. V.; Meury, M.; Dubey, B. N.; Schirmer, T.; Seebeck, F. P. *J. Am. Chem. Soc.* **2019**, 141 (13), 5275.
- (88) Mashabela, G. T. M.; Seebeck, F. P. *Chem. Commun.* **2013**, 49 (70), 7714.
- (89) Liao, C.; Seebeck, F. P. *ChemBioChem* **2017**, 18 (21), 2115.
- (90) Cumming, B. M.; Chinta, K. C.; Reddy, V. P.; Steyn, A. J. C. *Antioxid. Redox Signal.* **2018**, 28 (6), 431.
- (91) Halliwell, B.; Cheah, I. K.; Tang, R. M. Y. *FEBS Lett.* **2018**, 592 (20), 3357.
- (92) Grundemann, D.; Harlfinger, S.; Golz, S.; Geerts, A.; Lazar, A.; Berkels, R.; Jung, N.; Rubbert, A.; Schomig, E. *Proc. Natl. Acad. Sci.* **2005**, 102 (14), 5256.
- (93) Paul, B. D.; Snyder, S. H. *Cell Death Differ.* **2010**, 17 (7), 1134.
- (94) Richard-Greenblatt, M.; Bach, H.; Adamson, J.; Peña-Diaz, S.; Li, W.; Steyn, A. J. C.; Av-Gay, Y. *J. Biol. Chem.* **2015**, 290 (38), 23064.
- (95) Cheah, I. K.; Halliwell, B. *Biochim. Biophys. Acta - Mol. Basis Dis.* **2012**, 1822 (5), 784.
- (96) Servillo, L.; D'Onofrio, N.; Balestrieri, M. L. *J. Cardiovasc. Pharmacol.* **2017**, 69 (4), 183.
- (97) Rougee, M.; Bensasson, R. V.; Land, E. J.; Pariente, R. *Photochem. Photobiol.* **1988**, 47 (4), 485.
- (98) Seebeck, F. P. *J. Am. Chem. Soc.* **2010**, 132 (19), 6632.
- (99) Cheah, I. K.; Halliwell, B. *Biochim. Biophys. Acta - Mol. Basis Dis.* **2012**, 1822 (5), 784.
- (100) Wei, W.-J.; Siegbahn, P. E. M.; Liao, R.-Z. *Inorg. Chem.* **2017**, 56 (6), 3589.
- (101) Tian, G.; Su, H.; Liu, Y. *ACS Catal.* **2018**, 8 (7), 5875.
- (102) Todd, A. E.; Orengo, C. A.; Thornton, J. M. *Trends Biochem. Sci.* **2002**, 27 (8), 419.
- (103) Deechongkit, S.; Nguyen, H.; Powers, E. T.; Dawson, P. E.; Gruebele, M.; Kelly, J. W. *Nature* **2004**, 101.
- (104) Goncharenko, K. V.; Seebeck, F. P. *Chem. Commun.* **2016**, 52 (9), 1945.
- (105) Karshikoff, A.; Jelesarov, I. *Biotechnol. Biotechnol. Equip.* **2008**, 22 (1), 606.
- (106) Lavogina, D.; Enkvist, E.; Uri, A. *ChemMedChem* **2010**, 5 (1), 23.
- (107) Baker, E. N.; Hubbard, R. E. *Prog. Biophys. Mol. Biol.* **1984**, 44 (2), 97.
-



- 
- (108) Zhou, H. X.; Pang, X. *Chem. Rev.* **2018**, *118* (4), 1691.
- (109) Engi, P. *Chemical Probes for Mechanistic Enzymology*, University of Basel, 2017.
- (110) Cook, P. F.; Cleland, W. W. *Enzyme Kinetics and Mechanism*; Garland Science: London, 2007.
- (111) Gerfaud, T.; Chiang, Y. L.; Kreituss, I.; Russak, J. a.; Bode, J. W. *Org. Process Res. Dev.* **2012**, *16* (4), 687.
- (112) Wisniewski, K. *Org. Prep. Proced. Int.* **1999**, *31* (2), 211.
- (113) Endo, M.; Nakayama, K.; Majima, T. *J. Org. Chem.* **2004**, *69* (13), 4292.
- (114) Fenton, J. M.; Busse, B. M.; A, L. M. R. *Aust. J. Chem.* **2015**, *68*, 576.
- (115) Jagadish, B.; Guntle, G. P.; Zhao, D.; Gokhale, V.; Ozumerzifon, T. J.; Ahad, A. M.; Mash, E. a; Raghunand, N. *J. Med. Chem.* **2012**, *55*, 10378.
- (116) Braunshausen, A.; Seebeck, F. P. *J. Am. Chem. Soc.* **2011**, *133* (6), 1757.
- (117) Sassa, A.; Beard, W. A.; Shock, D. D.; Wilson, S. H. *J. Vis. Exp.* **2013**, No. 78, 1.
- (118) Vit, A.; Misson, L.; Blankenfeldt, W.; Seebeck, F. P. *Acta Crystallogr. Sect. F Struct. Biol. Commun.* **2014**, *70* (5), 676.

---

## 8 Acknowledgements

First and foremost, I would like to thank Prof. Florian P. Seebeck for giving me the opportunity to work in his group and letting me contribute to challenging and interesting projects during the last four years.

I would like to thank Prof. Thomas R. Ward for being my Co-Referee and for taking time to read my doctoral thesis.

I would like to thank Prof. Christof Sparr for chairing my PhD defense.

A huge thank you goes to all the lovable, happy and optimistic coworkers I had the pleasure to share the lab, coffee breaks and occasionally a beer with. I am truly thankful for all the good moments we shared over these years and hope that there are more to come. Thank you Cangsong Liao, Anja Stampfli, Alice Maurer, David Lim, Dzmitry Miarzlou, Florian Leisinger, Mariia Beliaeva, Jiaming Peng, Sebastian Flückiger, Marcel Meury, Pascal Engi, Kristina Goncharenko, Matthias Knopp, Roxana Lemnar, Laëtitia Misson, Julia Hildesheim and Carsten Baur.

A special thank you goes to the proofreading team Anja Stampfli and David Lim. I am more than grateful for all the time and energy they spent to read and discuss the manuscript.

As important as the support in the lab was the support outside the lab. Therefore, I would like to thank all my friends who have been helping me through these four years.

I would like to thank my family for all the support and trust throughout the years.

My deepest gratitude goes to Lu, for all the beautiful moments I could experience with her, all the patience she had with me and for being there when I needed her most. Without her, this would not have been possible.

---

# Reto Burn

Hardfeldstrasse 39, CH-4600 Olten, Switzerland • +41 79 763 59 24

[burn.reto@gmail.com](mailto:burn.reto@gmail.com) • DOB: 30<sup>th</sup> March 1991

Nationality: Switzerland • Single

...

## EDUCATION

Mar. 2015 - present **PhD in Chemistry, University of Basel**

PhD Thesis Supervisor: Prof. Dr. F. P. Seebeck

Investigation of a novel biosynthetic pathway in the anaerobic synthesis of ergothioneine and elucidation of the catalytic mechanism of the anaerobic ergothioneine biosynthetic enzyme EanB.

- Development of an HPLC assay for product isolation
- Developing and performing enzyme assays
- Recombinant protein production
- Cultivation of microorganisms
- Detection and isolation of bacterial thiols

Synthesis of small molecule inhibitors for the histidine N-alpha-methyltransferase EgtD to gain a deeper understanding of the binding mechanism for this enzyme.

- Designing enzyme inhibitors
- Development of synthetic routes

Synthesis of artificial substrates for the sulfoxide synthase, EgtB, and measurement of enzyme kinetics to gain insight into the reaction mechanism of this enzyme.

- Designing molecules to probe enzyme mechanisms

Feb. 2013 – Dec. 2014 **Master of Sciences in Chemistry and Molecular Sciences, University of Bern**

MSc Thesis: "Synthesis and Optimization of New Fluorescent Probes Containing Borinate Moieties for Protein Labeling"

MSc Thesis Supervisor: Dr. M. Lochner

Sept. 2009 – Sept. 2012 **Bachelor of Science in Biochemistry and Molecular Biology, University of Bern**

BSc Thesis: "Synthesis of Potential Agonists of the Serotonin 5-HT<sub>3</sub> Receptor"

BSc Thesis Supervisor: Dr. M. Lochner

Jun. 2009 **Maturität** Physics and Applied Mathematics, Gymnasium Neufeld (BE), Switzerland